Thesis Report

Performance-based Adaptation of Lateral Robotic Balance Assistance during Slackline Walking

by

Aneesh Ashok Kumar

to obtain the degree of Master of Science
at the Delft University of Technology,
to be defended publicly on Thursday May 14, 2020 at 1:30 PM.

Student number: 4738586

Project duration: August 1, 2019 – May 14, 2020
Thesis committee:

Prof. Dr. Ing. H. Vallery,	TU Delft, supervisor
Ir. A. Berry,	TU Delft, supervisor
Dr. Ir. J.C.F. de Winter,	TU Delft

An electronic version of this thesis is available at `http://repository.tudelft.nl/`.

TU Delft

Abstract

As part of the ongoing research on balance assistance at the Delft Biorobotics Lab, the goal of this project was to analyse the relevance of optimising the control action to each individual user. In order to explore the feasibility of tuning balance assistance based on task performance as well as controller assistance, an experimental study was conducted on the optimisation of lateral balance assistance during slackline walking. The task performance was quantified as the distance walked on the slackline. The balance assistance was provided by the RYSEN– an active Bodyweight Support (BWS) system used in gait training– in the form of lateral damping. The damping value was tuned over successive trials to optimise the trade-off between maximising the distance walked by the participants before loss of balance and minimising the lateral impulses applied by the RYSEN during each trial. The Covariance Matrix Adaptation Evolution Strategy (CMAES) was used for the automated optimisation of the lateral damping assistance. The performance of the CMAES algorithm was compared to participant performance in optimising the damping based on the same cost measure.

Using a final sample size of 15 healthy participants, comparisons were made between costs for trials conducted with Zero Damping (ZD), the optimal damping estimate returned by the algorithm (D_a) and the optimal damping estimate selected by the participants (D_h), with the expectation that lower trial costs would be returned by the optimal damping estimates.

No significant difference was found among the median cost measures of the three conditions ($p = 0.24$, Friedman's ANOVA). Significant differences were found between the corresponding distance measures ($p = 0.002$, Friedman's ANOVA), with significantly longer distances walked in D_a and D_h trials compared to ZD trials ($p = 0.003$ and $p = 0.005$ respectively), but no significant differences between the measures for D_a and D_h trials ($p = 0.61$). Analysis of the primary cost measures based on Grid Search (GS) trials indicated a shallow cost landscape with high variability. Post-hoc optimisation simulations were run using CMAES and Bayesian optimisation upon individual participant grid search data. Results indicated the possibility of better performance upon increasing the number of candidates sampled per generation and the initial step size used in the algorithm, using an alternative cost function with a quadratic distance cost component, or by using Bayesian optimisation for a comparable number of trial iterations.

Acknowledgement

I would like to thank my supervisors, Heike Vallery and Andrew Berry, for their guidance and mentorship throughout the course of this project. Andrew, my daily supervisor, was always available for discussions and advice. He provided invaluable sources of information on the scientific aspects of the project, as well as useful tips on the practical aspects. I am very grateful to him for his thorough and detailed feedback on my work.

I have learned a lot about effective and precise scientific communication from Heike, for which I am very thankful. Her sharp input and criticism during the weekly update meetings, with her insistence on high standards and attention to detail, played a huge role in my learning process throughout the project's duration.

I would like to thank Jan van Frankenhuyzen and Daniel Lemus for their ideas and advice during the design phase of the slackline anchoring setup, which greatly smoothened the design process and helped me arrive at a simple and feasible design for the anchors.

I learned about the functionalities of the RYSEN, as well as the practical aspects of its use, from Romain Valette and Nathan Fopma, for which I am very grateful. I also received useful tips on experiment protocol, participant interaction, and later on in statistical analysis from Nathan.

I would like to thank Patricia Bairnes and Saher Jabeen for their help in experiment design and the formulation of the experiment protocol. Patricia provided detailed guidance on the protocol formulation, while Saher volunteered to participate in an early pilot study, giving useful suggestions on the experiment procedure as well as the hypothesis test.

Working on the project at the Biorobotics Lab was an enriching experience. The lab had a nice work environment and a friendly atmosphere, and I really enjoyed my time with everyone there. In addition to the above-mentioned names, I want to express my thanks to my fellow lab mates–Christina, Roemer, Charlotte, Mahdi, Joris, Bram and Koos– for the useful suggestions I received from you all, including tips on presentation techniques and design ideas for the slackline anchor setup. The lunch and coffee conversations on wide-ranging topics were really enjoyable, as were the intense post-lunch table football matches.

I am grateful to all the participants of the study for the time and effort they put during their sessions, as slacklining is no easy task, and ironically is something that I still struggle to do. Special thanks to Rahul and Krishna for their invaluable support during the early pilot studies. Rahul especially helped out in the setup of the portable slackline used in initial pilot studies, and as the first volunteer to try the setup, his input on the effects of slacklining was invaluable.

I am also grateful to Ashwin Vijay, who along with Nathan and Krishna, provided useful peer-feedback on earlier drafts of this report.

The lunch sessions at the Aula– with Ashwin George, Syed, Rahul, Krishna, Sanjit and Rohit– were especially enjoyable and helped boost morale during phases of uncertainty. Special thanks to Ashwin George for his advice and useful perspective on multiple decisions involving the project. I learned a lot about data presentation techniques and Matlab and LaTeX functionalities from him.

I want to thank my flatmates Francisco, Paulius, and Sander for their positivity and encouragement during the course of the project. The lunch and dinner conversations, cycling trips, and game sessions were much needed breaks which helped clear my mind.

Lastly, I am deeply grateful to my parents and my brother Hareesh, for their constant support and belief in me. Whenever times were difficult, their encouragement and positivity really kept me going, and I have been able to put in my best efforts into this work because of them.

Contents

Table 1: Nomenclature.

COM	Centre of Mass.
COP	Centre of Pressure.
CMG	Control Moment Gyroscope.
CMAES	Covariance Matrix Adaptation Evolution Strategy.
BWS	Bodyweight Support.
BE	Baseline Evaluation. Experimental block implemented right after the familiarisation trials.
ZD	Zero Damping. Trial condition with no active lateral damping applied by the RYSEN
ADO	Algorithm-Driven Optimisation. Experimental block in which lateral damping is optimised by an algorithm
HDO	Human-Driven Optimisation. Experimental block in which participants optimise the lateral damping.
CC	Condition Comparison. Experimental block implemented right after the damping optimisation blocks
GS	Grid Search.
IQR	Inter-Quartile Range.
ISR	Initial Search Range. Defined as the range of damping parameters sampled by each participant in the first 5 HDO trials.
OSR	Overall Search Range. Defined as the range of damping parameters sampled by each participant over all the HDO trials.
D_{a}	Algorithm-estimated optimal damping value.
D_{h}	Optimal damping value estimated by the participant.
I_{m}	Maximum impulse along the user's mediolateral axis during a trial.
I_{lim}	Lateral impulse limit term used to scale the maximum impulse measure.
L	Distance walked by participant on the slackline during the trial.
L_{lim}	Maximum walkable distance on the slackline.
F_{AP}	Slingbar force component along the user's anteroposterior axis.
F_{ML}	Slingbar force component along the user's mediolateral axis.
v_{AP}	Slingbar velocity component along the user's anteroposterior axis.
v_{ML}	Slingbar velocity component along the user's mediolateral axis.

1
Introduction

1.1. Balance Control and Assistance

A person's ability to move around is one that is often taken for granted, yet is of great importance to a healthy and active life. A critical component of this activity is the ability to maintain balance, adapting to transitions in movement, changes in terrain and other external influences. For the average healthy adult, this is mostly a subconscious activity, achieved by the interplay between the sensory and motor pathways trained during one's early childhood.

However, maintaining balance becomes a challenge for the elderly [1, 2], and to those suffering from sensorimotor disorders. The causes of these disorders are wide-ranging and include muscle weakness (post-stroke condition [3], muscular dystrophy [4]), injuries to neural pathways (Parkinson's [5], cerebral palsy [6]), damage or loss of sensory feedback channels (visual, proprioceptive, or vestibular [7]), and even psychogenic factors (phobic postural vertigo [8]). The loss of balance control severely reduces the mobility of these individuals, and puts them at greater risk of severe injury due to falls. A fear of falling would inhibit them from trying to move around [9], and may result in delayed reactions to perturbations leading to increased risk of falls [10].

Overground standing balance is maintained by an interplay of multiple strategies– the ankle, hip and the change-of-support strategies [11]. The ankle strategy involves using dorsi- and plantarflexion, along with inversion and eversion muscle groups to move the Centre of Pressure (COP) about the projection of the Centre of Mass (COM) on the ground. In the hip strategy, the hip muscles are used to shift the load shared by each leg, and also to vary the angular momentum of the body. The change-of-support strategy is used in gait, as well as in quiet standing when the other two strategies cannot bring the COM in the support polygon. The relevance of each strategy depends on the nature of stance and the type of the terrain. For example, in normal stance with feet side-by-side, the ankle strategy is seen to dominate in the sagittal plane, while the hip strategy is more relevant in the frontal plane [11]. In tandem stance (with the feet in line), the sharing of the load would be more relevant in the sagittal plane, with ankle inversion-eversion being more dominant in the frontal plane [11].

A number of active gait rehabilitative/assistive devices have been developed to train and help individuals regain the ability to walk. These can be categorised based on the nature of the assistive forces/torques provided. Systems in contact with the ground or a fixed support can provide external forces on the body. They often incorporate bodyweight support, may apply actuations in the anteroposterior and/or mediolateral direction, and may be used for overground walking or with treadmill systems. Notable systems include the RYSEN (Motek BV, Amsterdam, The Netherlands [12]), the FLOAT (Reha-Stim Medtec AG, Schlieren, Switzerland [13]) and the Lokomat (Hocoma AG, Volketswil, Switzerland [14]). Meanwhile, portable lower-limb exoskeletons and exosuits, with actuators in parallel with the body's joints impart internal torques on these joints. Their primary function is to assist in gait, but some rehabilitation of balance strategies does occur [15]. Lastly, free-moment devices using reaction wheels [16] or Control Moment Gyroscopes (CMG) (GyBAR [17]) can exert moments on the body with respect to the inertial frame, using the principle of conservation of angular momentum in an inertial frame. These devices are portable and capable of exerting moments on the body without directly manipulating reaction forces to the ground or an external support frame.

The imposition of rigid joint constraints in some of these devices can have a few negative effects, such as user passivity and alteration from natural gait patterns, which reduces their effectiveness in rehabilitation compared to therapist-assisted rehabilitation [18]. Meanwhile, devices that allow users to generate their preferred movement patterns while assisting in aspects such as weight-bearing are shown to significantly improve participant performance [19]. Bodyweight unloading is especially useful in training patients with severe impairment, relieving the person's focus from load bearing and allowing him/her to focus on maintaining balance and in controlling foot placement. On the other hand, momentum-exchange devices that apply

free moments on body segments could be used to specifically assist people who have necessary strength for load bearing but suffer from sensorimotor impairments affecting balance strategies.

1.2. Adaptation of Assistance Parameters

1.2.1. Individual Variability

There is a lot of variability amongst individuals in terms of physical structure and neuro-muscular coordination, which can give rise to large differences among individuals in their optimal interaction with the assistive device. There are multiple ways to account for the variability, such as using compliant actuation [20], adaptive state estimation and intent recognition [21], or control adaptation based on outcome measurements [22, 23]. One approach is to minimise conflict between the user and the device, assisting the user in performing actions as per their intention. Adaptive oscillators quickly learn the user-defined frequencies of the repetitive components in activities such as gait, which are used to vary the time period of the reference trajectory cycles accordingly [24].

Assistance parameter adaptation could also be used to improve the performance of specific tasks, quantified by specific outcome measures. Adaptive control strategies [25] are often used in such frameworks, and they involve parameter adaptation in real-time to minimise errors in tracking reference position or velocity profiles. Other methods also exist, which could use cost measures such as reference errors, force estimates, or physiological measures, and involve parameter adaptation over different time intervals, such as each time-step, activity cycle, or task trial. The term *human-in-the-loop optimisation* is often used to broadly describe these methods [22, 23, 26, 27].

A systematic literature review was conducted by the author on the existing experimental implementations of real-time parameter adaptation frameworks, aimed at optimising various outcome measures in various upper- and lower-body motion tasks. It was observed that the adaptation method used to update the parameters could be an explicit law derived from system models, or an iterative optimisation method. The suitability of an adaptation method to the implementation depends on the complexity of the optimisation problem. This could be characterised by the relationship between the parameter and the performance metric, the uncertainties and physical limitations involved in their measurements, and the range of the parameter space being searched, including the search dimensionality.

Simple law-based methods are limited in applicability to frameworks where the performance-parameter mapping could be modelled/predicted. Thus, they are restricted to implementations either involving simple activities such as 1-D joint flexion or reaching, or using metrics such as position/velocity reference errors, which can be related to the parameters using dynamic models.

Optimisation-based methods could be used when the relationship between the parameters and the performance measures is not explicit. This is usually the case when using physiological measures such as EMG signals or metabolic estimates. The algorithms need to be sample-efficient when outcome measures have low sample rates, such as metabolic cost estimates, or any performance measure evaluated at the end of a trial. When measurements have high variability due to sensor noise or the system dynamics itself, robust algorithms are desirable.

The Covariance Matrix Adaptation-Evolution Strategy (CMAES) and Bayesion Optimisation algorithms have been successfully used to tune the control action of ankle and hip exoskeletons to minimise the estimated metabolic cost during gait [22, 26]. The cost estimates, based on respirometer measurements, suffer from noise and transient effects, requiring around 2 minutes of sampling time for reasonable estimates. A comparison between Bayesian Optimisation and Gradient descent was done by Kim et al. in finding optimal gait frequency for healthy participants based on metabolic costs, with Bayesian Optimisation reaching the optimal values in half the time as the Gradient descent method [23]. Meanwhile, CMAES was successfully used by Zhang et al. to perform a 4-parameter optimisation of ankle exoskeleton assistance, minimising user metabolic costs [22].

Sample-efficient convergence is especially attractive in human-in-the-loop optimisation because the human is a time-varying system. Stamina limitations lead to deterioration of participant performance over prolonged trials, and even in the absence of fatigue, the participants adapt their response to control action. It would be ideal to find the optimal parameters before the participants get fatigued, or lose their motivation, or develop compensatory strategies adapt to sub-optimal controller action. Improvement in skill level through consistent task repetition should also be accounted for.

1.2.2. Actuator Limitations

When tuning the parameters of an assistive device for an individual, the actuator limitations could ideally be factored into the selection process. Examples of such limitations include the power ratings of the motors used in exoskeletons and the maximum angular momentum that could be imparted by momentum-exchange devices. In the case of powered exoskeletons, insufficient assistance at particular instance could later lead to instability that system cannot recover from, due to limited actuation capability. It would be desirable to have the exoskeleton control action tuned such that the likelihood of assistance requirements ending up exceeding the motor power ratings is minimised.

Momentum-exchange devices work by the transfer of the angular momentum between the device (usually in the form of rotating flywheels) and the system. The magnitude of the total angular momentum that can be exchanged is limited by the physical properties of the system, restricting the magnitude and duration of exerted moments. The limitation on the angular impulse arises from the maximum flywheel angular velocity in reaction wheels, and the limited ability to reorient the momentum vector in CMGs. Specifically in the case of the GyBAR, which consists of a single CMG, assistive moments cannot be generated along the flywheel axis. Also, assistive torque can only be maintained in a specific direction for a limited period, before the flywheel becomes completely oriented in this direction. A control action that provides the necessary assistance such that the net impulse imparted by the device does not exceed the angular momentum constraint of the flywheel is therefore ideal in this situation.

1.3. Motivation of This Study

1.3.1. Optimisation of Balance Assistance with Limited Assistance

The Delft Biorobotics Lab is researching the use of gyroscopic actuators in wearable devices used for movement assistance and training. One of the goals is to build an assistive device that is portable and capable of specifically assisting balance-impaired people– a gyroscopic backpack that applies torques on the user's trunk [17]. As mentioned previously, such a device could specifically assist in maintaining balance and potentially help people with sensorimotor impairments to improve or relearn balance strategies used in stance and locomotion. Deciding on the nature of assistance provided could be crucial when aiming to maximise the effectiveness of a balance assistance device. Experiments were conducted with a prototype, involving standing and walking tasks with limited base of support in the sagittal or frontal plane, to compare control laws suitable for the backpack (spring, damper and spring-damper)[17]. A limited base of support was used with healthy participants so that balance control became challenging enough for differences in controller effectiveness to be observable. The controllers were compared based on the distance walked on a narrow beam before loss of mediolateral balance, for walking tasks, and the duration of stance on a narrow beam before loss of balance in the sagittal plane. While the damper controller showed the greatest improvement in task performance compared to unassisted baseline conditions, the feedback gains were set arbitrarily to a common value for all participants. Another important observation was that instances of actuator saturation during the trials resulted in immediate loss of balance, which is contrary to the objective. Therefore, the following question is explored in this study: Is it necessary, and possible to fine tune the controller to each individual's requirements, while minimising device action?

1.3.2. Research Goals

A systematic analysis of human-in-the-loop optimisation for motion tasks yielded no results pertaining specifically to balance assistance. Studies involving gait assistance optimisation focused on tuning the assistance of specific joints based on measures such as reference trajectory errors, interaction forces and metabolic costs. Thus, a research gap has been identified in the area of balance assistance optimisation. In addition, no device constraints were observed to be imposed in the collected literature, other than limits on the parameter search space.

Here we propose to study optimal balance assistance in a challenging locomotion task. As a representative example, we consider the task of walking as far as possible along a slackline while supported by the RYSEN cable robot.

The goal of the project is to analyse the necessity and effectiveness of fine-tuning controller assistance, specifically in the frontal plane, during a gait task that challenged user balance. The tuning of the assistance parameter is based on a task outcome measure– the distance walked before loss of balance, which is indicated

by stepping outside the base of support. This measure could be influenced by multiple factors other than the device assistance, such as the size, ability, and the motivation of the user, the specific strategy that is employed to maintain balance, and the occurrence of small 'mistakes', such as mis-steps, foot slips or some distractions that can affect balance. This results in complex and uncertain assistance-performance relationships that may challenge the search for an optimal assistance parameter.

An additional constraint is imposed while tuning for maximum performance, in the form of a limit on the impulse applied by the supporting device on the user during the task. This is imposed as a soft constraint, in the form of an exponential penalty that, together with the performance measure, are used to construct a cost function for the optimisation algorithm. Thus, a violation of this impulse limit does not lead to an end of the trial, but instead adds a penalty whose magnitude depends on the extent of the constraint violation. The trade-off between maximising task performance while minimising assistance constraint violations should ensure that unnecessary assistance is not provided to the user.

Thus, the research questions of the study are:

RQ1: Is it possible to use the distance walked on a slackline as a reliable measure to quantify the balance stability of an individual, for a given level of assistance? The reliability could be defined in terms of two components:

- What is the variance of this measure for an individual over a set of trials, for the same assistance conditions provided?
- What is the extent of shift in the mean or median value of the measure over a number of trials (e.g: 50-70 trials in a single session), due to participant adaptation or fatigue?

RQ2: Can the maximum lateral impulse provided by the RYSEN during the trial similarly be used as a reliable estimator of the extent of device assistance?
The lateral impulses during each trial are computed from measured lateral force timeseries.

RQ3: Assuming that the distance walked and the maximum lateral impulse are reliable quantifiers, are there lateral damping configurations that would provide an optimal trade-off between maximising balance stability and minimising device assistance?

RQ4: Considering that one or more optimal assistance parameter exists, how would an algorithm perform when compared to the users themselves in finding one such optimum over a range of trials? How is the parameter space explored in each case, and how do the final selections compare?

The following hypothesis is derived from **RQ3** and **RQ4**:

Hypothesis: Given a cost function that is dependent on the distance walked by the slackline and the maximum impulse applied on the participant during the trial, the cost measures associated to trials with optimal damping values– one returned by a suitable optimisation algorithm and the other identified by the participants themselves– are hypothesised to be significantly lower than cost measures associated to trials with zero lateral damping. There is a minimum residual impedance in the system during the zero lateral damping condition due to force-tracking limitations, but the other conditions are expected to have a controlled damping of lateral motion in addition to this residual impedance.

It is important to note that the research questions and the hypothesis are based on three implicit assumptions:

A1 The distance walked by the user on the slackline is positively correlated with the lateral damping coefficient.

A2 The maximum impulse applied by the RYSEN is positively correlated with the lateral damping coefficient.

A3 The distance walked on the slackline is positively correlated with the stability on the slackline.

From the above assumptions, it is concluded that a trade-off must exist between the distance walked along the slackline and the assistive impulse provided by the RYSEN.

Research questions **RQ1**-**RQ4**, along with the hypothesis, are addressed via an experimental implementation of a human-in-the-loop optimisation of slackline walking with RYSEN assistance, conducted with healthy participants. Post-hoc optimisation simulations with the experimental data are used to further address the questions **RQ3** and **RQ4**.

1.4. Report Structure

In Chapter 2, an overview of the experimental setup is first given in Section 2.1, including the assistive device, the slackline, and the implemented software framework. Following this, the selection of partipants, task activity and overall experiment procedure are explained in Section 2.2. In Section 2.3, the post-processing of the data to address the research questions is explained. Finally, in Section 2.4, the statistical tests used in the data analysis are explained.

Chapter 3 covers the experimental results, with the analysis of the primary outcome measures given in Section 3.1, followed by an analysis of the secondary outcome measures with changes in the assistance condition in Section 3.2. Section 3.3 covers the observations on the optimisation simulations conducted with experimental data.

In Chapter 4, the experimental results are discussed, study limitations are analysed, and alternatives to the cost function and optimisation algorithm are explored.

Finally, Chapter 5 summarises the findings of this study and provides recommendations for future studies.

2
Methodology

2.1. Experimental Setup

2.1.1. Assistive Device– RYSEN

The RYSEN (Motek Medical B.V., Amsterdam, NL) is a cable-driven 3-D overground Bodyweight Support (BWS) system, capable of applying forces in the vertical as well as horizontal directions [12]. The system is actuated by 5 motors: 2 for controlling vertical forces, 2 for applying forces in the forward-backward direction, and 1 for applying lateral forces. There are 2 parallel rails oriented in the forward direction, which is the main walking direction. Two cables, one passing through each rail, are used to track the motion of the participant and apply forces via a slingbar. Differences in force and velocity requirements in the vertical and horizontal planes led to the selection of a decoupling of actuation systems, which keeps the power requirements of the RYSEN lower than that of other overground systems like the FLOAT. A representation of the RYSEN research interface is given in Fig. 2.1. The global frame has its origin at one end of the workspace, furthest away from the cabinet and in the middle of the space between the rails. The X-axis is in the main walking direction, parallel to the rails and oriented to the cabinet. The positive Y-axis is oriented to the left when facing the cabinets, and the positive Z-axis is oriented upwards. In this study, during each trial, the anteroposterior axis of the participant is aligned to the X-axis, the mediolateral axis is aligned to the Y-axis, and the vertical axis is aligned to the Z-axis of the global coordinate system.

To start a session with a participant, a participant profile is first created in the user-interface, containing the height and weight of the participant. The allowable vertical force setpoints during normal stance or walking are in the range of $10-60\,\%$ of the participant's weight. The height of the participant is used to detect the onset of a fall and to increase vertical forces to prevent this. In case of a complete loss of balance, the entire weight of the participant can be supported. In addition to vertical support forces, the RYSEN can exert additional forces in the vertical, anteroposterior and mediolateral directions to assist or challenge the user. These forces could be in the form of impedance (virtual springs or dampers) or feedforward force trajectories. In this study, the RYSEN was used to provide varying degrees of damping assistance lateral to the main walking direction, resisting lateral motion of the slingbar from above the slackline on which the participants walked. This damping assistance was in addition to a vertical unloading force set to 11% of the participant's bodyweight, which was present in all trials. D-Flow (Motek BV, Amsterdam, The Netherlands), a visual programming tool, was used to set the damping value for each trial, based on input (csv) files generated via MATLAB (Mathworks, Natick, USA).

2.1.2. Balance Assessment Platform– Slackline

Slacklining is a balance-intensive activity in which a person stands or walks on a horizontal elastic webbing tensioned between two fixed anchors. The challenge involved in maintaining balance during slackline walking has two components– the limitation of the support polygon in the lateral direction, along with the low stiffness of the base of support. Slacklines are generally less than $5\,\text{cm}$ in width, which forces the usage of the tandem stance. Studies by Winter [11] show that ankle inversion-eversion is the generally dominant strategy in maintaining mediolateral balance in the tandem stance on the ground. However, this strategy is less effective on slacklines as the webbing would rotate along with ankle joint, being a 'false base of support'. The reduced effectiveness of typically dominant overground balancing strategies on slacklines makes them rather challenging to the inexperienced slackliner. Counter-rotation strategies using the torso, the arms and the non-stance leg are more effective, with experienced and skilled slackliners showing synergies in whole-body coordinated motion [28].

The Gibbon Classic slackline (ID Sports, Stuttgart, Germany) was used for the experiment. With a load rating of $40\,\text{kN}$, the Classic line is a high-stiffness polyester line that is suitable for slacklining at low heights.

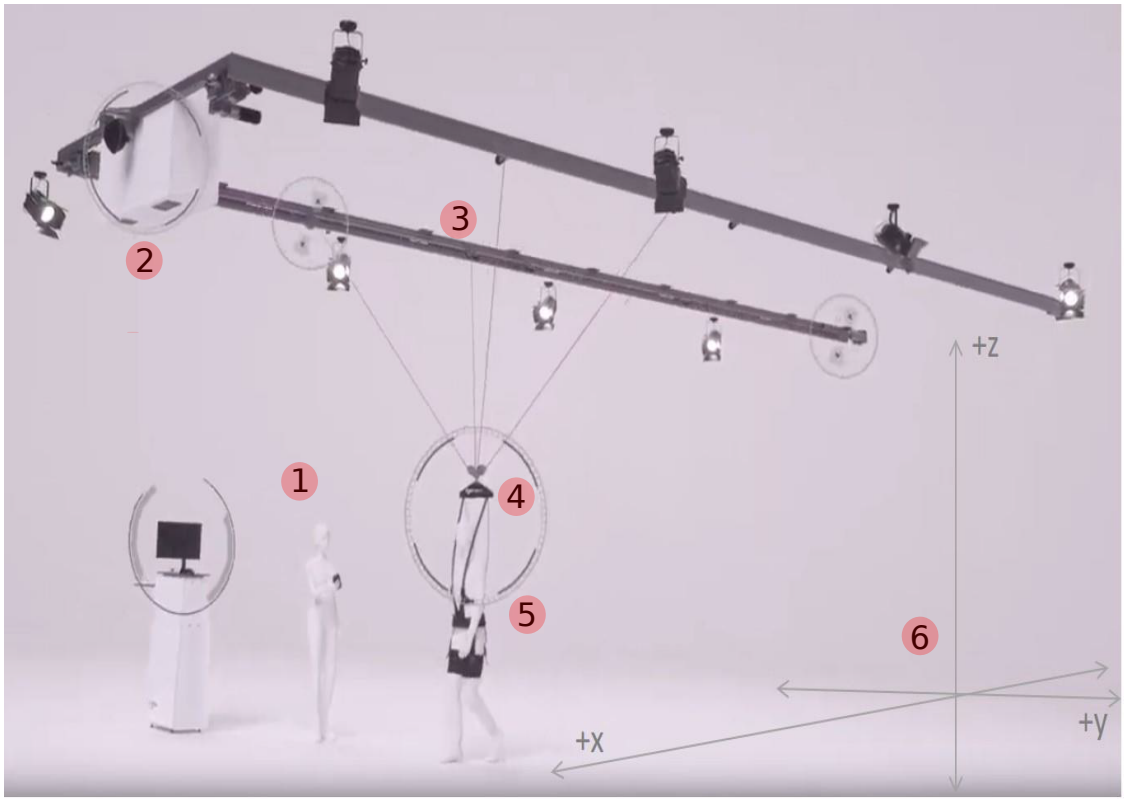

Figure 2.1: View of the RYSEN, with the following components: (1) control interface, via computer and mobile; (2) actuation unit, consisting of motors and transmission; (3) cable-pulley system with guide rails; (4) slingbar; and (5) body harness worn by participant. The global frame of reference (6) is also shown.

The slackline was used with 2 Gibbon SlackFrames (ID Sports, Stuttgart, Germany) and anchored to two floor-mounted steel plates at each end via a D-shackle and textile chord (additional information on the slackline anchoring setup is given in Appendix H). The slackline was set to a height of 0.5 m above the floor, and tensioned to have a sag of $0.35 - 0.37$ m when the participant steps on the mid-point of the slackline while attached to the RYSEN, with the vertical unloading set to 11% of the participant's weight. Fig. 2.6a shows the slackline setup. The slackline was aligned to the XZ plane of the RYSEN, so that the y-coordinate of the slingbar would be approximately zero when it is directly above the line. The walkable region on the slackline for the trials was between a starting point near one frame end and the position of the ratchet on the line, for a length of 5.5 m. To prevent injuries from loss of footing on the slackline, 2 cm thick exercise mats were placed on the floor below the walkable region of the slackline, extending to 1 m on either side of the slackline.

2.1.3. Setup Integration

Real-time data-processing

In addition to the provision of balance assistance, the RYSEN is also used to obtain information on participant performance, in the form of real-time slingbar position and force data. The data is processed in real-time by D-Flow and saved into csv files at the end of each trial. MATLAB scripts are used to read these files, as well as to set the damping parameter for the RYSEN via D-Flow.

The RYSEN is intended to produce a constant vertical force on the user, but limitations on force tracking capabilities can lead to increased vertical support forces upon sudden downward motion of the slingbar. A large downward displacement of the slingbar also results in increased vertical support to prevent falls. Since the focus of this experiment was on the effects of lateral forces on task performance, excessive reliance on the vertical support was undesirable. The reference point set for the vertical loading was 11% of the participant's weight. Slackline walking would involve significant vertical motion due to differences in vertical deflections at different positions of the line and vertical fluctuations arising from the oscillation of the line, therefore, some allowance for excess support could be made. The check for excessive BWS reliance was done in real-time via D-Flow, by checking if the vertical force at each time-step exceeded an allowable threshold (15% of

the participant's weight), with an alarm played when the cumulative duration of excess support during the trial exceeded 0.5 seconds. The real-time work-flow of the D-Flow application during each trial is represented in Fig. 2.2.

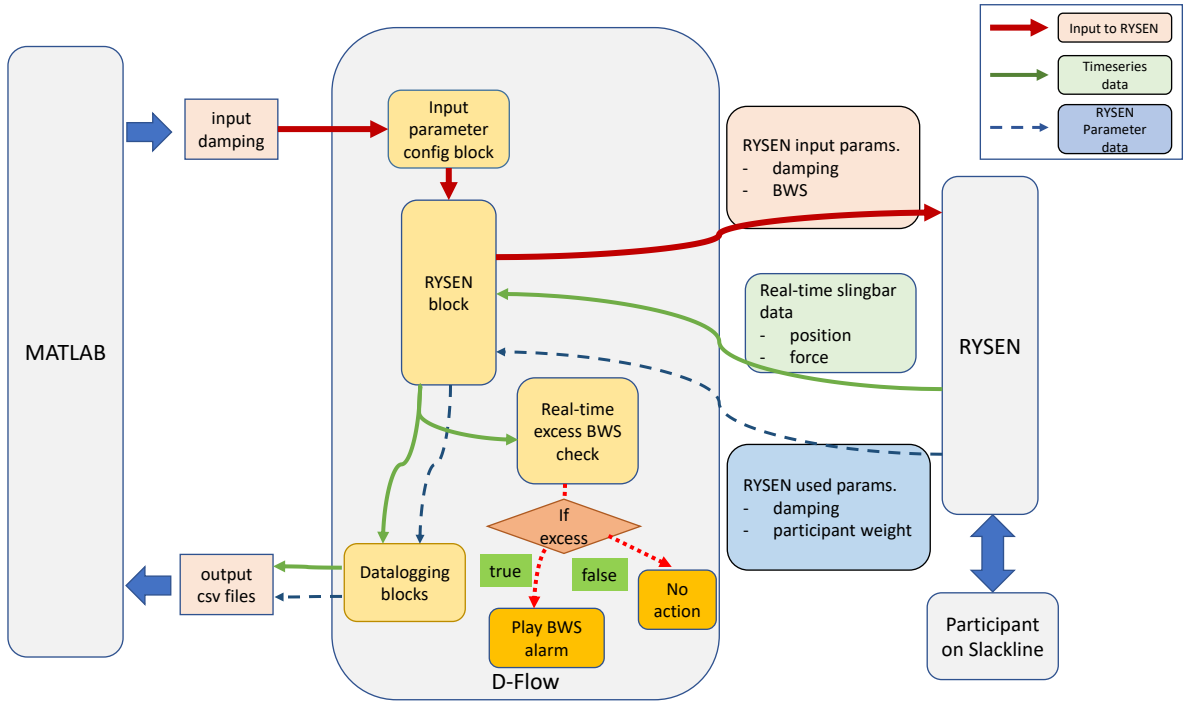

Figure 2.2: Real-time D-Flow workflow during each trial. MATLAB scripts are used to set the lateral damping parameters in the RYSEN via D-Flow before each trial. During the trial, position and force data from the RYSEN slingbar are processed and recorded in D-Flow, with a continuous check for excess BWS. At the end of the trial, the recorded data is saved, to be further processed by MATLAB scripts which then estimate the cost measure for the trial. The cost measure is used to set damping parameters for ensuing trials in the optimisation blocks of the experiment.

Estimation of Trial Outcomes

During each trial, slingbar position, orientation and force data were recorded as csv files via D-Flow, to be processed via MATLAB. The starting and ending of the recording were done manually by the experimenter. The position timeseries were used to determine the distance walked on the slackline, while the force timeseries were used to calculate lateral impulse timeseries as well as recheck for excessive bodyweight support. The distance walked and the maximum absolute value from the impulse timeseries were used to construct a cost measure for each trial. This cost measure was used as the basis for trial-by-trial tuning of the lateral damping provided by the RYSEN in the optimisation blocks of the experiment.

The timeseries data, recorded via D-Flow at a rate of roughly 300 Hz, were first filtered in MATLAB using a minimal-order low-pass IIR Butterworth filter, created using the *designfilt* function in MATLAB with the properties given in Table 2.1. Filtering was done to smoothen position timeseries data, which prevented the occurrence of sharp unrealistic peaks in velocity timeseries derived from them.

Table 2.1: Minimal order lowpass IIR filter applied (in MATLAB) on position and force data received from D-Flow.

Passband frequency (Hz)	10
Stopband frequency (Hz)	36
Passband ripple (dB)	1
Stopband attenuation (dB)	60

The start and stop of each trial recording was done manually via D-Flow, with the stopping done either after step-off, when the participant reached the end of the walkable distance, or when the excessive bodyweight support alarm was played. Thus, there was a risk of stopping the trial too late, with position and force values

during or after step-off influencing the cost measure. A possible example was the recording of a large lateral damping force during a voluntary step-off at the end of the walkable length. The lateral impulse caused by this should not be considered while estimating the trial cost.

To avoid this, the filtered timeseries data were then trimmed based on three separate checks:

1. **Excessive bodyweight support check:** As mentioned in the previous section, over-reliance on the bodyweight support could reduce the influence of lateral damping on the task performance. To avoid this, the bodyweight support applied on the participant at each instant was calculated in terms of the participant's weight using the vertical force timeseries data. With the set-point of the bodyweight support set to 11% of the participant's weight, the support was determined to be excessive if it exceeded 15% for a cumulative duration greater than 0.5 seconds. The check was applied for a cumulative duration per trial, e.g., if the support exceeded 15% for a duration of 100 ms early on in the trial and another 400 ms at a later instance, the support was determined as excessive. The end of the trial was trimmed to the instance at which the assistance became excessive (the end of this cumulative duration).

2. **Lateral position check:** The slackline was aligned to the centreline of the RYSEN, such that the lateral position of the slingbar should be close to zero when the person was on the slackline. The timeseries data were trimmed to the first and last time-steps during which the lateral position of the slingbar was within ±20 cm.

3. **Vertical velocity check:** To detect a step-off from the slackline, the timeseries data was trimmed to the last occurrence of a vertical velocity greater than 0.4 m/s in the downward direction. The vertical velocity timeseries was estimated from the filtered vertical position timeseries using the first-order divided difference and approximating each time-step to be 1/300 s.

Once the data was filtered and trimmed, the distance walked during the trial was computed as the magnitude of the difference between the maximum and the minimum values of the slingbar position in the walking direction. The impulse timeseries was computed from the lateral force timeseries in the following manner,

$$I(k) = I(k-1) + F_{\mathrm{y}}(k-1)(t(k) - t(k-1)) \tag{2.1}$$

where $I(k)$ is the impulse, $F_{\mathrm{y}}(k)$ is the force component lateral to the walking direction, and $t(k)$ is the time at the k^{th} step. The maximum absolute impulse value from this timeseries I_{m} was used as the impulse outcome measure.

$$I_{\mathrm{m}} = \max(|I(k)|) \tag{2.2}$$

The distance travelled by the slingbar along the length of the slackline during the trial was used as the distance measure L in the trial. It is computed as

$$L = \max(\boldsymbol{p}_{\mathrm{x}}) - \min(\boldsymbol{p}_{\mathrm{x}}), \tag{2.3}$$

where $\boldsymbol{p}_{\mathrm{x}}$ is the timeseries of the x-component of the slingbar position. The distance and impulse measures were used to determine cost measures for each trial, which are explained in the following section.

The distance, mediolateral impulse and BWS timeseries plots are shown for two example plots in Fig. 2.3. The timeseries data in both trials were trimmed based on the excessive use of BWS, with the cumulative duration of excess BWS exceeding 0.5 seconds.

Cost Function Structure

The distance component of the cost was set as a linear function of the form,

$$C_{\mathrm{dist}} = 10\left(1 - \frac{L}{L_{\mathrm{lim}}}\right), \tag{2.4}$$

where L is the distance walked by the participant before step-off, and L_{lim} is the maximum walkable distance for the experiment, which is 5.5 m. The range of C_{dist} is $[0, 10]$, with 10 corresponding to a distance of 0 m and 0 corresponding to L_{lim}. A linear function was chosen to avoid differences in behaviour of the cost function at different distance measures.

The maximum magnitude in the lateral impulse timeseries I_{m} was identified and used to compute the following cost.

$$C_{\mathrm{imp}} = \mathrm{e}^{\frac{I_{\mathrm{m}}}{I_{\mathrm{lim}}}}, \tag{2.5}$$

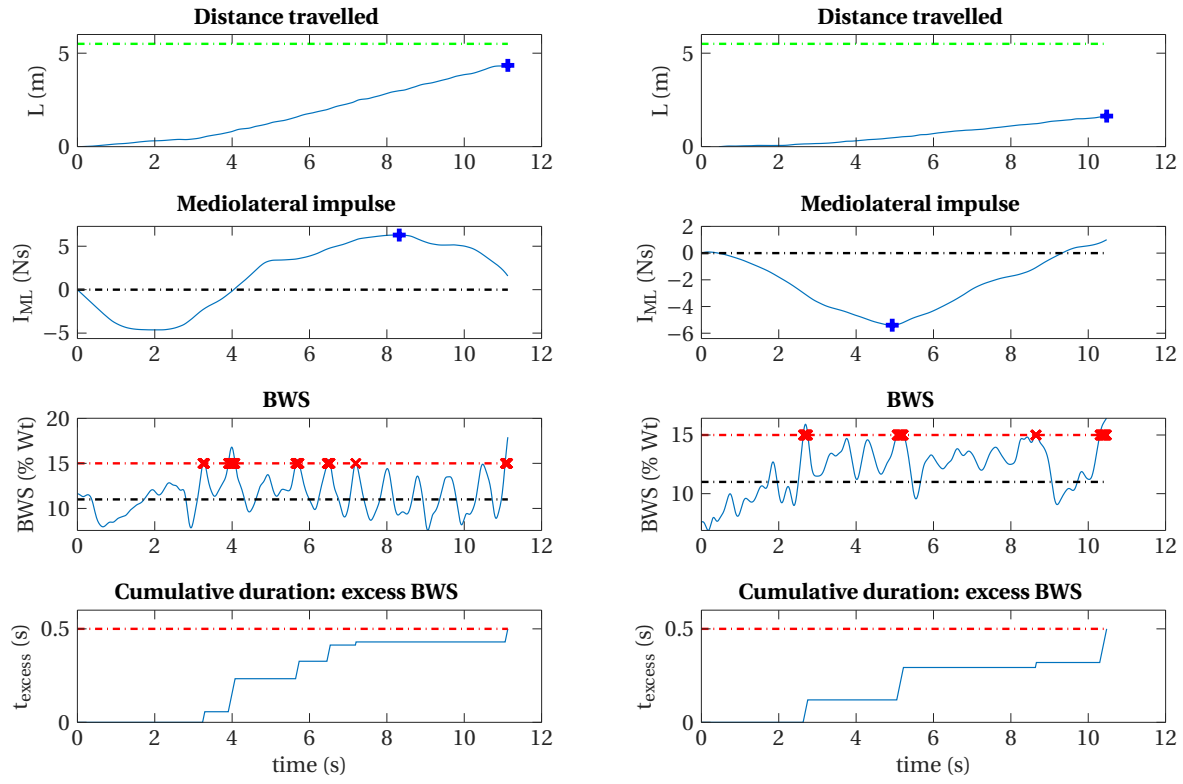

(a) (b)

Figure 2.3: Distance travelled along the slingbar, mediolateral impulse, BWS, and cumulative excess BWS duration plotted with respect to time for two separate trials. In the distance subplots, the maximum walkable distance is shown by the dashed line. The distance and maximum impulse measures are marked in the respective subplots by the blue '+' markers. In the BWS timeseries plots, the reference BWS level is indicated by the black dashed line and the allowable excess BWS threshold is indicated by the red dashed line. The periods of excessive support are indicated by the red 'x' markers. The maximum allowed cumulative duration of excess support, 0.5 seconds, is shown by the red dashed line in the duration subplots.

.

where I_{lim} is an impulse 'limit' that has been arbitrarily set to 5 Ns for the experiments, such that when I_{m} is greater than this value, the impulse cost rises rapidly. This cost term was set as an exponential function to set a soft constraint on the assistance provided: the RYSEN can apply lateral impulses greater than I_{lim}, but the resulting exponential increase in costs should cause the search strategy to avoid the associated damping value in subsequent iterations. The range of C_{imp} is $[1,\infty)$. The lateral assistance could have been quantified in terms of other variables such as an average of the lateral forces, or a power measure. It was decided to place a soft constraint on the maximum lateral impulse during a trial to emulate the limitation on the maximum impulse that a single CMG could impart before it enters singularity. Two things should be noted here however: (i) the RYSEN applies forces on the participant, whereas a CMG would apply torques, hence the impulses are different quantities, (ii) no physical limitation is actually applied on the impulse imparted by the RYSEN.

The total cost associated to a trial is therefore the sum of Eq. (2.4) and Eq. (2.5),

$$C = 10\left(1 - \frac{L}{5.5}\right) + \mathrm{e}^{\frac{I_{\text{m}}}{5}}. \tag{2.6}$$

Optimisation Method

The CMAES algorithm, developed by Hansen et al. [29], was to be used to search for the optimal damping parameter for each participant. CMAES is an evolutionary optimisation strategy which attempts to find the minimum of a cost function by randomly sampling candidate parameters from a (multivariate) normal distribution and updating the mean of the distribution, the orientation of its principal axes, and its overall scale over multiple generations. The mean of the distribution at each generation is the algorithm estimate of the minimum in that generation. In addition to adapting the mean over every generation based on the best

evaluated points, the algorithm independently varies the size and shape of the distribution over successive generations by adapting the overall standard deviation $\sigma^{(g)}$ and the covariance matrix $\boldsymbol{C}^{(g)}$ of the distribution over each generation g. As an example, the update of the distribution mean over successive generations of a 1-D implementation of the CMAES– used to find the minimum of a quadratic function– is shown in Fig. 2.4.

The algorithm is said to be robust to measurement noise and time-variance in the cost landscape, because it doesn't use the cost measurements directly, but instead estimates the distribution parameters for the next generation based on the ranking of the evaluated search points in each generation [30]. CMAES was successfully implemented in a four-dimensional human-in-the-loop optimisation problem [22], working well in black-box optimisation involving a time-varying system. Thus, even if there is a temporal shift in the cost map during a particular generation, for example due to fatigue or due to resumption of trials after an extended break (in the context of the experiment), the algorithm should work well as long as all the trials in the generation are similarly affected.

For the current study, a basic implementation of the algorithm was used, based on [29]. Each optimisation run consisted of 7 generations with 5 candidate parameters per generation. Each candidate damping parameter is implemented in a trial, and the corresponding cost measure is used to determine its fitness. The implemented workflow of the algorithm for each generation is listed below.

1. Generation of candidate parameters (damping values) from a normal distribution with a specified mean and standard deviation. Candidates generated outside the search space $[0,75]$ NS/m were reset to the boundary values.

2. Estimation of cost measures (fitness) of each candidate parameter. In the experimental implementation, the cost measures were calculated from the timeseries data obtained for each trial via D-Flow.

3. Ranking of candidate parameters based on order of increasing cost measure. The best μ candidates ($\mu = 3$ in the experimental implementation) with the lowest cost measures were identified as parents for the next generation.

4. Computation of the distribution mean of the next generation. The weighted average of the parent candidates was used as the mean for the next generation. The parent candidates were weighed in the decreasing order of their ranking, with the highest weight assigned to the candidate with lowest cost. *The weights do not depend on the values of the cost measures themselves, but only upon their ranking.*

5. Update of the distribution covariance matrix. The covariance matrix was updated based on the rank-1 and rank-μ updates (see Appendix A).

6. Step-size adaptation. Step-size adaptation in each generation is based on the displacement of the distibution mean over successive generations, encoded as an evolutionary path variable (see Appendix A).

Further details on the algorithm, selected hyperparameters and relevant code segments are given in Appendix A.

Being the first study involving balance assistance optimisation on a slackline, the decision to tune a single parameter was made to avoid the possibility of redundancy with multiple solutions, and to clearly identify the effect of a single assistance parameter (in this case, damping) on performance. This makes the covariance matrix update redundant– in a one-dimensional search, the algorithm only has to control the step-size of the distribution. Although the main strength of CMAES is handling parameter spaces with high dimensionality, it is nevertheless a method applicable for a parameter space with a single dimension.

A summary of the in-experiment data processing via MATLAB is shown in Fig. 2.5.

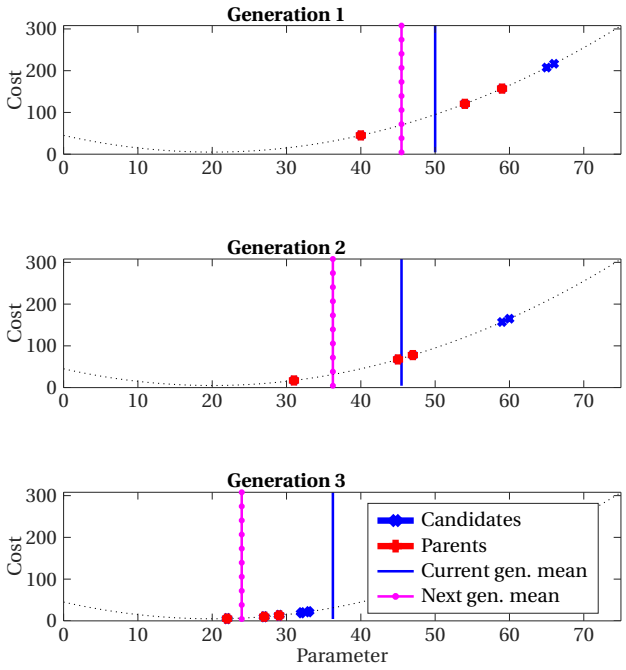

Figure 2.4: Example plots showing the working of the CMAES algorithm over three successive generations in a 1-D optimisation problem. The underlying cost function whose minimum is to be found, is plotted in dotted lines. Five candidate parameters are evaluated in every generation. The centre of the distribution in each generation is the weighted mean of the best three candidates of the previous generation. The step-size of the distribution is also adjusted in in each generation based on path followed by the distribution mean in the previous generations (see Appendix A for further information).

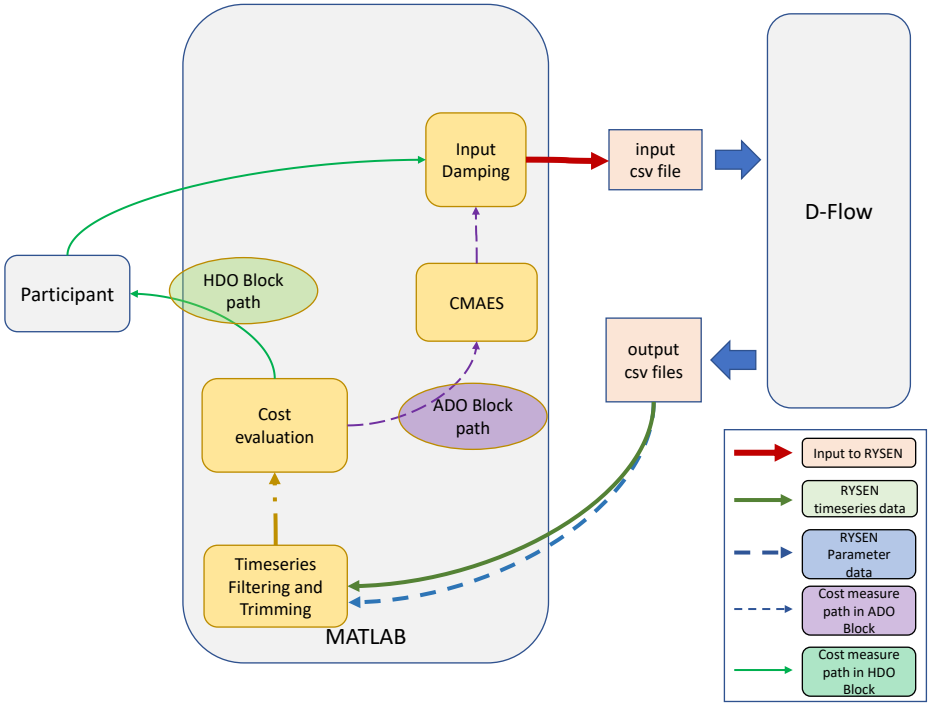

Figure 2.5: Online data-processing (in between trials) via MATLAB. The cost measure pathways are only shown for the two optimisation blocks (Algorithm Driven Optimisation block and Human Driven Optimisation block, explained further ahead in Section 2.2.3) in the experiment, where the damping values in the ensuing trials are dependent on cost measures of the previous trials.

2.2. Experiment Procedure

2.2.1. Participant Selection

A sample size of 16 was set for the study. Assuming a normal distribution of outcome measures in the sample set, an a-priori sample size estimation was done using GPower [31] for a repeated measures ANOVA analysis, considering the comparison of individual task performance for three conditions: without any lateral damping, with the damping parameter obtained with the optimisation algorithm, and with the damping parameter finalised by the participant. Meanwhile, the participant was assumed to perform with a reasonable consistency when repeating measurements with the same impedance parameters (keeping a correlation estimate of 0.8 between repeated measurements).

These experiment parameters were set to allow the identification of an expected medium effect size ($f = 0.25$), with a probability of incorrect rejection of null hypothesis, $\alpha = 0.05$ and probability of incorrect acceptance of null hypothesis, $\beta = 0.20$. The expected effect size is an assumption and not based on pilot data.

The experiments were conducted with 16 healthy participants [12 male, 4 female, age = 25 ± 1.6 years, height = 1.76 ± 0.08 m, weight = 71 ± 8 kg, (Mean $\pm$ Standard deviation)] who have no known history of sensorimotor impairment that might affect their balancing ability. Recent ankle or back injuries, or pregnancy were the remaining exclusion criteria. This study was conducted under the recommendations of the TU Delft Human Research Ethics Committee (approval letter 949). Informed consent was given by all subjects prior to participation. See participation criteria and consent form in Appendix G.

(a) (b) (c)

Figure 2.6: (a) Slackline used for the experiment, with the slackframe tripods at both ends. Exercise mats are placed below the walkable region. A foot stool is placed at the starting position, to reduce the initial difficulty of maintaining balance on the line. (b) Task requirement– walking on the slackline with short steps and arms folded. (c) Example of crouching on the slackline to maintain balance, which can lead to increased BWS.

2.2.2. Trial Activity

The experiment involved multiple trials of walking on the slackline from a fixed start position, with the RYSEN always providing BWS with or without mediolateral damping. A foot stool was placed under the start position to reduce the initial difficulty in stepping on the line. In order to maintain sufficient task difficulty throughout the experiment, participants were asked to walk on the line with short steps, and with their arms folded (see Fig. 2.6b). Each trial was started with the participant placing one foot on the slackline at the start position, and ended upon one of the following events:

1. Loss of balance resulting in a step-off.
2. Completion of the maximum walkable length– the walkable length of the slackline was 5.5 m, from the start position to location of the ratchet on the line. Participants were asked to step off the line before

stepping on the ratchet.

3. Excessive reliance on the vertical support of the RYSEN. As mentioned in the previous section, a real-time check was placed on the BWS to avoid excess vertical support. When BWS exceeded the allowable threshold beyond a cumulative duration, an alarm sound was played, at which point the participant could step off the slackline. Since the trial recording is stopped manually by the experimenter, an excess BWS check is also applied to the timeseries data exported to MATLAB, with the timeseries beyond the instance of excess support being trimmed. The main purpose of the real-time BWS check was to avoid unnecessary walking of the participants on the slackline beyond the instance of excess support. Fig. 2.6c shows an example of how participants could crouch while on the slackline to improve stability, which could possibly increase the BWS due to residual impedance in the vertical direction.

2.2.3. Experiment Blocks

Each experiment consisted of a single session by an individual participant. The participant did multiple trials of walking on the slackline, all of which involved some form of assistance from the RYSEN. The RYSEN applied BWS (11% of the participant's weight) in all the conditions.

The experiment could be divided into six blocks, as shown in Fig. 2.7:

1. Initial training block– In order to remove initial learning effects and to allow the participant to explore suitable balancing strategies, 25-27 trials were conducted with the RYSEN providing BWS. All the trials were with Zero Damping (ZD) in the mediolateral axis. In the first 10-12 trials, the participant was allowed to use their arms to maintain balance. For the remaining 15 trials, the participant was asked to keep their arms folded and to take short steps. The participants were especially asked to identify a preferred starting foot and learn to balance without relying excessively on the BWS.

2. Baseline Evaluation (BE) block– The participant did 5 ZD trials to evaluate an initial baseline performance level.

3. Algorithm Driven Optimisation (ADO) block– In this block, the CMAES algorithm was used to find an optimal lateral damping parameter that minimises the cost score of the participant, in the range of $0-75\,\mathrm{Ns/m}$. This block consisted of 35 trials for each participant, with the algorithm returning an estimate of the optimal damping value, D_a, to be evaluated in a later block.

4. Human Driven Optimisation (HDO) block– Here, the participant was asked to optimise the cost measure themselves by searching for the optimal damping value over successive trials. The cost score was explained to decrease with a greater distance walked on the line, and increase exponentially with higher lateral impulses applied by the RYSEN. Each trial in this block was with a damping value of the participant's choice, and the same damping value could be resampled multiple times. At the end of each trial, the participant could view their cost history in the form of a cost-damping plot, showing the previously selected damping values and the associated costs. The participant had up to 35 trials to identify a suitable damping assistance, but they could stop early if they were satisfied with a particular damping value. The last sampled damping value was used as the solution of this block (D_h).

5. Condition Comparison (CC) block– In this block, performances of the D_a and D_h damping values were compared with the ZD condition by having the participant do 5 trials with each condition in a randomised order. The randomisation order, implemented using the randperm function in MATLAB, was set differently for each each participant, to remove any effects of trial order.

6. Grid Search (GS) block– Here, a parameter cost grid was constructed for the participant by conducting trials with damping values uniformly sampled from the search range in a randomised order. For the first 6 participants (F1-F6), 16 search points (parameter values in intervals of 5 Ns/m) were sampled with one trial per parameter, but due the high variability in cost measurements observed in the trials for the same parameter result (non-consecutive repetition), each parameter was sampled thrice for the remaining 10 participants (F7-F16), with fewer search points (11 points in 10 percent intervals of the search range). This was done to use the median cost measures at each grid point, reducing the effect of outlier trials.

The blocks were conducted as per the above order, except for the ADO and HDO blocks, whose order was randomised to remove systematic effects of condition order, such as learning or fatigue. Breaks were provided in between the experimental blocks, or after every 15-20 trials, to avoid participant fatigue. After each break, the block trials were preceded by one or two unrecorded ZD trials to refamiliarise the participant to the task. Fig. 2.7 shows the summarised experiment procedure with the 6 experimental blocks.

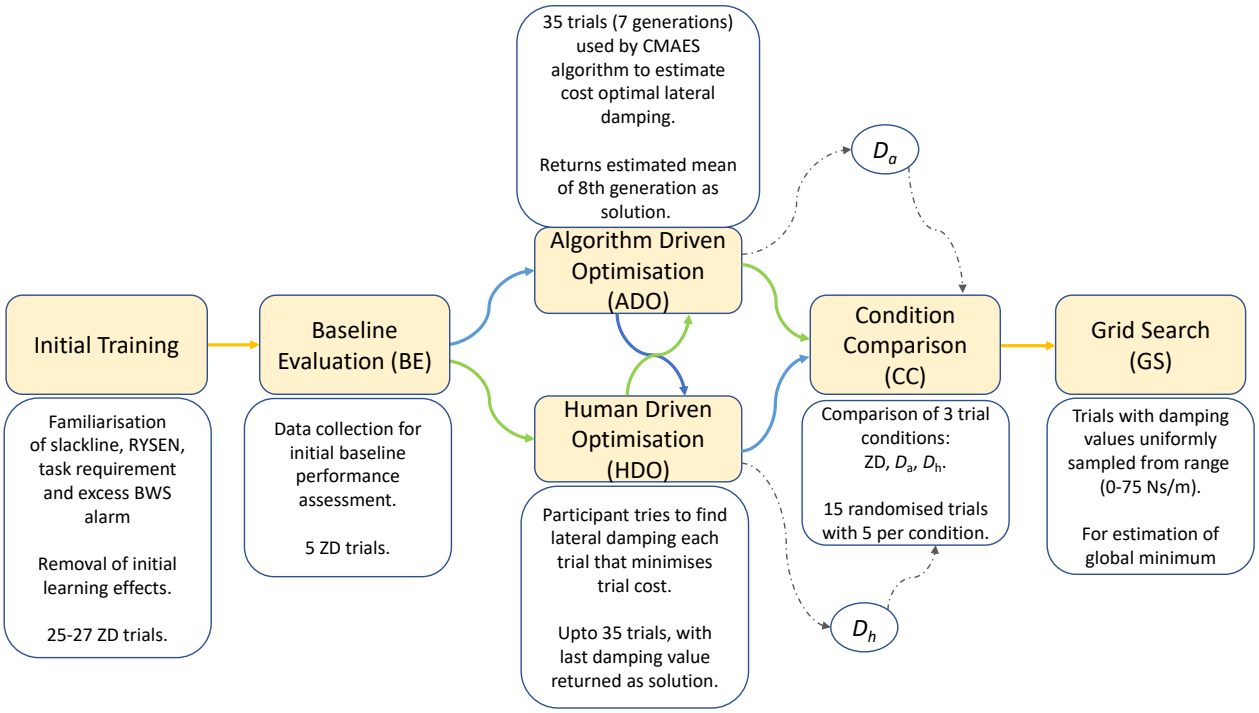

Figure 2.7: Summarised experiment procedure. The green and blue arrows show the two alternative experiment block orders.

2.3. Data Analysis

2.3.1. Final Included Set

The results of one participant (F16) were not considered for analysis due to insufficient motivation observed in the trials, with the participant showing no effort to maintain balance and relying entirely on the system. For the generation of cost grids and the analysis of secondary outcome measures, GS block results of participants F1-F6 were not included, as each grid point was sampled only once, leading to unreliability from outlier trials. Thus, the results of 15 participants were included in the final analysis, 9 of which had usable GS trial results.

2.3.2. Primary Outcome Measures

The distance walked on the slackline and the maximum lateral impulse generated in each trial, along with the associated cost, were the experimental outcome measures used to analyse each research question and the hypothesis.

Research questions **RQ1** and **RQ2** focus on the suitability of the distance and impulse measures to be used as indicators of task performance and device assistance respectively. The stochastic variability in these measures were analysed to partly address these questions. The variability of the cost, the distance and the impulse measure for each participant, was quantified as the Inter-Quartile Range (IQR, difference between the 25^{th} and 75^{th} percentiles) of the measure for each damping condition. The IQR was used here because of its relative robustness to outliers for small sample sizes (five trials per condition per participant), when compared to the standard deviation. No statistical comparison is done on the variability across the conditions.

To evaluate the long-term shift in the outcome measures over 50-70 trials, the measures from the ZD

trials of the BE (pre-optimisation trials) and the CC (post-optimisation trials) blocks were compared. For each participant, the median cost measure and the associated distance and impulse measures from each condition were used in the comparison.

The results of the GS block trials of participants F7-F15 were used to study the shape of the cost landscape, as well as the dependence of the distance and the impulse measures on lateral damping for each participant. For each participant, the median cost measure at each damping parameter in the grid was used as the representative measure for the grid point, along with the distance and impulse measures associated to the median cost trial.

Research questions **RQ3** and **RQ4** ask about the existence of an optimal trade-off between task performance maximisation and device assistance minimisation, achievable at one or more damping parameter values. To test the related hypothesis that participants would return significantly lower costs in trials with the estimated optimal damping assistance than in ZD trials, a comparison was made between the costs associated to ZD trials and trials with damping values returned by the algorithm and the participant. For this, the median cost trials of each participant, for the D_a, D_h and ZD conditions from the CC block were used.

To evaluate the performance of the algorithm in the experiment, the minimum costs of the first generation of the ADO blocks were compared to the minimum costs of the last (7^{th}) generation. A comparison of the minimum costs was made because, with each generation, the algorithm shifts the mean of the estimated distribution closest to the parent candidate with lowest cost (by computing the weighted mean of the parameters with the lowest three costs of the generation). A significant reduction in minimum costs over generations could imply that the algorithm has managed to improve its estimate of the optimal damping parameter over the initial guess, assuming time-invariance in the participant's skill level and fatigue. To quantify the exploration of the search space, the range of sampled damping values, as well as the range covered by the distribution means over all the generations, was determined for each ADO block implementation. The final step-sizes of the algorithm were also listed for each ADO block implementation.

The ADO and HDO block solutions were also compared to the global minima from the GS results of F7-F15. The median costs of the trials associated to the ZD condition (implemented in the GS block), the nearest grid points to D_a and D_h– $\hat{D}_a$ and $\hat{D}_h$, and the the grid point with the lowest median trial cost D_{gmin}, were used in this analysis.

To quantify the explorative behaviour of participants in the HDO trials, an Initial Search Range (ISR) and Overall Search Range (OSR) were computed for each participant. The ISR was the the range of damping values sampled in the first five trials of the HDO block, where the participant did not have sufficient prior information on the cost landscape. The OSR was the range of damping values sampled over the entire set of HDO trials. To understand the exploitative component of the search strategies and the tendency to improve confidence in the cost estimates, the frequency of resampling previously evaluated damping parameters was analysed, quantified as the average resampling frequency and the average consecutive resampling frequency and computed for each participant.

2.3.3. Secondary Measures

To get further insight on the effect of different damping values on balance stability on the slackline, the following secondary trial outcome measures were analysed using the GS block results of participants F7-F15– RMS of mediolateral slingbar velocity (v_{ML}), mean anteroposterior velocity (v_{AP}), RMS of mediolateral slingbar force (F_{ML}), RMS of anteroposterior slingbar force (F_{AP}), and mean BWS.

During a step-off from the slackline, a sudden increase in the lateral and vertical components of slingbar forces and velocities can be expected. The in-experiment automated trimming may not sufficiently remove the step-off phase from all trials. To avoid the potential influence of step-offs, an additional 0.5 seconds was trimmed from the ends of the trials before the computation of the secondary outcome measures.

The shifts in secondary outcome measures that could indicate participant stability and reliance on the RYSEN– RMS v_{ML}, mean v_{AP}, and mean BWS– over 50-70 trials, was studied by comparing these measures from the ZD trials of the BE (pre-optimisation trials) and CC (post-optimisation trials) blocks.

2.3.4. Post-hoc Simulated Optimisation

Motivation

Research questions **RQ3** and **RQ4** ask whether an optimal trade-off exists between task performance and device assistance, and whether the selected algorithm is capable of finding this optimal setting. To further explore these questions, alternative cost functions and algorithm settings were compared in a post-hoc anal-

ysis. First, the effect of changing different hyperparameters on algorithm performance was analysed. Next, an alternative cost function was used to compare algorithm performance in finding the optimal trade-off upon a reweighing of the distance and impulse cost components. Finally, the performance of the CMAES algorithm is compared to the Bayesian optimisation algorithm in finding the optimal trade-off.

Cost Map Construction

In order to recreate the stochastic nature of experimental human-in-the-loop optimisation, noisy cost grids were created for the simulations, using the distance and impulse grids for a single participant. Since the GS blocks for F7-F15 evaluated each grid point thrice, the variability in the distance and impulse measures could be estimated for individual participants using this data. A uniform variability was assumed throughout the grid, with standard deviations for the distance and impulse measures of the participant computed by averaging the standard deviations of these measures at each grid point. The median distance and impulse measures at each evaluated grid point were meanwhile interpolated to obtain estimated measures for the unevaluated damping values, with a resolution of 1 Ns/m. These median grids were used as the mean function values in normal distribution models for the distance and impulse measures with corresponding standard deviations. For each damping input, these models could then be sampled from to simulate the variability in the experimental cost measure.

Evaluation Metrics

To account for the stochastic parameter sampling nature of the algorithms, comparisons were made between optimisation sets consisting of 100 optimisation runs, with each optimisation run being an independent search for the minimum cost, with the same algorithm settings and initial guess.

The damping values at the global minimum (D_{gmin}) and maximum (D_{gmax}) of each cost map were defined as the damping values with the lowest and highest mean costs respectively. These values and their respective mean costs were used to determine the success rates of the algorithm over the total number of optimisation runs N_{r}, for a given cost function and set of algorithm hyperparameters.

To determine convergence rates to the global minimum, histograms showing the relative proportion of solutions at different regions were plotted for a set of optimisation runs, and the RMS of the differences between solution values D_{a}^{i} and D_{gmin} was computed as,

$$\text{RMS}(\Delta D) = \frac{1}{N_{\text{r}}}\sqrt{\Sigma_{i}^{N_{\text{r}}}(D_{\text{a}}^{i} - D_{\text{gmin}})^2}, \tag{2.7}$$

where D_{a}^{i} is the optimal damping estimate returned in the i^{th} optimisation run. To determine the rate of achieving costs close to $C(D_{\text{gmin}})$, a relative cost metric ΔC_{r} was computed for each run, and plotted in a histogram. ΔC_{r} was defined as the difference between the mean cost associated to the returned solution D_{a} and the global minimum as a fraction of the difference between the global maximum and minimum costs,

$$\Delta C_{\text{r}} = \frac{C(D_{\text{a}}) - C(D_{\text{gmin}})}{C(D_{\text{gmax}}) - C(D_{\text{gmin}})}, \tag{2.8}$$

to account for the different shapes of the cost maps that were tested. Finally, the mean value of the relative cost was computed for each optimisation set.

$$\text{mean}(\Delta C_{\text{r}}) = \frac{1}{N_{\text{r}}}(\Sigma_{i}^{N_{\text{r}}}\Delta C_{\text{r}}^{i}). \tag{2.9}$$

Effect of Algorithm Parameters

To analyse the effect of varying algorithm parameters, $N_{\text{r}} = 100$ optimisation runs each were simulated for 4 sets of CMAES hyperparameters, as given in Table 2.2. Set I consisted of the experiment-implemented cost function and hyperparameters. The default population size $\lambda = 5$ was set based on empirical formula for population size (see Appendix A), and the number of generations was set accordingly to $N_{\text{g}} = 7$ to have a total trial budget of 35. Set II was used to study the effect of increase in initial step size, while sets III and IV were used to check the effect of increasing the number of trial generations while keeping the same population size.

Effect of Reshaping the Cost Function

To analyse the effect of restructuring the cost function, the default cost function is compared with the following alternative:

Table 2.2: CMAES hyperparameter sets used in the optimisation simulations, in addition to the mean value used to generate the first generation, D_0

Set	D_0 (Ns/m)	σ_0 (Ns/m)	λ	N_g
I	5	15	5	7
II	5	30	5	7
III	5	30	8	6
IV	5	30	8	12

Quadratic distance cost component: To avoid low costs being associated to trials with very low distances walked, while maintaining a sufficient weight to assistance cost component, a quadratic distance cost could be used, such as:

$$C = \left(10\left(1 - \frac{L}{5.5}\right)\right)^2 + \mathrm{e}^{\frac{I_{\max}}{5}}. \tag{2.10}$$

Using a quadratic distance cost component, trials with a low distance walked could have a high cost.

The alternative option is evaluated using CMAES parameter Sets I and III from Table 2.2.

Comparison with Bayesian Optimisation
Bayesian Optimisation had not been considered for the experimental implementation, due to its potential performance limitation with time-varying cost measures. However, if considering a limited number of trials, temporal shifts in task performance, due to fatigue or learning, could be kept to a minimum. Using the *bayesopt* function in MATLAB with default hyperparameter settings (see Table 2.3), the algorithm was tested for 100 runs each on the default cost function and the quadratic cost function, with a budget of 30 trials per optimisation run.

Table 2.3: Algorithm control parameter options influencing the search strategy of the *bayesopt* function.

Option	Explanation	Default Parameter
'AcquisitionFunctionName'	Name of the acquisition Function used to select each subsequently sampled point	'expected-improvement-per-second-plus'
'ExplorationRatio'	Exploration tendency in algorithm	0.5
'GPActiveSetSize'	Number of evaluated points used to construct Gaussian Process model, to which subsequent evaluations are fit.	300

2.4. Statistical Analysis

All statistical tests in this study were conducted for a significance level $\alpha = 0.05$, with the Bonferroni correction used when applicable. To evaluate the original hypothesis, a comparison was to be made between the cost measures of the ZD, D_a and D_h conditions from the set F1-F15. The sample set for each condition was tested for normality using the Shapiro-Wilks test, implemented with the *swtest* function (MATLAB, File Exchange). The tests showed that the sample sets significantly deviated from the normal distribution model. Thus, non-parametric tests were used for evaluating the hypothesis. First, a test for significant difference among the three conditions was done using Friedman's ANOVA method. If a statistical difference was found, Wilcoxon signed-rank tests were conducted between each condition pair. The same procedure was followed in the comparison of the associated distance and impulse measures.

The comparison of the ADO and HDO block solutions with the global minima and the ZD conditions in the GS block was also done with the Friedman's ANOVA method, followed by pairwise Wilcoxon signed-rank tests.

The comparison of the minimum costs of the first and last generations of the ADO block trials, as well as the comparison of all outcome measures for the pre- and post-optimisation ZD trials were done with Wilcoxon signed-rank tests.

3
Results

3.1. Primary Outcome Measures

3.1.1. Optimality of Solutions

Hypothesis Test

A comparison was made between median trial costs of the ZD, D_a and D_h conditions from the CC block, after removing between-subjects differences by computing costs relative to the ZD trial costs. No significant differences were found among the three conditions ($p = 0.2466$) using Friedman's ANVOA, for $\alpha = 0.05$. However, as seen in Fig. 3.1a, D_a and D_h conditions have lower median costs.

Looking at the cost components of the median cost trials– the distance walked and the maximum lateral impulse terms, once again relative to the ZD condition– a significant difference was found among the 3 conditions for the distance measures ($p = 0.002$), but not for the impulse measures ($p = 0.34$) (refer Figs. 3.1b and 3.1c). Using pairwise Wilcoxon signed-rank tests and with Bonferroni-corrected significance level for three comparisons, $\alpha = 0.016$, the median distances walked in the D_a and D_h conditions were found to be significantly greater than in the ZD condition ($p = 0.003$ and $p = 0.005$ respectively), but no significant difference was found between D_a and D_h ($p = 0.61$).

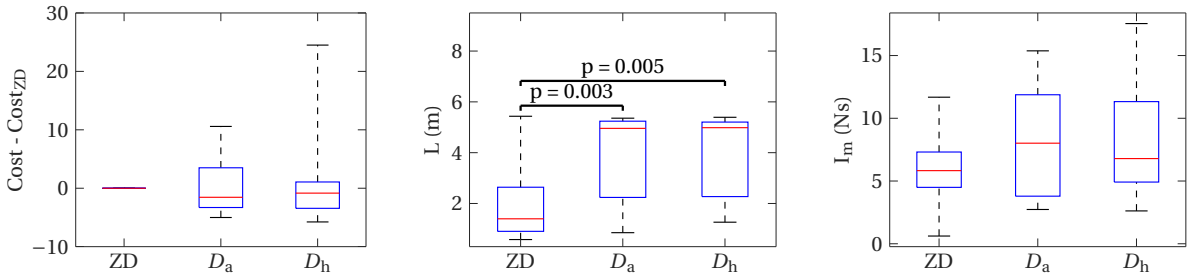

Figure 3.1: Comparison of (a) median trial costs and corresponding (b) distance and (c) impulse measures for ZD, D_a, and D_h conditions for all participants. While significant difference is not observed due to high variability in the D_a and D_h solutions, the median cost in these conditions are slightly lower than in the ZD condition.

Comparison with Global Minima

To compare the cost measures obtained for the D_a and the D_h with the global optimum parameter found in the GS blocks, the GS block results for the set F7-F15 ($n = 9$) were checked. In this analysis, the median trial costs of the grid points that were closest to the D_a and D_h values ($\hat{D}_a$ and $\hat{D}_h$) were compared to the global minima D_{gmin}, along with ZD condition in the grid search. A significant difference was observed among the 4 conditions in the cost measures ($p = 3.4 \times 10^{-5}$), all differences being with the global minima (refer Fig. 3.2).

3.1.2. Suitability of Cost Component Measures

Short-term Variability

The variability in cost, distance, and impulse measures are defined for each participant from the CC block trials, using the Inter-Quartile Range (IQR) for the trials corresponding to ZD, D_a and D_h conditions. The observed IQR values for each measure are shown in the boxplots in Figs. 3.3a to 3.3c. Large between-subjects differences can be seen in the cost variability for the optimal damping conditions. The median IQR in the distance walked is 2 m for the ZD trials and around 1 m for the optimal damping trials. The impulse measures

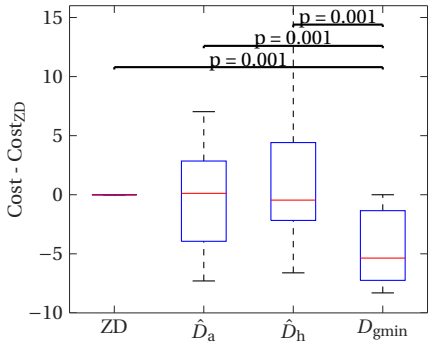

Figure 3.2: Comparison of median trial costs for ZD, nearest neighbours of D_a and D_h, and the GS global minima for participants F7-F15. The pairwise comparisons, made for the Bonferroni-corrected significance level $\alpha = 0.05/6$, showed significant differences between the global minima and the other three conditions.

have a median IQR of 2 Ns for the ZD trials and 3 – 5 Ns for the optimal damping trials. The differences in the impulse IQR across participants is noticeably larger for the optimal damping trials.

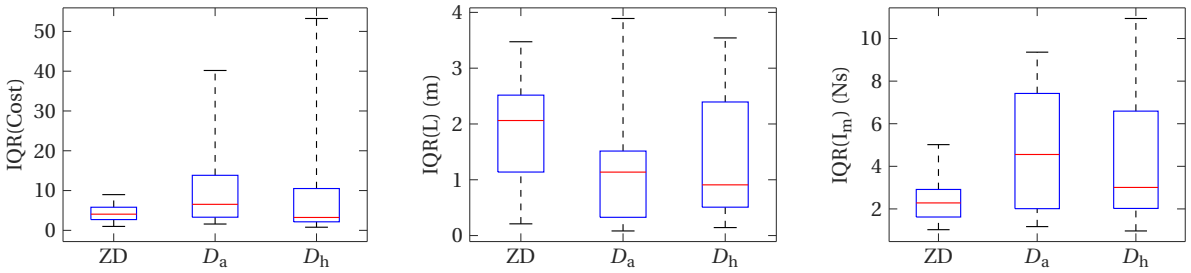

Figure 3.3: Inter-quartile ranges observed in (a) cost, (b) distance and (c) impulse measures for ZD, D_a, and D_h conditions for all participants.

Long-term Drift

Fig. 3.4 shows the box-plots comparing median costs and the corresponding distance and impulse measures for the ZD trials in the BE and CC blocks of all participants in F1-F15. No significant differences were observed on the cost ($p = 0.44$), distance ($p = 0.20$) or impulse measures ($p = 0.44$). Looking at individual shifts in baselines, 9 out 15 participants had lowered their median trial costs; 7 out of 15 participants had increased their median distance walked by at least 0.1 m, while only 4 decreased their median distance walked by at least 0.1 m.

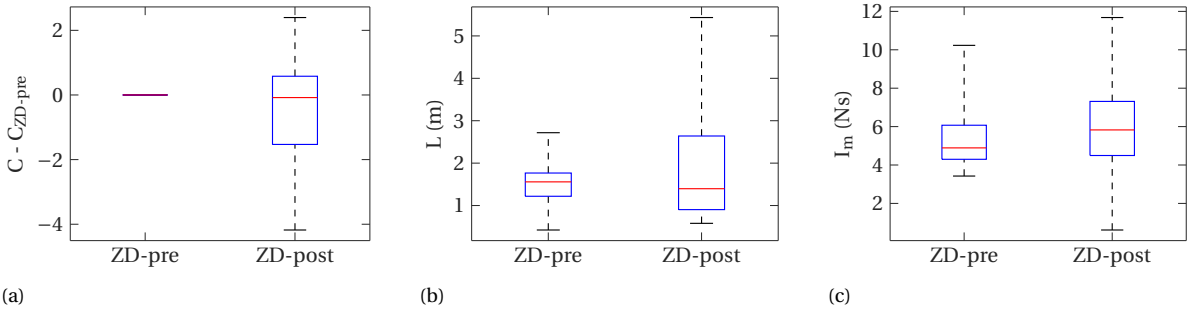

Figure 3.4: Comparison of cost measures for ZD trials conducted in the baseline evaluation and the condition comparison blocks for F1-F15 ($n = 15$): (a) Median trial costs, (b) Corresponding distance measures, (c) Corresponding impulse measures.

Effect of Damping

The effect of damping on the overall shape of the cost-map, as well as the distance and impulse measures are plotted based on the GS trial results for F7-F15. The damping values are expressed as percentages of the maximum damping value (75 Ns/m). The median cost measures from all participants are plotted in Fig. 3.5. Using the distance and impulse measures corresponding to each participant's median grid cost, respective grids are plotted in Fig. 3.6a and Fig. 3.6b. The median distance measure shows a sudden increase from 2 to 5 m with an increase in damping from 20 to 30% of the maximum. Thus, at least half the participants were capable of walking nearly the maximum distance at 30 % of maximum damping. The impulse damping plot shows a small but steady increase in the median impulse measure upon an increase in damping, with the median value increasing from about 7 Ns/m at zero damping to about 9 Ns/m at 90% maximum damping. The median impulse and distance measures both show a sudden decrease at the maximum damping value. Individual distance- and impulse-damping plots for participants F7-F15 are given in Appendix C.

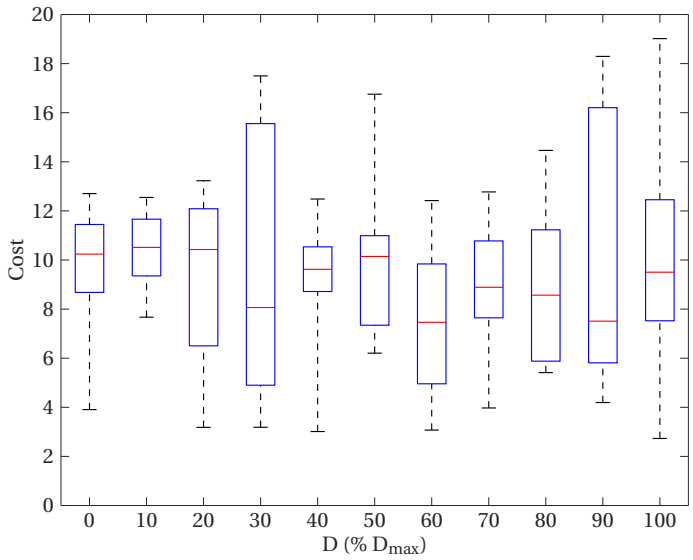

Figure 3.5: Boxplots showing the range of the participant costs at each grid point, based on GS trials for F7-F15. The damping values are expressed as a percentage of the maximum possible damping. The overall median cost does not follow a clear trend with the damping.

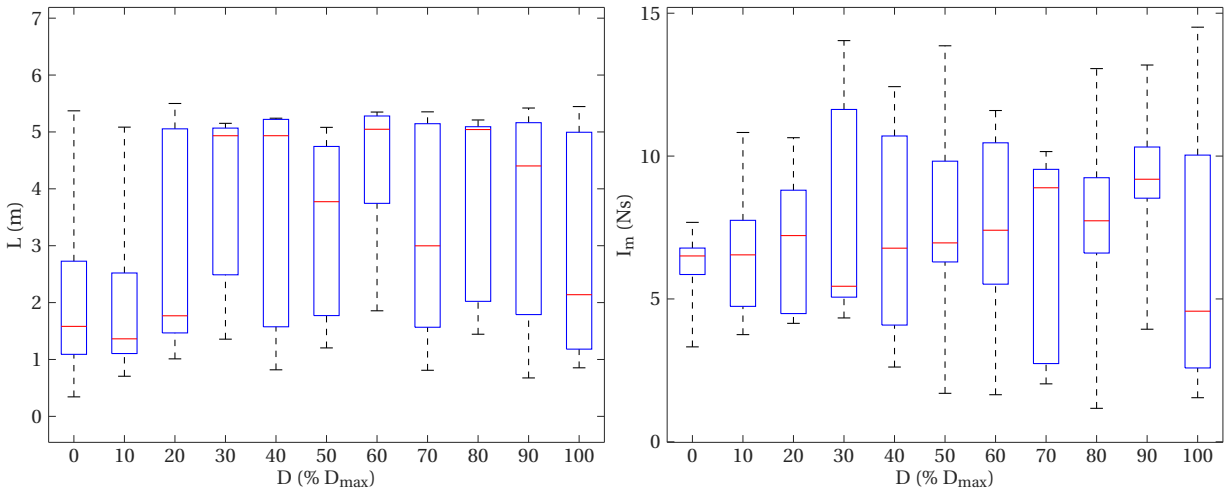

(a) (b)

Figure 3.6: Boxplots showing (a) distance walked by each participant vs damping, and (b) the maximum lateral impulse vs damping, for F7-F15.

3.1.3. Performance of CMAES Algorithm

To check the performance of the CMAES algorithm in reducing trial costs, a comparison was made between the minimum costs of the first and last generations for each participant in F1-F15. No significant difference was found between the cost measures of the first and last generation ($p = 0.5$). Fig. 3.7a shows the minimum costs of each generation in the ADO blocks of all the participants, measured relative to the first generation. Interestingly, the cost measures show a decreasing trend from the first generation, until an increase from the sixth to the seventh generation.

Table 3.1 shows the results of each ADO block in F1-F15. D_{start} is the mean of the distribution used to generate the first generation, which has been randomly set for each participant. In addition to the returned solution values D_{a}, the range of the sampled damping values, the range of the generation means, the step size for the final generation σ_{f}, and the median cost difference between the D_{a} and ZD CC block trials are also listed. The D_{a} values are distributed throughout the overall damping range, and the algorithm has sampled more than 50% of the damping range in all implementations except for F8, which has the lowest sample range of 26. The range of the distribution means, which is the net displacement of the estimated optimum over all the generations, has a low median value of 17.4, indicating that the shifts in the algorithm distribution over successive generations were generally low. Fig. 3.7b shows the trajectories of the distribution means over generations for the ADO block implementations. The means of the eighth generation, which are the algorithm-returned D_{a} values, are often close to the initialised means of the first generation. The final step size, which encodes the displacement of the population means over successive generations and determines the range of the sampled values in the final generation, is larger than the initial step-size ($\sigma_0 = 15$) in four implementations (F4, F6, F10 and F14). This could have been caused by large shifts of the distribution means due to changes in locations of the best sampled values in the initial generations, or poor convergence due to a shallow cost landscape. Among these four participants, all but F14 had higher median D_{a} cost compared to the baseline.

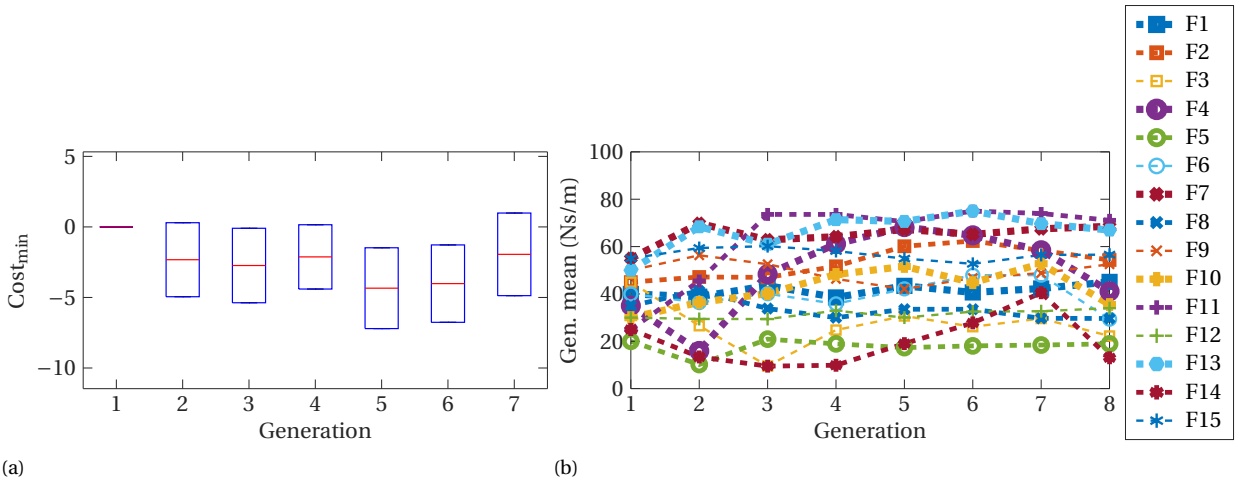

Figure 3.7: (a) Boxplot showing the minimum trial costs of each generation, relative to the first generation, for the ADO block trials of F1-F15. The minimum costs show a decrease over successive generations, although no significant difference was found between the first and the last generations (b) Trajectories of the distribution means over generations for individual ADO block implementations.

3.1.4. Search Patterns in HDO Blocks

Table 3.2 shows the initial and final damping values in the HDO block of each participant (D_0 and D_{h} respectively), along with the number of trials taken per block N_{HDO}, the Initial Search Range (ISR)– the range of damping values covered in the first 5 trials, the Overall Search Range (OSR)– the range of damping values covered over all trials, the average resampling frequency– the average number of times a particular damping value is resampled, and the average consecutive resampling frequency– the average number of times a damping value is consecutively resampled, for each participant. The differences between the median costs of D_{h} and ZD trials from the CC block are also shown as indicators of the optimality of the D_{h} values.

The initial damping values are distributed throughout the search range, although more than half the par-

Table 3.1: Start point, estimated optimum, sampled range, generation mean range and final step size for each ADO block in F1-F15. The median cost difference between the D_a and ZD trials from the CC block are also displayed.

Participant	D_{start} (Ns/m)	D_a (Ns/m)	Sampled Range (Ns/m)	Distribution Mean Range (Ns/m)	σ_f (Ns/m)	$C(D_a) - C(ZD)$
F1	40	45	49	6.6	8.5	-4.4
F2	45	54	64	17.4	12.0	-3.7
F3	45	22	75	35.4	13.0	2.9
F4	35	41	75	52.3	30.1	10.6
F5	20	19	49	10.7	3.4	-0.6
F6	40	29	68	18.6	33.1	9.4
F7	55	68	54	14.8	5.8	-1.5
F8	35	29	26	11.6	8.5	-1.6
F9	50	52	38	14.3	10.5	8.3
F10	30	35	75	22.8	23.7	3.7
F11	25	71	75	50.0	10.9	-2.4
F12	30	34	38	4.6	5.2	-5.0
F13	50	66	59	25.0	11.0	-2.2
F14	25	13	75	31.0	28.0	-1.1
F15	55	56	54	7.5	6.1	-3.6
Median	-	41	59	17.4	10.9	
Range	-	13-71	26-75	4.6-52.3	3.4-33.1	

Table 3.2: Search characteristics of individual HDO blocks of participants F1-F15.

Participant	D_0 (Ns/m)	D_h (Ns/m)	N_{HDO}	ISR (Ns/m)	OSR (Ns/m)	Average re-sampling frequency	Consecutive resampling frequency	$C(D_h) - C(ZD)$
F1	20	35	35	10	47	3.5	3.2	0.1
F2	20	20	25	45	65	1.8	1.0	-1.8
F3	20	7	25	5	50	2.3	1.8	-0.1
F4	50	20	25	40	40	3.1	1.4	11.3
F5	75	15	25	75	75	3.1	1.6	1.2
F6	30	25	30	50	75	2.5	1.4	24.5
F7	5	30	25	15	55	2.8	2.3	-3.6
F8	15	47	35	20	70	1.8	1.1	-5.8
F9	10	27	15	10	40	1.7	1.3	22.1
F10	50	10	15	35	50	1.7	1.3	-4.2
F11	37	5	15	22	75	1.7	1.4	0.6
F12	10	40	25	65	75	2.8	2.8	-2.0
F13	5	55	15	70	70	2.1	1.4	-5.2
F14	75	0	10	65	75	2.0	1.1	-0.8
F15	40	40	25	20	55	3.1	2.5	-3.0
Median:	20	25	25	35	65	2.3	1.4	
Range:	5-75	0-55	10-35	5-75	40-75	1.7-3.5	1.0-3.2	

ticipants started in the lower half of the damping range. Meanwhile, 11 out of the 15 final values are in the lower half of the damping range. Figs. 3.8a to 3.8d show the damping and cost trajectories of participants F1, F3, F11, and F13 respectively. These plots show that moving from low to high damping values is likely to be accompanied by an increase in trial cost. However, steady resampling of high damping values, as done by F1, can show lower associated costs.

Upon looking at individual HDO block trials, distinct characteristics were observed in the search strategies. Some participants were cautious in the initial trials, sampling within a specific region of the damping range. Participants F1, F3, F7, F8, F9, and F11 especially sampled with search steps less than 20 Ns/m in the first 5 trials of the block. On the other hand, participants F2, F5, F6, F12, F13 and F14 were exploratory– they

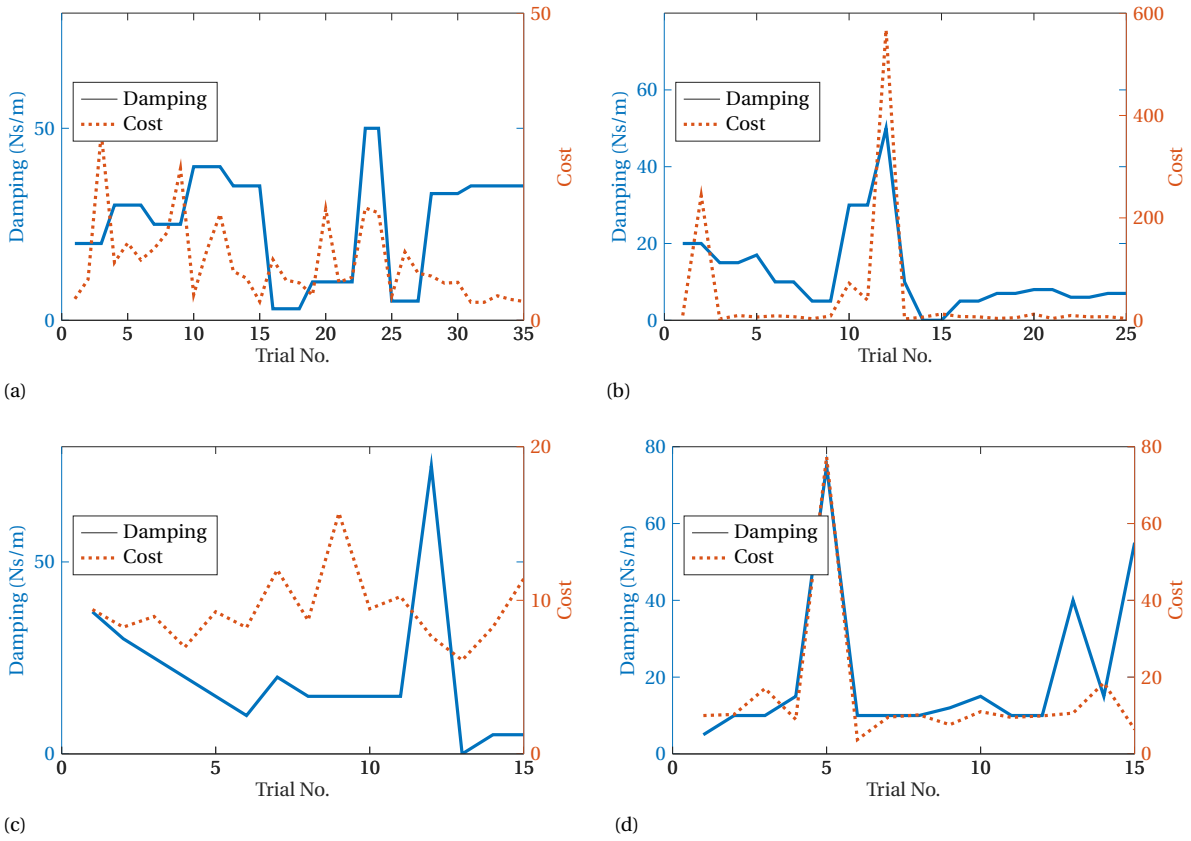

Figure 3.8: Trial-wise damping and cost trajectories for HDO blocks of participants (a) F1, (b) F3, (c) F11, and (d) F13. F1 and F3 show a higher tendency to resample previous estimated damping values, when compared to F11 and F13.

selected damping values below 15 Ns/m and above 60 Ns/m within the first 5 trials itself. Participants F4, F10 and F15 followed a balanced search strategy– they took initial search steps upto 20 Ns/m but did not explore the extremes of the damping range.

3.2. Secondary Outcome Measures

3.2.1. Effect of Damping

Fig. 3.9a shows the effect of damping on the RMS of v_{ML}, considering data of participants F7-F15. The measure decreases with increase in damping, while there is no clear trend in the RMS of F_{ML} for different damping assistances provided to the participants (Fig. 3.9b).

Meanwhile, Fig. 3.10a indicates a very weak positive correlation between damping and the mean v_{AP}. At the same time, a very weak negative correlation is observed in the RMS F_{AP}, per trial, in Fig. 3.10b.

3.2.2. Long-Term Shift in Measures

Looking at differences in secondary measures across the ZD trials of the BE and CC blocks, Wilcoxon signed-rank tests were used to compare RMS v_{ML}, mean v_{AP}, and mean BWS. A significant difference is observed in RMS v_{ML} ($p = 0.0006$) and mean v_{AP} ($p = 0.021$) as seen in Figs. 3.11a and 3.11b, indicating significantly reduced lateral oscillations and faster gait. No significant difference is observed for mean BWS ($p = 0.19$, refer Fig. 3.11c), but the median BWS is slightly lower for the CC block ZD trials.

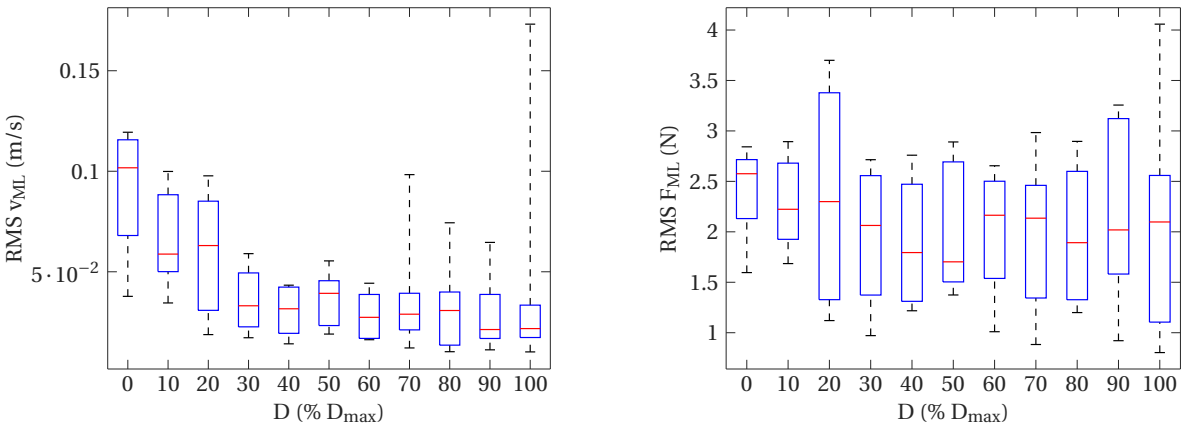

(a) (b)

Figure 3.9: Effect of damping on (a) rms(v_{ML}) , (b) rms(F_{ML})

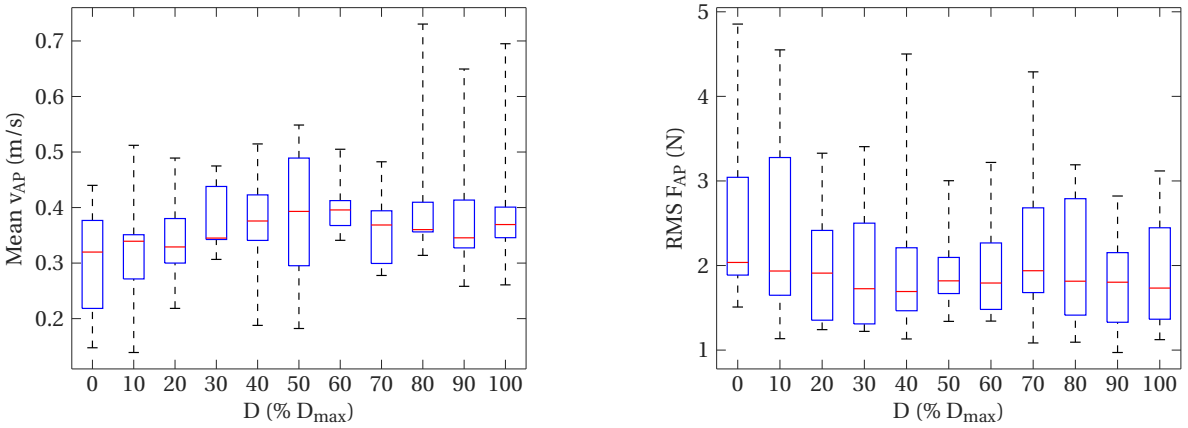

(a) (b)

Figure 3.10: Effect of damping on (a) Mean antero-posterior velocity, (b)Mean antero-posterior forces

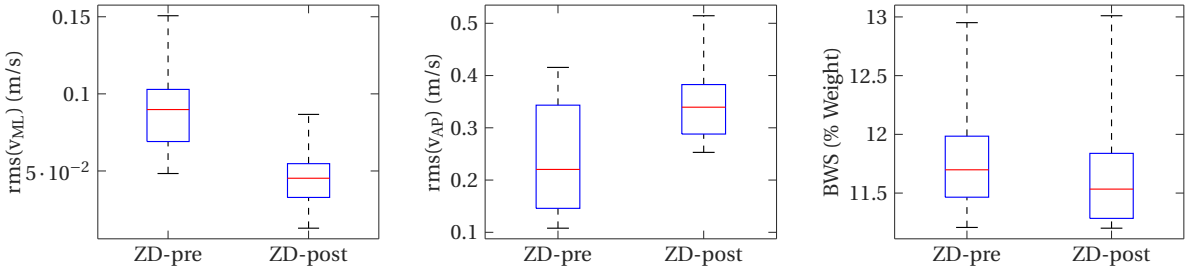

(a) (b) (c)

Figure 3.11: Change in (a) RMS v_{ML}, (b) Mean v_{AP}, (c) mean BWS, for ZD trials conducted in BE and CC blocks for F1-F15.

3.3. Post-Experiment Simulations

Table 3.3 shows the results of the simulated optimisation runs. Cost map plots and histograms showing the distribution of algorithm solutions and associated costs are shown for each simulation set in Appendix D.

The RMS of the deviations of each solution from the global minimum, RMS (ΔD) for the simulations with CMAES hyperparameter Set I is 24.6 Ns/m. Randomly selecting a damping value from the search range a 100

times is seen to result in RMS (ΔD) between 19 – 23 Ns/m. This implies that, for the given cost function, start point and hyperparameters, the CMAES algorithm is more likely than a random guess to converge to a local minimum away from the global best.

The results of simulations with Set II, where σ_0 is increased from 15 to 30 Ns/m, are marginally better, while there is a marked improvement in converging to the global minimum with Set III and Set IV, without there being a big difference between the two. Simulations with the quadratic distance cost component showed slightly improved results for parameter Set III in terms of convergence to the global minimum.

Results with Bayesian Optimisation were better for both the default cost function and the quadratic cost function, with lowest deviations from the global minimum as well as the lowest relative cost difference amongst all the simulation runs, even with the lowest trial budget of 30 trials per optimisation run.

Table 3.3: Results of simulated optimisation runs looking at the effects of different CMAES hyperparameter sets, a quadratic distance cost component, as well as a comparison with Bayesian optimisation.

Optimisation Algorithm	Cost function	Hyperparameter Set	Trial Budget	RMS(ΔD) (Ns/m)	Mean (ΔC_r)
CMAES	Default	I	35	23.7	0.28
		II	35	20.9	0.27
		III	48	15.8	0.21
		IV	96	14.3	0.16
	Quadratic	I	35	24.7	0.44
		III	48	13.6	0.22
Bayesian Opt.	Default	NA	30	12.8	0.15
	Quadratic	NA	30	7	0.07

4
Discussion

4.1. Suitability of Primary Outcome Measures for Quantifying Balance Stability

The distance measure shows some dependence on the provided lateral damping, with significant differences observed between trials with zero and non-zero damping from CC blocks of F1-F15 (see Fig. 3.1b). However, the fact that no significant differences were observed between distance measures for D_a and D_h possibly indicates that increasing damping beyond a certain level has little impact on the distance walked. It could be that the lack of significant difference was due to a ceiling effect from limited task difficulty. Grid search results show that the median distance walked by participants F7-F15 reaches 5 m at about 30% of the maximum damping (see Fig. 3.6a). As expected, the distance walked by each participant shows a noticeable level of variability in different trials with the same damping assistance. This arises due to other factors affecting balance, such as the oscillations of the slackline and changes in participant effort. Some participants were found to be more susceptible to using excess BWS, although not consistently, which could affect the distance measure recorded for different trials and contribute to the variability.

The impulse measure, on the other hand, did not show significant differences between zero and non-zero damping trials (see Fig. 3.1c). Individual GS block results also did not show a noticeable relationship between damping and the maximum impulse measure, except for a slight increase when compared to zero-damping trials. An investigation of ZD trials indicated that the lateral impulse usually reached its maximum towards the end of the trial (see Figs. E.1a and E.1b). This is despite the trimming of the force and position timeseries based on position and force limit checks before the estimation of the cost measures. Impulse values as high as 10-12 Ns were observed in ZD trials (see Fig. E.2a). The higher than expected values are partly due to residual impedance in the RYSEN in the lateral direction, and partly due to safety mechanisms in the RYSEN that arise upon the onset of falls (sudden downward motion the slingbar). The maximum impulse in a trial could therefore occur independently of the set damping assistance, especially for low damping values. A post-hoc analysis of the maximum impulse measures for the F7-F15 GS trials (see Appendix C), with an additional 0.5 seconds trimmed from the end of each trial, showed that the maximum impulse measure reduced by an average of 0.5 Ns, with the maximum reduction being around 4 Ns.

To further understand the effects of damping and BWS on slackline balance, simulations were conducted with a simple two-segment (legs and trunk) pendulum model of the human: the human effort in the form of feedback-controlled hip joint torque, and the RYSEN assistance in the form of vertical BWS forces and different levels of lateral damping at the trunk COM (see Appendix F). Simulations with different levels of damping assistance did not show large differences in lateral impulses for different levels of damping. It should however be noted that the hip torque gains were optimally tuned by the *lqry* function in MATLAB, with the selected $\boldsymbol{Q}$ and $\boldsymbol{R}$ matrices not based on actual human performance data. The simulation results should not be seen as a quantitative reference of human balance performance on slacklines, but could be used to suggest differences among various levels of assistance.

The cost measure constructed from the distance and impulse measures had the limitation of having a shallow landscape with high variability. For example, in the ADO block trials, the CMAES algorithm generally sampled over more than half of the search space (the median sampled range was 59 Ns/m, see Table 3.1), but the distribution means generally showed low displacements over successive generations (see Fig. 3.7b and Table 3.1). This suggests that the cost measure showed a low dependence on the damping parameter. The usage of an exponential impulse cost component, to prioritise the minimisation of assistance over the maximisation of performance, was not effective due to the overall low dependence of the impulse measure on the damping assistance. Thus, the exponential impulse cost was effectively an injector of additional random noise into the cost function based on the distance walked during trials. This could have reduced the effectiveness of the algorithm in searching for an optimal damping value, given the limited number of trials

available.

The CMAES implementation by Zhang et al. [22], as well as the Bayesian optimisation implementations by Kim et al., Ding et al. [23, 26], used steady metabolic cost estimates that were estimated by fitting a first-order model over a period of transient metabolic data, which reduced the stochasticity of the cost measure.

A study on the challenge provided by beam walking on lower-limb prosthesis users, by Sawers and Hafner [32], indicated that participants generally took 6-8 trials to achieve a steady performance on a beam. In the current study, participants were familiarised to the ZD condition, with an initial familiarisation block, as well as 1-2 ZD trials after each break in the session. However, no familiarisation was provided for trials with damping assistance. Large changes in damping parameters across consecutive trials, especially in the ADO, CC and GS blocks, where the participant was unaware of the damping level used, could have affected the steadiness of the participant and increased performance variability.

One of the commonly observed issues with the applied cost measure was that for the same participant, trials with very short distances walked had lower costs than trials in which the maximum distance was reached, due to the dominating effect of the exponential impulse component. To avoid such situations, a nonlinear distance cost could also be considered, so that damping values that provide little assistance (i.e., resulting in very small distance measures) are avoided. The quadratic distance cost component was seen to increase the steepness the cost landscape, leading to better performance by the optimisation algorithm in the post-hoc optimisation simulations, especially when using Bayesian optimisation.

While the cost measure showed no overall trend when comparing baseline conditions (ZD trials before and after the optimisation blocks, see Fig. 3.4a), an overall increase in mean anteroposterior velocity v_{AP} and decrease in RMS mediolateral velocity v_{ML} was observed from the ZD trials for F1-F15 (see Figs. 3.11a and 3.11b). The decrease in RMS v_{ML} could indicate higher stability on the slackline, while the increase in mean v_{AP} is possibly due to an increased confidence level and steadiness in walking. Similar effects are not observed in the distance walked or the overall cost measure (see Figs. 3.4b and 3.4c). It should be noted that both the distance and maximum impulse metrics, being single values computed at the end of each trial, are not direct indicators of balance stability, and are affected by multiple factors, such as task motivation, mental fatigue, as well as potential changes in the slackline over the course of each experimental session.

4.2. Algorithm Performance

The experimental implementation of the CMAES algorithm did not perform as well as expected in finding the optimal damping values. The lack of significant differences between the median and minimum costs over the first and last generations of the ADO blocks could partially be attributed to the algorithm's susceptibility to local minima, for the given hyperparameters and trial budget.

One of the possible reasons for the unsatisfactory performance of the CMAES is a small population size per generation λ and initial step size σ_0, which can reduce exploration. The algorithm does not use the cost measures directly but uses them to rank the candidates in each generation and select the best candidates to create the next generation. It does not use measurements of the previous generations, other than in the evolutionary path variables. Thus, if an otherwise sub-optimal damping value has a low-cost measurement in the initial generations, the algorithm is likely to shift to its vicinity in the next generation. With the algorithm only looking at the best members of each generation and the step size tending to decrease with each generation, a small population and step size could end up reinforcing an initial shift to a damping region, whether it is near a global or local minimum.

A study on the effect of population size on CMAES performance with different multimodal test functions by Hansen and Kern [33] showed that the success rate– success was defined there as termination of optimisation upon function value decreasing below a threshold– improved with increasing population size. The appropriate population size, however, not only depended on the number of dimensions of the search but also on the type of test function, with the appropriate population size (for a 95% success rate) ranging from 4 to 200 for a two-dimensional search. The population size selected for the experimental implementation in this study was based on the empirical formula suggested in [30]. It should be noted that the analyses and empirical formulae are based on a minimum search dimension of 2, where the covariance matrix is relevant. Little formal information was found on the appropriate initialisation of the step-size, possibly due to the greater focus on improving step size adaptation, reducing dependence on the initialisation. A recommendation to use an initialisation value of one-third of the search range was later found in the standard MATLAB implementation of the CMAES algorithm.

The solution returned by the algorithm was the weighted mean of the best three candidate values of the

seventh generation. If the algorithm had a large step size at this point, this value could potentially be computed from candidates that are on either side of local maxima. However, an increasing step size is also an indicator of a flat cost landscape and might call for restructuring the cost measure.

For the experimental implementation, σ_0 was arbitrarily set to 15, i.e., one-fifth of the search range. Post-hoc simulations with this step size (CMAES parameter Set I) gave poor results, with a lot of the returned solution values located in local minima or even maxima (see Fig. D.1a). Increasing the σ_0 to 30 (Set II) marginally improved performance, while increasing λ from 5 to 8 further improved results (see Figs. D.1b and D.1c). This suggests that the performance of the algorithm in the experiment could have improved with a higher population size and initial step size.

Simulations with Bayesian Optimisation showed more promising results, giving solutions close to the global optimum with both the default cost function and quadratic cost function (see Figs. D.3a and D.3b). With the trial budget for these simulations set to 30, the assumption of time-invariance in the cost measures is reasonable.

While simulated optimisation runs could be used to determine optimal algorithm hyperparameters or compare the performance of different algorithms, it is important to note the assumptions involved in such analysis. In this study, the cost maps have been constructed based on noisy distance and impulse measures, with the randomness in both measures assumed to be normally distributed and independent of the provided damping assistance itself. The second assumption is due to insufficient number of measurements at each grid point, which cannot be used to reliably estimate the variability at each point. The standard deviation of each measure was obtained by averaging the standard deviations computed at each grid point. This method of computation gives a lower estimate than the actual average standard deviation, which would be computed as the RMS of the standard deviations at each grid point.

Also, the measures are assumed to be time-invariant, which should be a reasonable assumption when considering a budget of less than 50 trials, and assuming that initial learning effects have been removed with a enough familiarisation trials.

4.3. Participant Performance in Parameter Selection

The set of participant-selected damping values D_h did not show significant differences with the CMAES solutions D_a in terms of outcome measures (see Fig. 3.1a). However, participants tended to end up choosing values in the lower half of the damping range (see Table 3.2). Meanwhile, a study by Fricke et al. on manual and automated tuning of robot assistance in gait training showed that manual tuning usually resulted in higher assistance values than the algorithm [34]. It should be noted that the study incorporated participants with neurological disorders, the manual tuning was done by a therapist, and that it was not based on minimising the same performance measures as the algorithm.

A visual inspection of HDO block results of individual participants indicated that shifting from a low to high damping in consecutive trials was likely to result in an increased cost measure. This sudden increase could have caused participants to avoid higher damping values and instead increase their own efforts to maintain balance. In addition, some participants, such as F3, F5 and F14, explicitly indicated a tendency to maximise their performance while relying more on their own skill, resulting in the preference of lower damping values and a high level of human effort.

A variety of sampling strategies were observed in the HDO block trials, with a few participants systematically re-evaluating search points in consecutive trials to minimise associated cost uncertainty while others resorted to randomly sampling from the damping range. Nearly all participants tended to show both strategies over the entire course of the HDO block. All participants resampled at least some of the evaluated damping values, with the lowest average resampling frequency being 1.67. Most participants eventually evaluated both low and high damping values with a median search range of 65 Ns/m.

Participants generally showed high motivation, especially in the initial stages of the HDO block trials, as they were in control of the assistance level, and were tasked with minimising trial costs. However, this motivation sometimes decreased over time, with some participants observing that attempting to stay on the slackline for a longer duration was more likely to incur higher costs when compared to giving up early upon losing balance. The high random variability observed in cost measures for the same damping assistance, as well as inconsistent changes in cost measures upon changes in damping, often caused participants to reduce the focus on finding the optimal damping and instead reduce the trial costs for a selected damping value.

4.4. Setup Limitation

The RYSEN, being a support system intended to retrain gait function for people with balance-related neuromuscular impairments, cannot be used without a minimum level of BWS, which increases in case of sudden downward motion of the slingbar. Prior to the main experiment, pilot studies were conducted by the author with narrow beam walking tasks with and without BWS from the RYSEN. Results indicated that the minimum BWS of 10% of the user's weight could noticeably improve the distance walked on the beam before loss of balance, resulting in ceiling effects.

According to recent documentation received on a parameter-estimation study of the RYSEN, the residual lateral damping in the ZD condition was 64 Ns/m. In the current study, considerable lateral forces were measured in ZD trials, with the mediolateral force timeseries showing high negative correlations to the mediolateral slingbar velocity timeseries (see Appendix E). These damping forces, in addition to the BWS, can noticeably reduce the difficulty of slackline walking.

Thus, even with the minimum possible assistance by the RYSEN, the task of slackline walking itself may not have been sufficiently challenging for all participants, with most participants being able to complete the maximum distance on the slackline on multiple occasions with both low and high levels of damping assistance. Participants with a limited prior experience on slacklines (less than two or three previous occasions) were able to reach the maximum distance on the slackline early on in the session, in spite of the instructions to walk with short steps and arms folded, as well as the restriction placed on excessive BWS support.

At the same time, the lateral damping exerted by the RYSEN may not assist the user beyond a certain limit, due to the compliance of the harness and the straps connecting the user to the slingbar. As seen in Fig. 3.9a, the RMS v_{ML} measure reaches a near-constant value beyond 40% of the maximum damping level. High damping levels may bring down the lateral motion of the slingbar, but the user's trunk can still have a noticeable lateral displacement with the slingbar. This also limits the usability of mediolateral slingbar velocity as a reliable indicator of balance stability on the slackline.

Thus, a different balance-assistive device could be used in future implementations of balance assistance optimisation, which has a lower influence on participant performance in the baseline condition, and has fewer compliant linkages between the point of actuation and the user.

4.5. Recommendations for Balance Assistance Systems

From this study, the implementation of balance assistance in the form of damping shows promise, as there are clear improvements in the distance walked on the slackline when a non-zero damping value is applied. The effectiveness of the damping controller compared to the spring and spring-damper controller was already shown in the beam walking experiments conducted with the GyBAR [17]. Simulations with the slackline balance model showed a reduction of 14% in the peak hip joint torque required to stabilise the system for the condition with 11% BWS and a damping of 64-75 Ns/m, as compared to the condition with only BWS (see Fig. F.2). However, the difference in peak hip torque was more drastic when comparing simulations with no BWS and 11% BWS, with the 11% BWS condition showing a 25% reduction in peak torque (see Fig. F.2).

The experimental results suggest that the optimisation of balance assistance, based on performance measures such as the distance walked before a complete loss of balance on a challenging platform, while possible, is not a straightforward task, due to the multiple factors influencing such measures. Prior to the optimisation of assistance, it would be advantageous to familiarise the user to the task at different levels of device assistance, to avoid skill-adaptation phases during the experiment. Familiarisation trials could also be provided in between optimisation trials, especially when there are large transitions in the assistance level. To account for the resulting large number of trials, the initial device familiarisation phase could be implemented in a separate session.

The lateral impulse measure, used in this study to quantify the assistance received during each trial, did not behave as expected, partially due to the limited force tracking capabilities, residual impedance, and safety mechanisms of the RYSEN. Prior to the use of this metric, its relationship with the damping parameter could have been further explored. Alternative assistance metrics that could be considered for future implementations include the mechanical power provided by the device, or a metric based on the assistance parameters. An assist-as-needed policy could be incorporated into the optimisation approach, by iteratively reducing the device assistance in successive trials when a minimum level of performance is consistently achieved by the user.

5
Conclusion

The goal of the study was to find whether lateral balance assistance could be tuned to optimise a trade-off between maximising task performance and minimising device assistance. The distance walked on a slackline in a trial, for a given level of damping assistance provided by the RYSEN, was chosen as the performance metric, while the maximum lateral impulse imparted by the RYSEN during the trial was selected as the assistance metric. Two estimates of the optimal damping parameter– one returned by the CMAES algorithm, and the other returned by the participants– were compared to a baseline assistance condition with zero lateral damping.

The distance metric seems to show a positive correlation to the damping assistance, but no clear relation is observable between damping and the maximum impulse metric. The task difficulty was possibly insufficient for a number of participants, leading to the maximum distance being reached in a large number of trials even without the use of maximum damping assistance. Meanwhile, the residual impedance of the RYSEN, as well as safety checks in the system for fall prevention, often led to large variations in the impulse measures. The above factors, in addition to the exponential cost framed from the impulse measure, resulted in a shallow cost landscape with high variability, due to which the experiment-implemented optimisations were not entirely successful.

Post-hoc optimisation simulations indicated that a larger population size and initial step size could have improved the performance of CMAES, and Bayesian Optimisation showed even more promise with a comparable trial budget.

Bibliography

[1] N. Benjuya, I. Melzer, and J. Kaplanski, "Aging-induced shifts from a reliance on sensory input to muscle cocontraction during balanced standing," *The Journals of Gerontology Series A: Biological Sciences and Medical Sciences*, vol. 59, no. 2, pp. M166–M171, 2004.

[2] C. A. Laughton, M. Slavin, K. Katdare, L. Nolan, J. F. Bean, D. C. Kerrigan, E. Phillips, L. A. Lipsitz, and J. J. Collins, "Aging, muscle activity, and balance control: physiologic changes associated with balance impairment," *Gait & posture*, vol. 18, no. 2, pp. 101–108, 2003.

[3] S. Niam, W. Cheung, P. E. Sullivan, S. Kent, and X. Gu, "Balance and physical impairments after stroke," *Archives of physical medicine and rehabilitation*, vol. 80, no. 10, pp. 1227–1233, 1999.

[4] E. Hammarén, G. Kjellby-Wendt, and C. Lindberg, "Muscle force, balance and falls in muscular impaired individuals with myotonic dystrophy type 1: a five-year prospective cohort study," *Neuromuscular Disorders*, vol. 25, no. 2, pp. 141–148, 2015.

[5] S. Rahman, H. J. Griffin, N. P. Quinn, and M. Jahanshahi, "Quality of life in parkinson's disease: the relative importance of the symptoms," *Movement disorders: official journal of the Movement Disorder Society*, vol. 23, no. 10, pp. 1428–1434, 2008.

[6] C. Andersson and E. Mattsson, "Adults with cerebral palsy: a survey describing problems, needs, and resources, with special emphasis on locomotion," *Developmental Medicine and Child Neurology*, vol. 43, no. 2, pp. 76–82, 2001.

[7] T. Masud and R. O. Morris, "Epidemiology of falls," *Age and ageing*, vol. 30, no. suppl_4, pp. 3–7, 2001.

[8] S. Krafczyk, V. Schlamp, M. Dieterich, P. Haberhauer, and T. Brandt, "Increased body sway at 3.5–8 hz in patients with phobic postural vertigo," *Neuroscience letters*, vol. 259, no. 3, pp. 149–152, 1999.

[9] H. W. Lach, "Incidence and risk factors for developing fear of falling in older adults," *Public health nursing*, vol. 22, no. 1, pp. 45–52, 2005.

[10] R. Tisserand, T. Robert, P. Chabaud, M. Bonnefoy, and L. Chèze, "Elderly fallers enhance dynamic stability through anticipatory postural adjustments during a choice stepping reaction time," *Frontiers in human neuroscience*, vol. 10, p. 613, 2016.

[11] D. A. Winter, "Human balance and posture control during standing and walking," *Gait & posture*, vol. 3, no. 4, pp. 193–214, 1995.

[12] M. Plooij, U. Keller, B. Sterke, S. Komi, H. Vallery, and J. Von Zitzewitz, "Design of rysen: an intrinsically safe and low-power three-dimensional overground body weight support," *IEEE Robotics and Automation Letters*, vol. 3, no. 3, pp. 2253–2260, 2018.

[13] H. Vallery, P. Lutz, J. von Zitzewitz, G. Rauter, M. Fritschi, C. Everarts, R. Ronsse, A. Curt, and M. Bolliger, "Multidirectional transparent support for overground gait training," in *2013 IEEE 13th International Conference on Rehabilitation Robotics (ICORR)*. IEEE, 2013, pp. 1–7.

[14] S. Jezernik, G. Colombo, T. Keller, H. Frueh, and M. Morari, "Robotic orthosis lokomat: A rehabilitation and research tool," *Neuromodulation: Technology at the neural interface*, vol. 6, no. 2, pp. 108–115, 2003.

[15] H. K. Kwa, J. H. Noorden, M. Missel, T. Craig, J. E. Pratt, and P. D. Neuhaus, "Development of the ihmc mobility assist exoskeleton," in *2009 IEEE International Conference on Robotics and Automation*. IEEE, 2009, pp. 2556–2562.

[16] E. Aoki, H. Konosu, H. Kimura, T. Wojtara, and S. Shimoda, "Balance device," Dec. 22 2015, uS Patent 9,216,132.

[17] D. Lemus Perez, "Gyroscopic assistance for human balance," Ph.D. dissertation, Delft University of Technology, 2019.

[18] J. Hidler, D. Nichols, M. Pelliccio, K. Brady, D. D. Campbell, J. H. Kahn, and T. G. Hornby, "Multicenter randomized clinical trial evaluating the effectiveness of the lokomat in subacute stroke," *Neurorehabilitation and neural repair*, vol. 23, no. 1, pp. 5–13, 2009.

[19] M. Visintin, H. Barbeau, N. Korner-Bitensky, and N. E. Mayo, "A new approach to retrain gait in stroke patients through body weight support and treadmill stimulation," vol. 29, no. 6, pp. 1122–1128.

[20] A. J. Veale and S. Q. Xie, "Towards compliant and wearable robotic orthoses: A review of current and emerging actuator technologies," *Medical engineering & physics*, vol. 38, no. 4, pp. 317–325, 2016.

[21] B. Achili, T. Madani, B. Daachi, and K. Djouani, "Adaptive observer based on mlpnn and sliding mode for wearable robots: Application to an active joint orthosis," *Neurocomputing*, vol. 197, pp. 69–77, 2016.

[22] J. Zhang, P. Fiers, K. A. Witte, R. W. Jackson, K. L. Poggensee, C. G. Atkeson, and S. H. Collins, "Human-in-the-loop optimization of exoskeleton assistance during walking," vol. 356, no. 6344, pp. 1280–1284.

[23] M. Kim, Y. Ding, P. Malcolm, J. Speeckaert, C. Siviy, C. Walsh, and S. Kuindersma, "Human-in-the-loop bayesian optimization of wearable device parameters."

[24] T. Lenzi, M. C. Carrozza, and S. K. Agrawal, "Powered hip exoskeletons can reduce the user's hip and ankle muscle activations during walking," *IEEE Transactions on Neural Systems and Rehabilitation Engineering*, vol. 21, no. 6, pp. 938–948, 2013.

[25] K. Tsakalis and P. Ioannou, "Adaptive control of linear time-varying plants," *Automatica*, vol. 23, no. 4, pp. 459–468, 1987.

[26] Y. Ding, M. Kim, S. Kuindersma, and C. J. Walsh, "Human-in-the-loop optimization of hip assistance with a soft exosuit during walking."

[27] N. Thatte, H. Duan, and H. Geyer, "A sample-efficient black-box optimizer to train policies for human-in-the-loop systems with user preferences," vol. 2, no. 2, pp. 993–1000.

[28] K. Kodama, Y. Kikuchi, and H. Yamagiwa, "Whole-body coordination skill for dynamic balancing on a slackline," in *JSAI International Symposium on Artificial Intelligence*. Springer, 2015, pp. 528–546.

[29] N. Hansen, S. D. Müller, and P. Koumoutsakos, "Reducing the time complexity of the derandomized evolution strategy with covariance matrix adaptation (CMA-ES)," vol. 11, no. 1, pp. 1–18. [Online]. Available: http://www.mitpressjournals.org/doi/10.1162/106365603321828970

[30] N. Hansen, "The cma evolution strategy: A tutorial," *arXiv preprint arXiv:1604.00772*, 2016.

[31] F. Faul, E. Erdfelder, A.-G. Lang, and A. Buchner, "G* power 3: A flexible statistical power analysis program for the social, behavioral, and biomedical sciences," *Behavior research methods*, vol. 39, no. 2, pp. 175–191, 2007.

[32] A. Sawers and B. J. Hafner, "A study to assess whether fixed-width beam walking provides sufficient challenge to assess balance ability across lower limb prosthesis users," *Clinical rehabilitation*, vol. 32, no. 4, pp. 483–492, 2018.

[33] N. Hansen and S. Kern, "Evaluating the CMA evolution strategy on multimodal test functions," in *Parallel Problem Solving from Nature PPSN VIII*, ser. LNCS, X. Yao *et al.*, Eds., vol. 3242. Springer, 2004, pp. 282–291.

[34] S. S. Fricke, C. Bayón, H. Van Der Kooij, and E. H. van Asseldonk, "Automatic versus manual tuning of robot-assisted gait training in people with neurological disorders," *Journal of neuroengineering and rehabilitation*, vol. 17, no. 1, p. 9, 2020.

[35] D. A. Winter, *Biomechanics and motor control of human movement*. John Wiley & Sons, 2009.

A
CMAES Information

In each generation, the algorithm samples and evaluates the cost measurements of λ candidates, randomly sampled from the distribution. The mean of the distribution is calculated in each generation using the weighted average of μ candidates of that generation ($\mu < \lambda$) with the best fitness (lowest cost measurements). The weights of each candidate are assigned based on the order of their cost scores, so that the mean is closest to the best scoring candidate.

The random sampling of candidates in each generation can be expressed by the following equation,

$$\boldsymbol{x}_k^{(g+1)} \sim \boldsymbol{m}^{(g)} + \sigma^{(g)} N(\mathbf{0}, \boldsymbol{C}^{(\mathbf{g})}), \text{ for } k = 1, ..., \lambda, \tag{A.1}$$

where $\boldsymbol{m}^{(g)}$ is the mean, $\sigma^{(g)}$ is the overall step size or scale, and $\boldsymbol{C}^{(g)}$ is the covariance matrix of the normal distribution in the g^{th} generation.

The code segment related to the candidate generation in the MATLAB implementation of CMAES is shown below.

```
for k=1:lambda % this run generates the candidate parameters that
    are stored as input files for D-Flow!
  n_c = k;
  candidate_param = round(xmean + sigma * B * (D .* randn(N,1))); %
      m + sig * Normal(0,C)
  %%% Applying constraints on search space
  candidate_param = x_in_bounds_fn(candidate_param,lb,ub);
  arx(:,k) = candidate_param;

  Candidate_set(:,k,n_g) =arx(:,k);
end
```

The calculation of the mean of the next generation can be expressed as,

$$\boldsymbol{m}^{(\mathbf{g+1})} = \boldsymbol{m}^{(g)} + c_m \sum_{i=1}^{\mu} w_i \, (\boldsymbol{x}_{i:\lambda}^{(g+1)} - \boldsymbol{m}^{(\mathbf{g})}), \tag{A.2}$$

where $\boldsymbol{x}_{1:\lambda}^{(g+1)}$ is the set of the evaluated candidates of the current generation, sorted in increasing order of the cost score,
w_i is the weight of the i^{th} candidate, such that $w_i > w_{i+1}$, and
$c_m \leq 1$ is the learning rate which is usually set to 1, based on empirical results [30].

The adaptation of the distribution mean over successive generations is implemented in the function as shown below.

```
[arfitness, arindex] = sort(arfitness);  % sort candidates based on
    cost measures
xold = xmean; % mean of the generation which has just been
   evaluated
xmean = ((1-cmean) * xold) + cmean *arx(:,arindex(1:mu)) * weights;
     % recombine best members of current gen to construct the mean
    of the next generation
```

The update of the covariance matrix and the step sizes are done using separate evolution paths p_c and p_σ , that factor in the shift in the position of the distribution means over successive generations and are

themselves updated by exponential smoothening with learning rates c_c and c_σ. The exploitation of the search history in this form is supposed to increase robustness to noisy measurements (rank-1 update) [29] . The covariance matrix update also considers the distances of the μ best candidates of each generation from the generation means, which increases the speed of the search for the optimum (rank-μ update) [29]. A different learning rate c_μ is used for the rank-μ update.

The covariance matrix is updated for each generation using the formula,

$$\boldsymbol{C}^{(g+1)} = (1 - c_1 - c_\mu \sum_{j=1}^{\lambda} w_j)\boldsymbol{C}^{(g)} + c_1(p_c^{(g+1)} p_c^{(g+1)T}) + c_\mu \sum_{i=1}^{\lambda} w_i y_{1:\lambda}^{(g+1)} (y_{1:\lambda}^{(g+1)})^T, \tag{A.3}$$

where c_1 is the learning rate of the rank-one update,
c_μ is the learning rate of the rank-μ update,
$p_c^{(g+1)}$ is the evolution path of the covariance matrix, used to preserve sign information when updating the covariance matrix, and
$y_{1:\lambda}^{(g+1)} = (x_{1:\lambda}^{(g+1)} - \boldsymbol{m}^{(g)})/\sigma^{(g)}$.
The covariance matrix is expressed in terms of a diagonal matrix D and an eigenvector matrix B, such that $C^{(g)} = B^{(g)}(D^{(g)})^2 B^{(g)T}$.

The step-size is updated over each generation by the following equation,

$$\sigma^{(g+1)} = \sigma^{(g)} \exp\Big(\frac{c_\sigma}{d_\sigma}\Big(\frac{||p_\sigma^{(g+1)}||}{\mathrm{E}||\mathrm{N}(0,\mathrm{I})||} - 1\Big)\Big), \tag{A.4}$$

where
$p_s^{(g+1)}$ is the evolution path of the step size, which increases with the Mahalanobis distance between the means of successive generations, (i.e., when optimal solution is away from the current estimate), and
d_σ is a damping term which limits changes in the step size. The step size increases when the evolutionary path is larger than the expected deviation from the mean for a random normal distribution, i.e., when the shifts in the mean over successive generations is not likely to be by random chance.

The implementation of the covariance matrix and step-size adaptation in the MATLAB function is given below.

```
%%%% Step 5: Cumulation: Update evolution paths
ps = (1-cs) * ps ...
      + sqrt(cs*(2-cs)*mueff) * invsqrtC * (xmean-xold) / sigma; %
         evolution path term for sigma
hsig = sum(ps.^2)/(1-(1-cs)^(2*counteval/lambda))/N < 2 + 4/(N+1);
   % term using ps used in pc
pc  = (1-cc) * pc ...
      + hsig * sqrt(cc*(2-cc)*mueff) * (xmean-xold) / sigma;

% Adapt covariance matrix C
artmp = (1/sigma) * (arx(:,arindex(1:mu)) - repmat(xold,1,mu));  %
   mu difference vectors
C = (1-c1-cmu) * C ...                    % regard old matrix
     + c1 * (pc * pc' ...                 % plus rank one update
             + (1-hsig) * cc*(2-cc) * C) ... % minor correction if
                hsig==0
     + cmu * artmp * diag(weights) * artmp'; % plus rank mu update

% Adapt step size sigma
sigma = sigma * exp((cs/damps)*(norm(ps)/chiN - 1));
```

The parameters used in the experimental implementation of the algorithm are given in Table A.1.

Table A.1: Hyperparameter values used for the CMAES algorithm with search dimension $N = 1$ [30].

Hyperparameter	Empirical formula	Value used
λ	$\sim 4 + (3\log(N))$	5
μ	$\sim \lambda/2$	3
$\boldsymbol{w}'_i$	$\log(\mu + 1/2) - \log(i_{1:\mu})$	[1.25 0.56 0.15]
$\boldsymbol{w}_i$	$\frac{1}{\sum_{i=1}^{\mu} w'_i} \boldsymbol{w}'_i$	[0.64 0.28 0.08]
μ_{eff}	$\frac{(\sum_{i=1}^{\mu} w_i)^2}{\sum_{i=1}^{\mu} w_i^2}$	2.03
σ^0	-	15
N_{g}	-	7
c_{c}	$\frac{(4+\mu_{\text{eff}}/N)}{(N+4+2\mu_{\text{eff}}/N)}$	0.67
c_σ	$\frac{\mu_{\text{eff}}+2}{N+\mu_{\text{eff}}+3}$	0.67
d_σ	$1 + 2\max(0, \sqrt{\frac{\mu_{\text{eff}}-1}{N+1}} - 1) + c_\sigma$	1.67
$\boldsymbol{p}_c^0$	0	
$\boldsymbol{p}_\sigma^0$	0	
c_m	1	
c_1	$\frac{2}{(N+1.3)^2+\mu_{\text{eff}}}$	0.273
c_μ	$\min\left(1 - c1, 2\frac{(\mu_{\text{eff}}-2+1/\mu_{\text{eff}})}{(N+2)^2+\mu_{\text{eff}}}\right)$	0.095

B
Individual Optimisation Block Trajectories

Figs. B.1 and B.2 show the damping values sequentially selected by participants in their respective HDO block trials, and the associated cost measures. To avoid losing information due to individual spikes in costs, cost values greater than 100 have been saturated to this value in the plots.

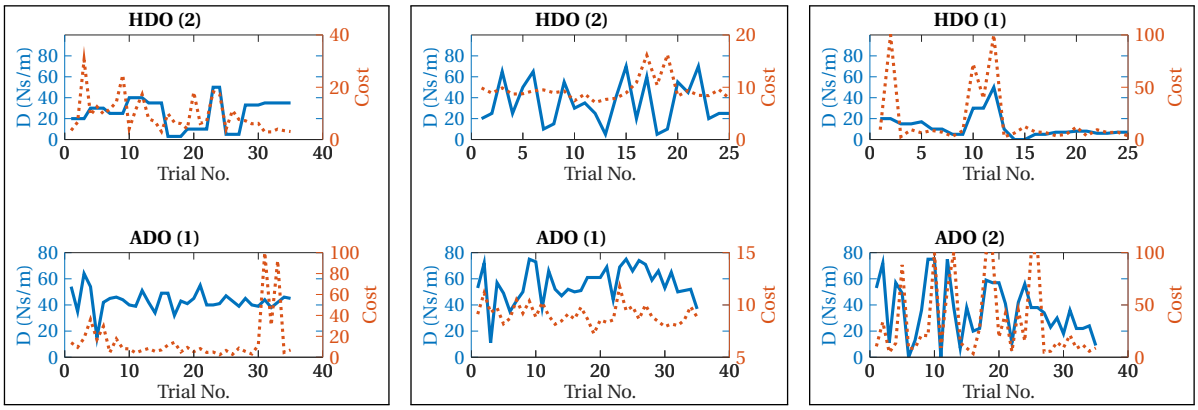

(a) F1

(b) F2

(c) F3

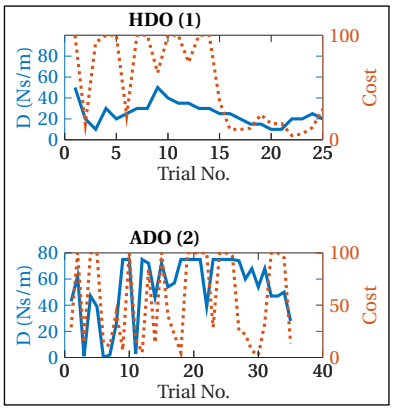

(d) F4

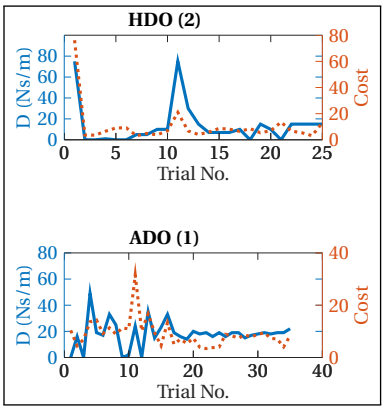

(e) F5

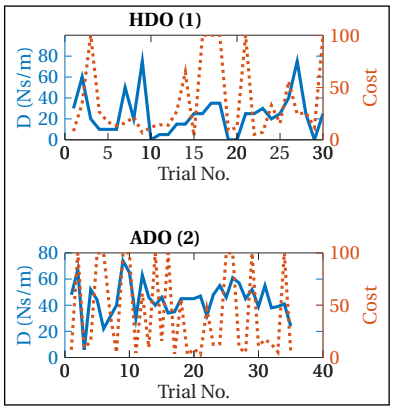

(f) F6

Figure B.1: Trial-wise damping and cost trajectories for ADO and HDO blocks of participants F1-F6. The order in which the blocks are implemented are given in parenthesis next to the titles.

(a) F7 (b) F8 (c) F9

(d) F10 (e) F11 (f) F12

(g) F13 (h) F14 (i) F15

Figure B.2: Trial-wise damping and cost trajectories for ADO and HDO blocks of participants F7-F15. The order in which the blocks are implemented are given in parenthesis next to the titles.

C
Grid Search Results F7-F15

The distance and maximum impulse measures for GS block trials of F7-F15 are plotted in Figs. C.1 and C.2 with respect to the damping values, expressed as a percentage of the maximum damping (75 Ns/m). To observe the effect of trimming out an additional 0.5 seconds from the end of each trial on the maximum impulse, recomputed maximum impulse values I_{mnew} are plotted alongside the originally used impulse measures.

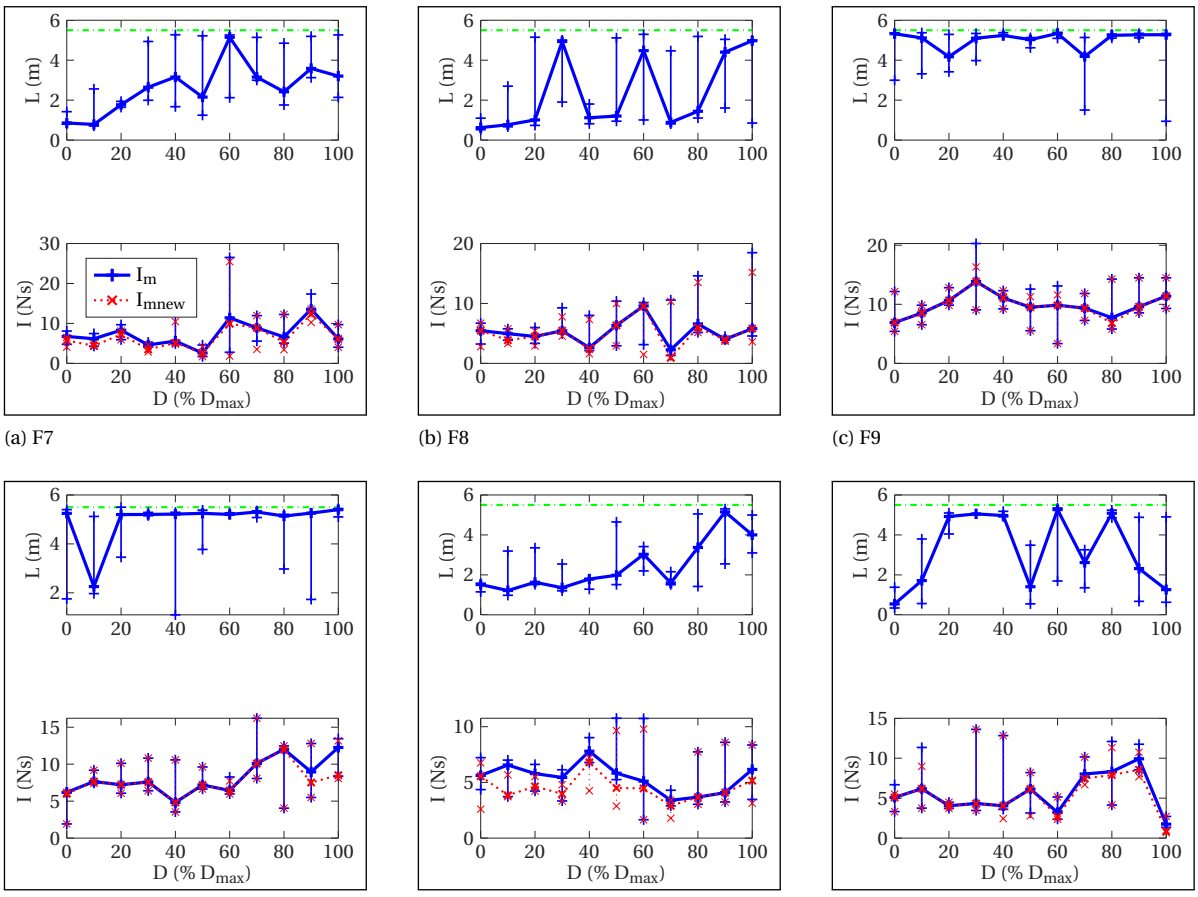

(a) F7 (b) F8 (c) F9

(d) F10 (e) F11 (f) F12

Figure C.1: Plots of individual distance and impulse measures for GS block trials of F7-F12. The median measures corresponding to each damping value are plotted in thick lines, with the corresponding ranges plotted as vertical lines.

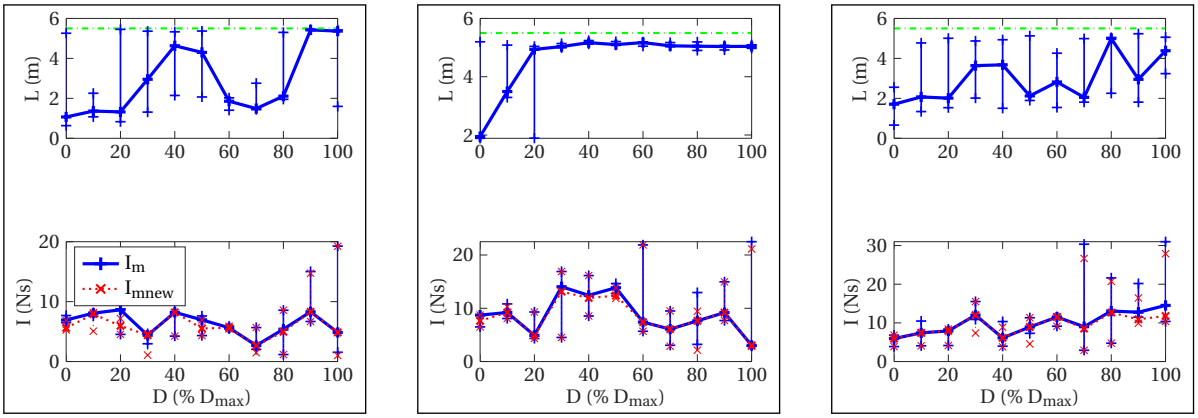

(a) F13 (b) F14 (c) F15

Figure C.2: Plots of individual distance and impulse measures for GS block trials of F13-F15. The median measures corresponding to each damping value are plotted in thick lines, with the corresponding ranges plotted as vertical lines.

Similarly, the RMS mediolateral velocity and mean anteroposterior velocity measures from the GS block trials of F7-F15 are plotted with respect to the damping values, expressed as a percentage of the maximum damping (75 Ns/m), in Figs. C.3 and C.4.

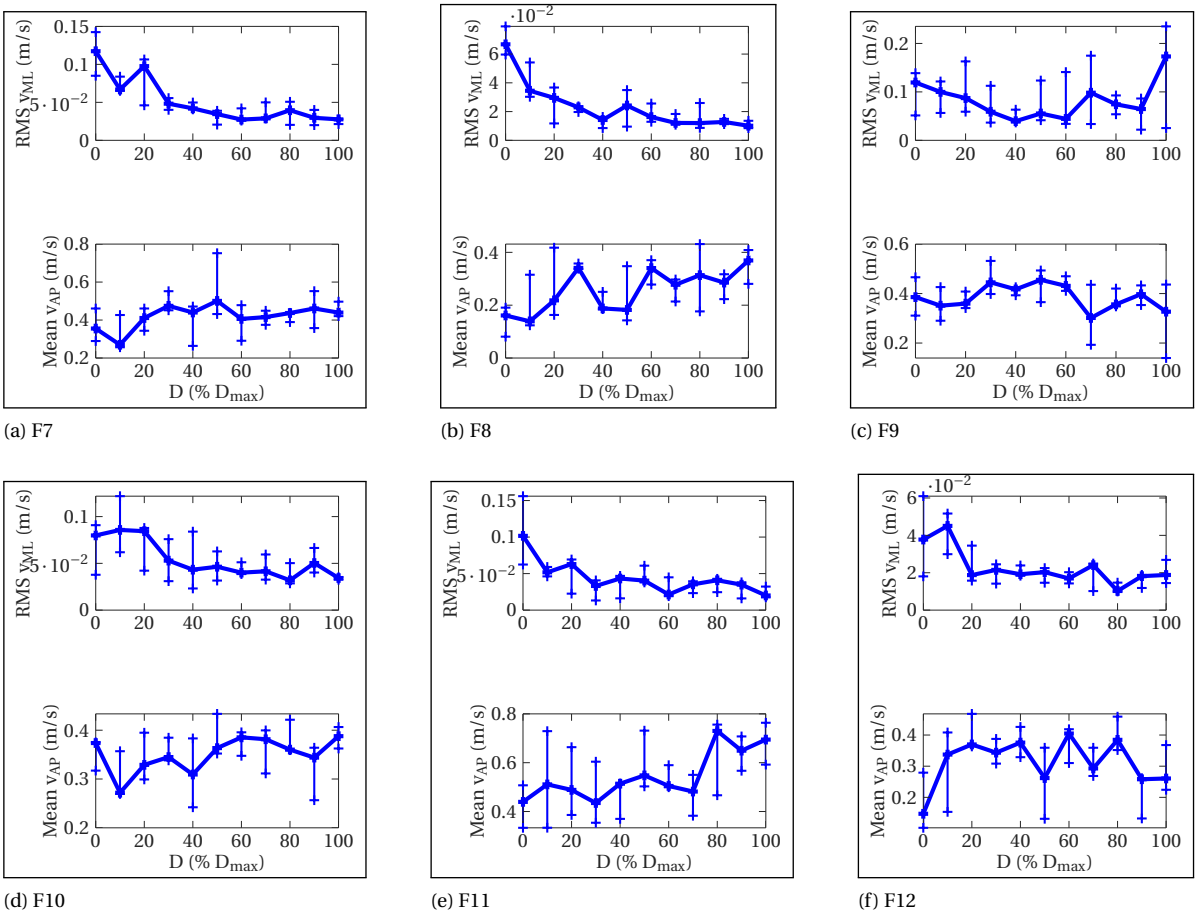

(a) F7 (b) F8 (c) F9

(d) F10 (e) F11 (f) F12

Figure C.3: Plots of individual RMS v_{ML} and mean v_{AP} measures for GS block trials of F7-F12. The median measures corresponding to each damping value are plotted in thick lines, with the corresponding ranges plotted as vertical lines.

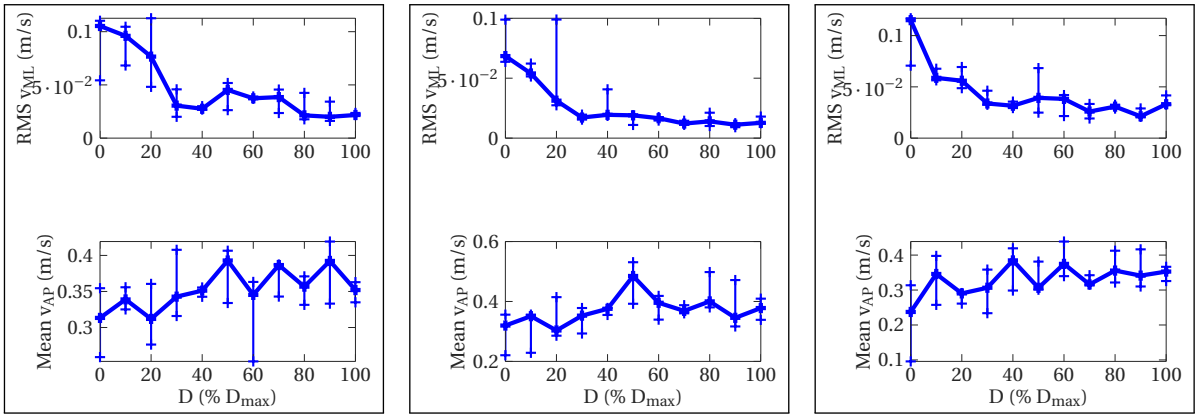

(a) F13 (b) F14 (c) F15

Figure C.4: Plots of individual RMS v_{ML} and mean v_{AP} measures for GS block trials of F13-F15. The median measures corresponding to each damping value are plotted in thick lines, with the corresponding ranges plotted as vertical lines.

D
Simulated Optimisation Results

The results of the simulated optimisation runs, conducted with CMAES algorithm with hyperparameter Sets I-IV (Table D.1) for the default cost function are shown in Figs. D.1a to D.1d. Figs. D.2a and D.2b show the results of optimisation runs with hyperparameter Set I and III for the quadratic distance cost component. Figs. D.3a and D.3b show results for Bayesian optimisation runs conducted with the default and quadratic cost maps. The difference between the returned algorithm solutions and the global minimum in each optimisation set is quantified by RMS(ΔD_r), and visualised in the damping solution histogram shown with each subfigure. In addition, the difference between the algorithm solution costs and the global minimum costs is normalised to the difference between the global maximum and minimum costs, and quantified by the mean(ΔC_r) along with the visualisation through relative cost difference histograms.

The cost measure has a flat profile in Figs. D.1a to D.1d, with the global minimum D_gmin in between $30-40\,\mathrm{Ns/m}$. In the first two cases, a large proportion of the solutions returned by the algorithm are at a local minimum near the initialised search distribution mean (start point), resulting in a large RMS (ΔD_r). Simulations conducted with the random sampling of 100 parameter values from the search range, each value considered as a solution value, showed similar RMS(ΔD_r) values. The average relative cost difference from the global minimum is also quite high, due to a number of solutions returned from all over the search space. Using CMAES parameter Set II (higher initial step size) shows a some reduction in RMS(ΔD_r). Increasing the population size (Set III), followed by the number of generations (Set IV) each steadily brings down these measures.

The use of the quadratic distance cost function component shows more definite gradients in the cost landscape (Figs. D.2a and D.2b). The global minimum meanwhile has moved to a slightly higher damping value. Algorithm Set I still results in poor performance, with a higher mean(ΔC_r) than in Fig. D.1a. Algorithm Set III shows a similar performance as in Fig. D.1c, with a slightly lower RMS(ΔD_r). Comparing the damping solution histograms of Fig. D.1c and Fig. D.2b, a noticeable difference can be observed in the spread of the solutions, with low damping solutions being avoided in Fig. D.2b.

Bayesian Optimisation shows the highest quality in the solutions, with the lowest deviations from the global minima for both the default cost function and with the quadratic distance cost component. Simulations with the quadratic distance cost component show the best results amongst all the optimisation sets, with RMS(ΔD_r) and mean(ΔC_r) being around half the values for the Bayesian Optimisation simulations with the default cost function.

Table D.1: CMAES hyperparameter sets used in the optimisation simulations, in addition to the mean value used to generate the first generation, D_0

Set	D_0 (Ns/m)	σ_0 (Ns/m)	λ	N_g
I	5	15	5	7
II	5	30	5	7
III	5	30	8	6
IV	5	30	8	12

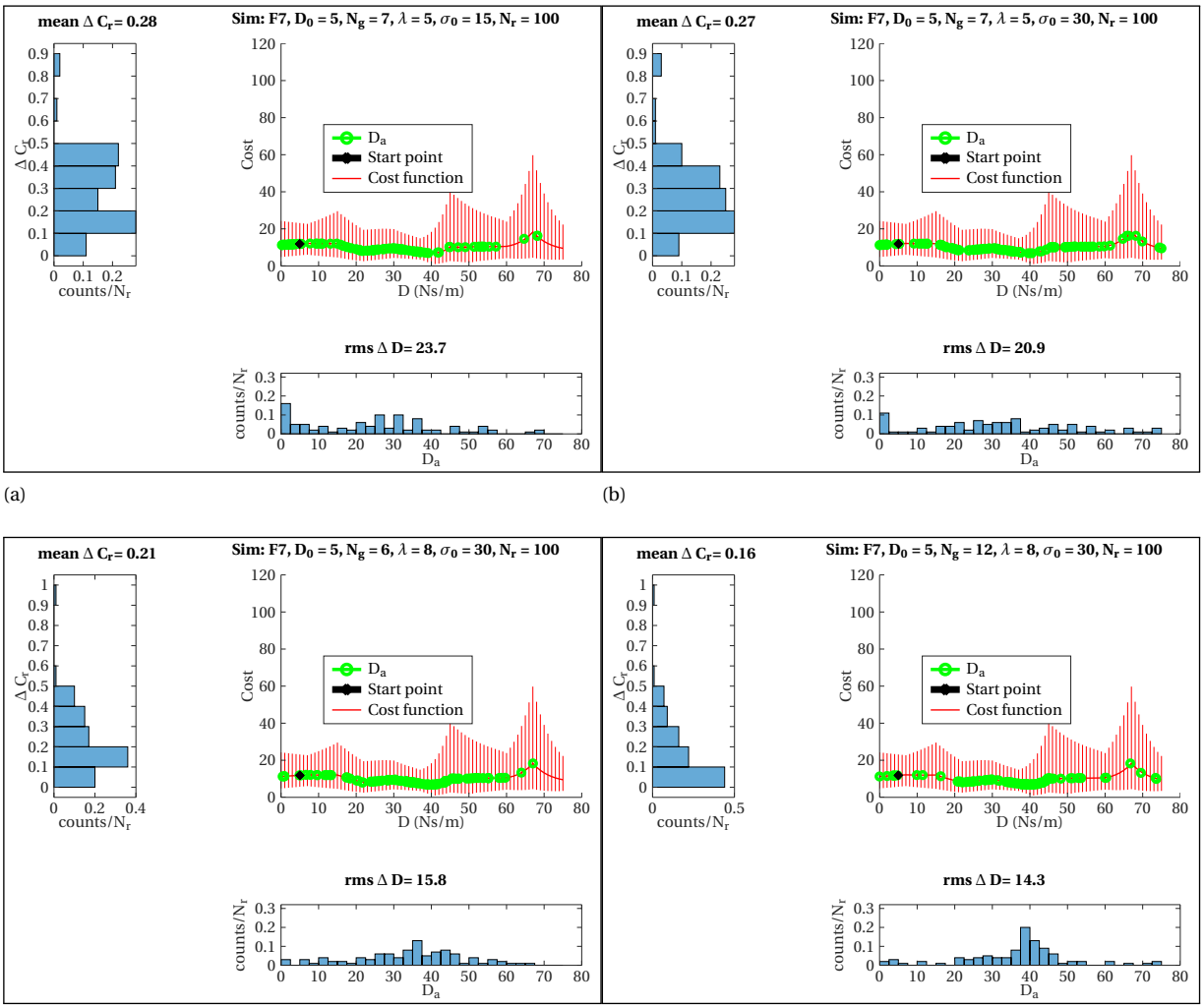

Figure D.1: CMAES simulation results for F7, using CMAES parameter sets (a) I, (b) II, (c) III and (d) IV. The damping histogram below each cost-damping plot shows the relative number of algorithm solutions D_a in each 2.5 Ns/m interval of the damping range. The cost histogram to the left of each cost-map shows the relative number of algorithm solutions with the corresponding ΔC_r.

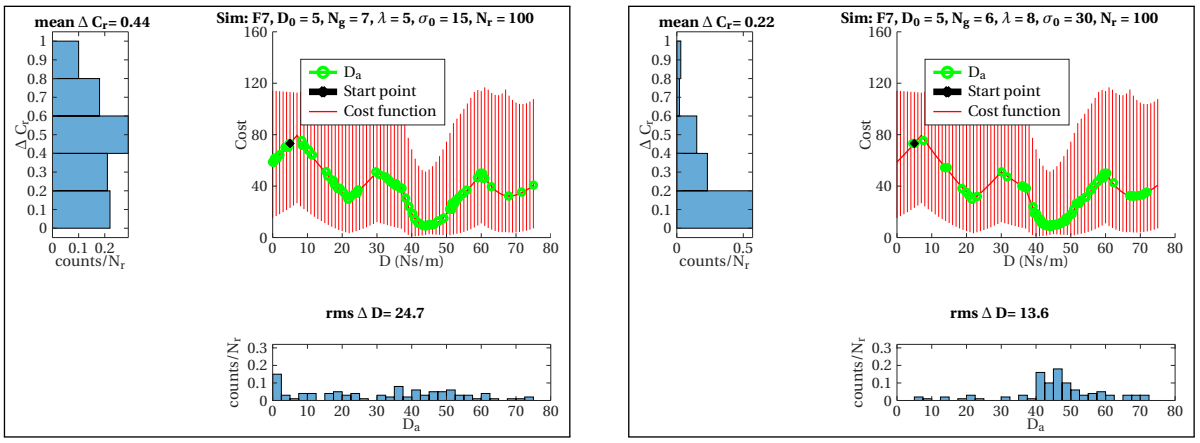

(a) (b)

Figure D.2: CMAES simulation results for F7 with the quadratic distance cost component are shown when using CMAES parameter sets (a) I and (b) III. The damping histogram below each cost-damping plot shows the relative number of algorithm solutions D_a in each 2.5 Ns/m interval of the damping range. The cost histogram to the left of each cost-map shows the relative number of algorithm solutions with the corresponding relative cost difference ΔC_r.

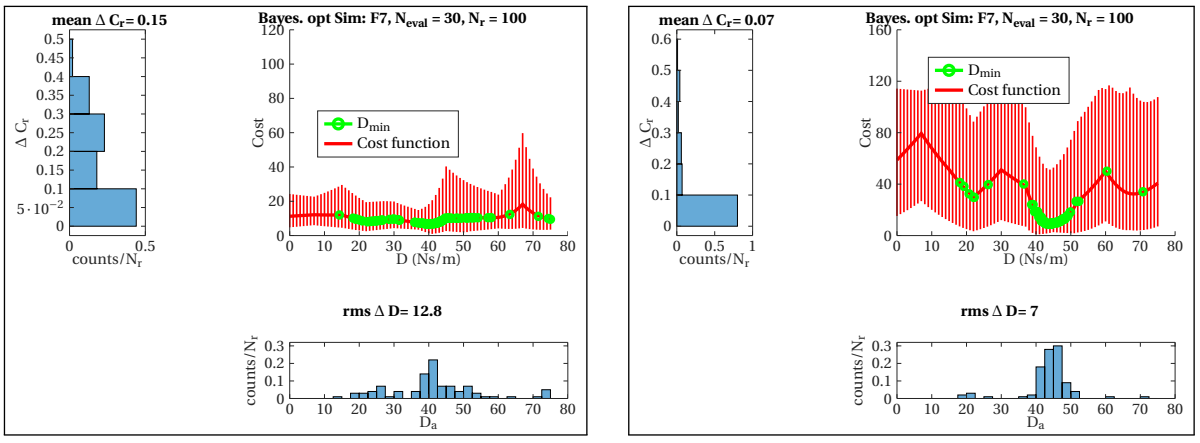

(a) (b)

Figure D.3: Bayesian optimisation simulation results for F7, using (a) default (linear) and (b) quadratic distance cost component. The damping histogram below each cost-damping plot shows the relative number of algorithm solutions D_a in each 2.5 Ns/m interval of the damping range. The cost histogram to the left of each cost-map shows the relative number of algorithm solutions with the corresponding relative cost difference ΔC_r.

E
Observations on Lateral Forces

Experimental results indicated a very low dependence of lateral impulse on the set damping value. To better understand this low dependence, an analysis of trials with and without lateral damping was done, looking at lateral position, velocity and force timeseries, as well as BWS timeseries data of individual trials. Visual inspection of individual trial data showed the presence of noticeable lateral impedance even in ZD trials, as can be seen in Fig. E.2a. The Pearson correlation coefficient between F_{ML} and v_{ML} timeseries data for this trial was -0.97, indicating a strong damping component in the residual impedance. More than 75% of the ZD trials in the BE and CC blocks had correlation coefficients above 0.7.

The active damping component in the RYSEN is designed to be assistive, i.e., only the movement of the slingbar away from a specific position (in this case, from above the slackline) should be resisted. As seen in Fig. E.2b, the measured lateral damping forces show some correspondence to the expected forces but show occassional deviations, which could be partially due to the system's limited force tracking abilities and partially due a coupling with the vertical BWS forces.

Fig. E.1a shows the occurrence of the maximum impulse measure normalised to the corresponding trial durations, in the ZD trials of the BE and CC blocks, while Fig. E.1b shows the same for GS block trials. In both sets of trials, a large proportion of the maximum impulse measures occur at the ends of the trials, which is likely due to an increase in lateral forces during step-off.

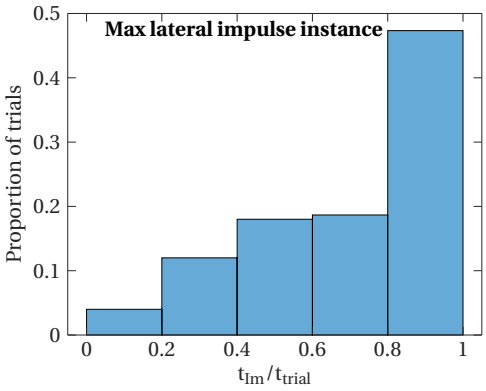

(a) ZD trials (BE and CC block)

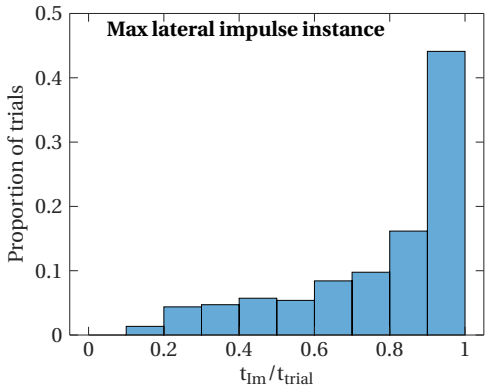

(b) GS block trials (F7-F15)

Figure E.1: Histograms showing the frequency of occurrence of the maximum impulse with respect to individual trial durations, for (a) ZD trials from the BE and CC blocks of F1-F15, (b) GS block trials of F7-F15

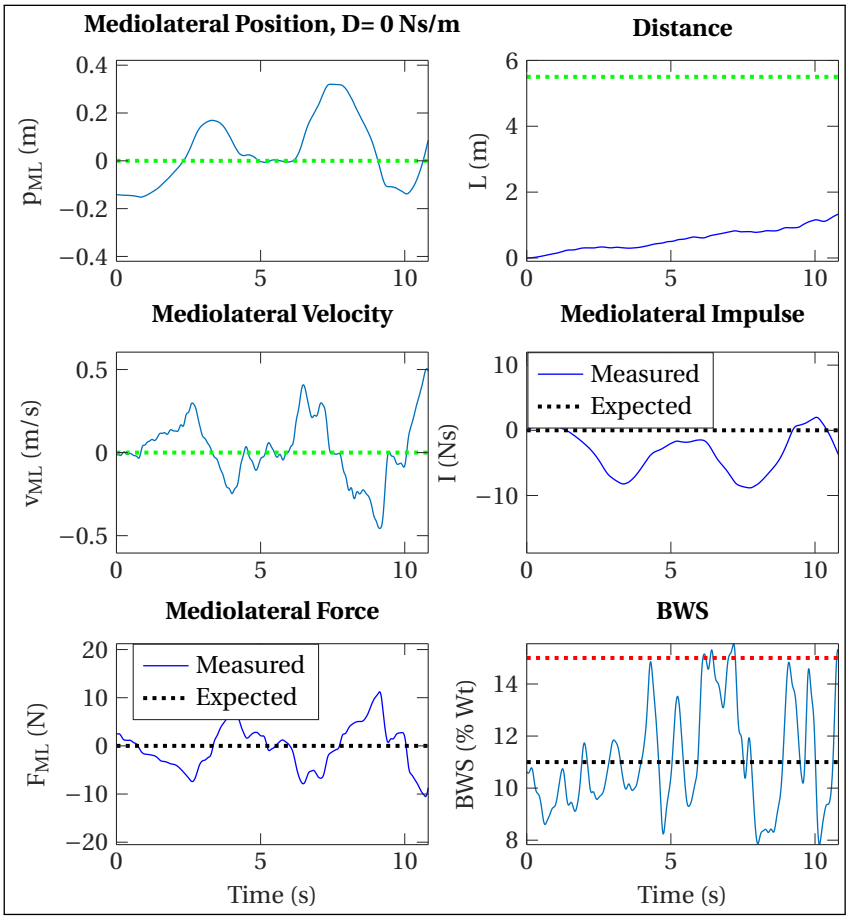

(a) Zero Damping

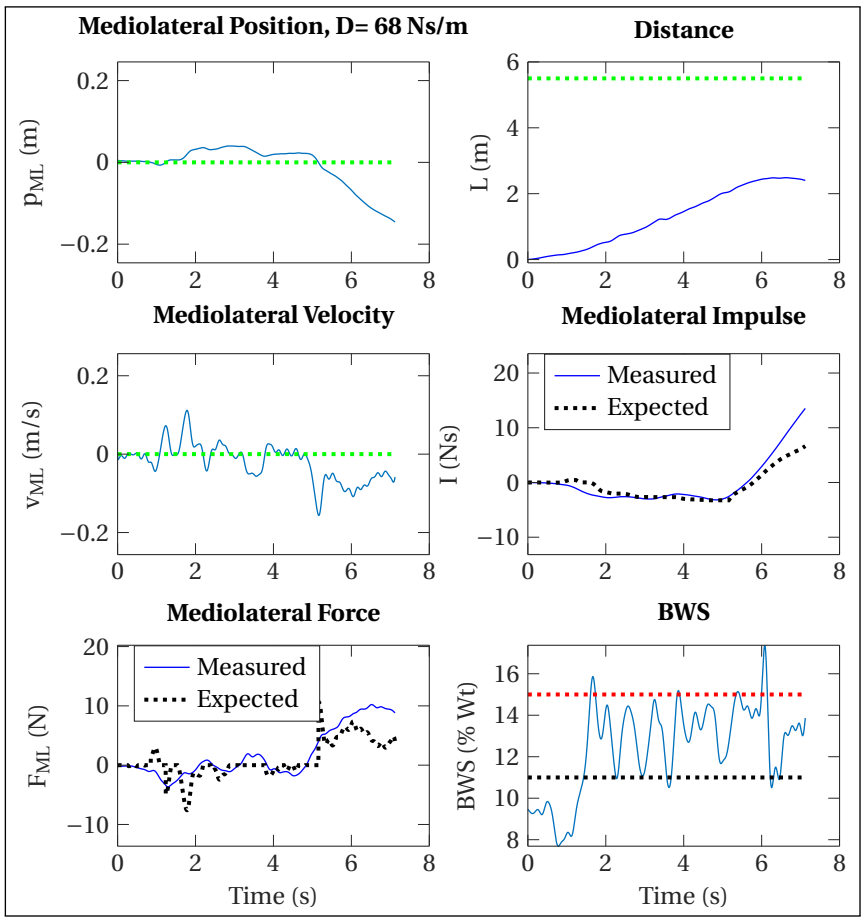

(b) High Damping

Figure E.2: Plots of mediolateral slingbar position, velocity and forces, as well as distance travelled, mediolateral impulse and BWS timeseries data for (a) a ZD trial by F6 and (b) a trial with $D_a = 68\,\mathrm{Ns/m}$ for participant F7.

F
Slackline Balance Model Analysis

F.1. System Model

To better understand the dynamics involved in slackline balancing, especially under the effect of BWS and lateral damping assistance, a slackline balance model was created in MATLAB. The human-slackline system model is based on the slackline-balance model developed by Heike Vallery and used as part of an assignment in the course 'Human and Robot Locomotion', with the human modelled as a three-segment pendulum and the slackline modelled as parallel spring-damper system.

The original pendulum model consisted of three segments: the base (legs), the trunk and the arms (both arms modelled as a single segment), with the base and trunk segments connected at the hip joint and the trunk and arm segments connected at the shoulder joint. Each segment was modelled as a rigid link with a given mass, length and inertia. The human-effort in maintaining balance was in the form of stabilisation torques applied at the hip and shoulder joints. In this study, the arms are considered as a part of the trunk, since participants were asked to fold their arms in the experiments of the main study. The two-segment pendulum model is therefore to be stabilised by hip torques.

The slackline behaviour is the same as defined in the original model, and consists of stiffness and damping elements acting in parallel, with the damping ratio set to 0.5. The stiffness and damping terms are not directly set, but are derived from the static equilibrium condition applied for a given vertical sag of the slackline under the weight of the human. The deflection of the slackline gives rise to forces at the foot of the human, with both vertical and horizontal components.

In addition to human-effort component, external stabilisation forces are considered in the analysis, in the form of upward BWS and lateral (horizontal) damping. In a simplification of the actual behaviour of the RYSEN, the forces acting on the slingbar have been assumed to act directly at the trunk, neglecting the compliance of the connecting elements– the user harness and the connecting straps. The lateral damping can be anisotropic– with resistance provided only against trunk motion away from the vertical, or isotropic– with damping applied against trunk motion in both directions. The damping action provided by the RYSEN is designed to be anisotropic, to ensure that the device provides only assistive damping forces to the user. However, residual forces applied by the RYSEN in the 'zero-damping' (ZD) condition show isotropic damping behaviour. Also, due to force-tracking limitations and a safety limit on the rate of change of forces on the slingbar, the applied lateral force does not immediately switch from zero to the setpoint value upon a change in direction of motion.

A labelled representation of the modelled system is given in Fig. F.1. The nomenclature of the key components are given in Table F.1.

The system configuration can be fully explained by the following generalised coordinate vector $\boldsymbol{q}$

$$\boldsymbol{q} = \begin{bmatrix} x_b & y_t & \phi_b & \phi_t \end{bmatrix}^T. \tag{F.1}$$

Thus, the state vector of the system can be defined as

$$\boldsymbol{X} = \begin{bmatrix} \boldsymbol{q} \\ \dot{\boldsymbol{q}} \end{bmatrix}. \tag{F.2}$$

The full derivation of the equations of motion is not included in the report due to the complexity involved.

The hip torque is regulated by full-state feedback control, with the control gain vector tuned as an output-weighed linear quadratic regulator. The output variables considered are the base and trunk angles and angular velocities ϕ_b, ϕ_t, $\dot{\phi}_\mathrm{b}$ and $\dot{\phi}_\mathrm{t}$ respectively. The reference equilibrium state is determined as,

$$\boldsymbol{X}_\mathrm{eq} = \begin{bmatrix} 0 & 0.5l_\mathrm{b} - d_\mathrm{st} & 0 & 0 & 0 & 0 & 0 & 0 \end{bmatrix}^T. \tag{F.3}$$

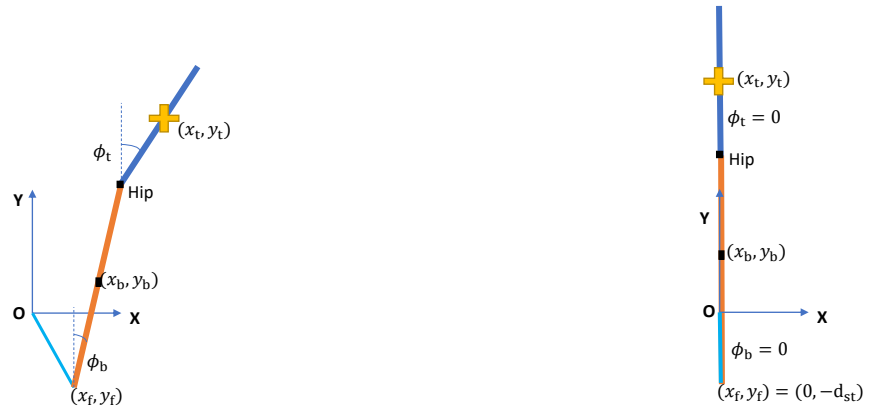

Figure F.1: Slackline balance model, with the reference equilibrium state shown in the right. The point of action of the assistive forces is at the trunk COM, indicated by the '+' sign.

Table F.1: Nomenclature of the different components of the slackline model.

Term	Definition
(x_b, y_b)	x- and y-coordinates of the COM of the base segment.
(x_t, y_t)	x- and y-coordinates of the COM of the trunk segment.
ϕ_b	angle between the base segment and the Y-axis, measured clockwise (radian).
ϕ_t	angle between the trunk segment and the Y-axis, measured clockwise (radian).
(x_f, y_f)	x- and y-coordinates of the COM of the foot.
g	Acceleration due to gravity (m/s^2)
m_b	Mass of base segment (kg)
m_t	Mass of trunk segment (kg)
l_b	Length of base segment (m)
l_t	Length of trunk segment (m)
d_{st}	vertical sag of the slackline under the weight of the human, under static equilibrium (m).
k_s	stiffness of the slackline (N/m).
c_s	damping of the slackline (Ns/m).
D	lateral damping applied at the trunk COM (Ns/m)

To determine the optimal gain vector, the human-slackline-RYSEN system model is first numerically linearised about this equilibrium state. The diagonal $\boldsymbol{Q}$ matrix used to weigh the output error terms is,

$$\boldsymbol{Q} = \text{diag}(\begin{bmatrix}0.5 & 0.5 & 1 & 1\end{bmatrix}), \tag{F.4}$$

while $\boldsymbol{R} = 10$ is used to weigh the participant's effort, i.e., hip torque. The optimal gain vector is then computed using the *lqry* function in MATLAB.

F.2. Simulation Conditions

Numerical simulations of the system were performed for the following initial condition, with the base and trunk segments oriented 10° anticlockwise and 10° clockwise, respectively, to the y-axis.

$$\boldsymbol{X}_{\text{init}} = \begin{bmatrix} 0 & 0.5l_{\text{t}} - d_{\text{st}} & -\frac{10\pi}{180} & \frac{10\pi}{180} & 0 & 0 & 0 & 0 \end{bmatrix}^T. \tag{F.5}$$

The initial condition was set such that simulations in all the 4 conditions achieve stability. Each simulation was run with *ode45* solver in MATLAB for a period of 5 seconds, with a time-step size of 0.01 seconds.

The model parameters used in the simulation are given in Table F.2.

Table F.2: Model parameters used in the simulation. The segment masses and lengths are based on anatomical data from [35], considering the upper segment as the head, arms and trunk (HAT) and the lower segment as two legs.

Parameter	Value
g	9.81 m/s^2
m_{b}	23 kg
m_{t}	49 kg
l_{b}	0.95 m
l_{t}	0.85 m
d_{st}	0.3 m
k_{s}	$\frac{(m_{\text{b}}+m_{\text{t}})g}{d_{\text{st}}}$
c_{s}	$\sqrt{k_{\text{s}}(m_{\text{b}}+m_{\text{t}})}$

The conditions considered in the simulation are:

1. **No Assistance:** In this condition, no assistive forces are provided at the trunk COM. The model is entirely stabilised by hip torque.

2. **Ideal ZD:** In this condition, an upward force (BWS) which is 11% of the human's total weight is applied at the trunk COM. This condition represents the ideal baseline condition in the RYSEN.

3. **Real ZD:** In this condition, an isotropic lateral damping of 64 Ns/m is applied at the trunk COM, along with the BWS. This condition represents an actual baseline condition in the RYSEN.

4. **Maximum Ideal Damping:** In this condition, an anisotropic damping of 75 Ns/m is applied at the trunk COM, along with the BWS. This condition represents an ideal maximum lateral damping condition in the RYSEN.

F.3. Observations and Model Limitations

The timeseries plots of trunk COM position, lateral velocity, lateral forces and impulses on the trunk, and the hip torques have been shown in Fig. F.2. The main difference observed in model behaviour between the conditions is in the initial hip torque applied to stabilise the human. The lateral impulses generated in the Real ZD condition are larger in magnitude than the impulses generated in the Maximum Ideal Damping condition, and with opposite sign.

The optimal hip torque gains for each simulation condition are plotted for each state variable in Fig. F.3. The optimal gains show a decrease upon moving from simulation condition 1-4, with very little difference between the optimal torque gains for the Real ZD and the Maximum Ideal Damping conditions.

Comparing the peak hip torques in each condition with respect to the No Assistance condition, it was found that the peak torques in the Ideal ZD condition was 75% of the unassisted peak torque, while the Real ZD and Maximum Ideal Damping conditions had very similar peak hip torques, at 64 % and 62 % of the unassisted peak hip torque. It was interesting to note that the Real ZD condition, in which damping occurs against stabilising as well as destabilising movements, reduces peak hip torque to nearly the same values as the Maximum Ideal Damping. The assumed magnitude of the lateral damping in the Real ZD condition is quite close to the magnitude of the Maximum Ideal Damping condition. **Running a simulation with the Real ZD damping set to 75 Ns/m revealed identical timeseries profiles– including peak hip torques, to the Maximum Ideal**

Damping Condition, indicating that anisotropic damping was no better than isotropic damping. Assuming no error in the model, the identical behaviour of the model under both forms of damping could be due to the low magnitude of lateral forces involved. To further understand this result, the generalised acceleration vector was computed at the same initial condition, for different values of the assistive lateral force at the trunk COM. Upon changing the lateral force from -100 N to 100 N, the acceleration terms changed as follows: 8% difference in $\ddot{x}_b$, 2% difference in $\ddot{y}_b$, 7% difference in $\ddot{\phi}_b$, and 6 % difference in $\ddot{\phi}_t$. The low changes in accelerations for a complete change in the sign of the force terms, suggests that, for the scale of lateral forces seen in the simulation, the effect of anisotropy–essentially, the sudden changes in damping force from zero to non-zero value, based on the position and the velocity of the trunk COM– is negligible in the model.

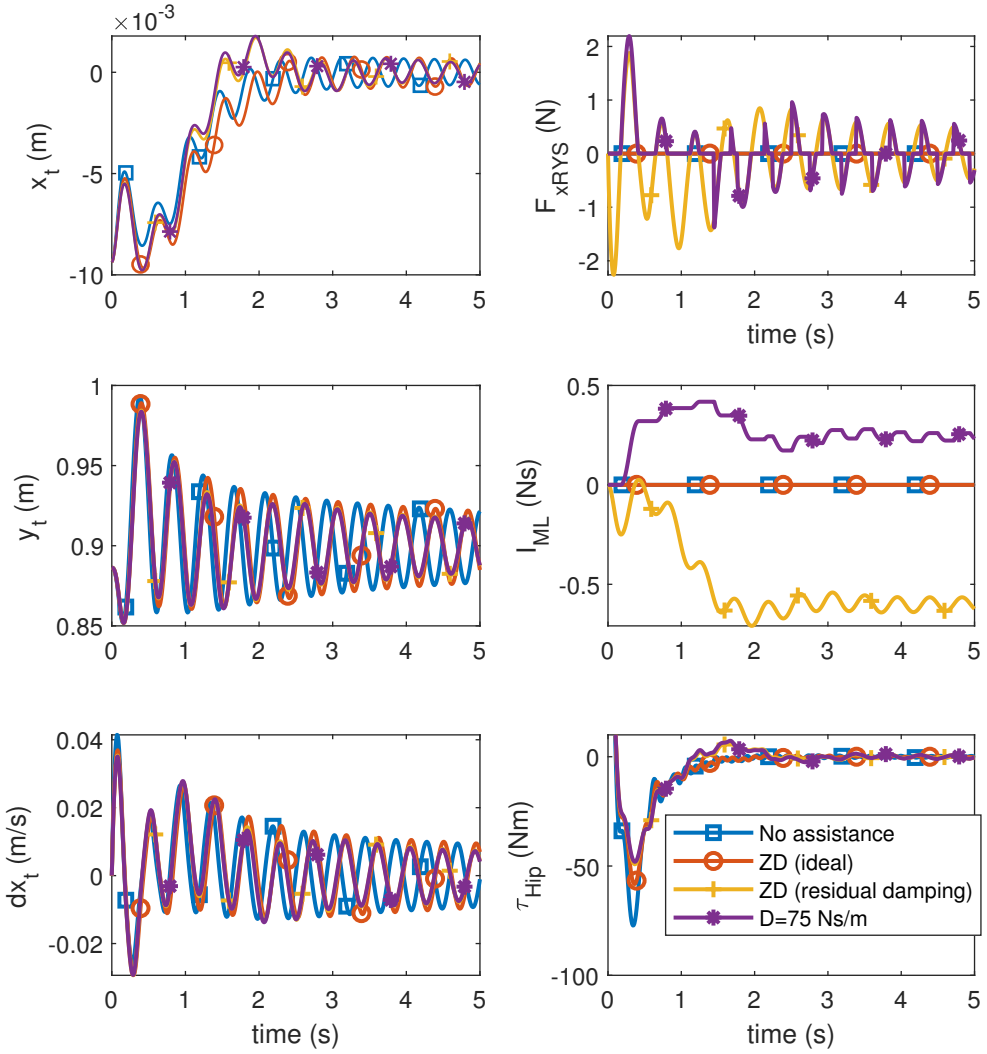

Figure F.2: Plots of trunk COM x-coordinate, y-coordinate, lateral trunk COM velocity, lateral force, lateral impulse and hip torque vs time for simulations with no assistance, ideal ZD condition, real ZD condition, maximum lateral damping conditions.

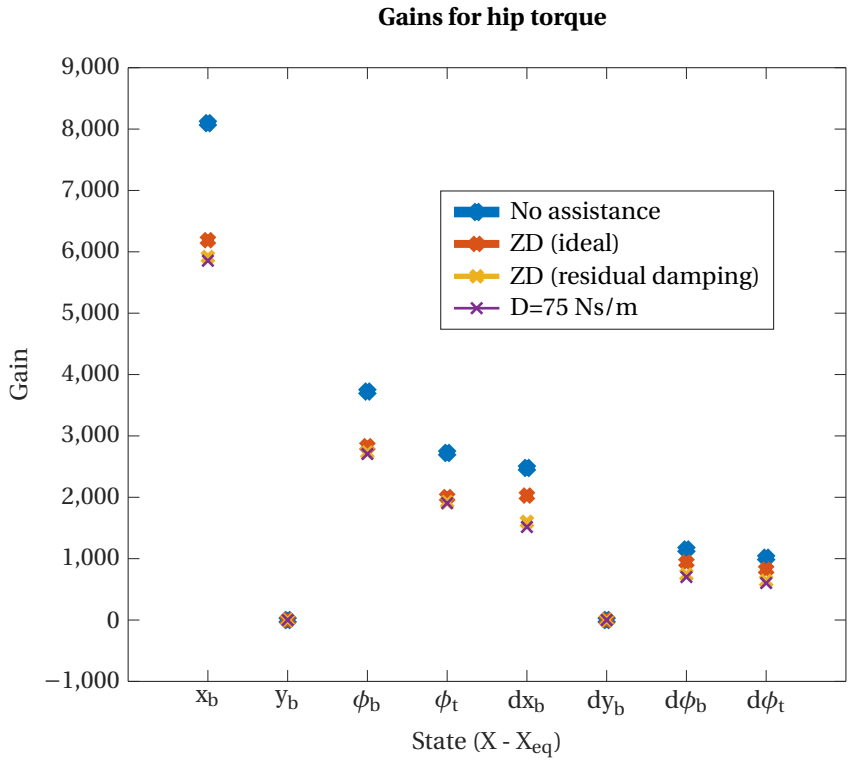

Figure F.3: Optimal gain values for each state variable, considering balancing without any assistance, with only 11% bodyweight support, with the maximum possible damping in the RYSEN, and with the maximum possible stiffness in the RYSEN.

G
Informed Consent Form

Informed Consent Form

Research Study: Optimisation of lateral balance assistance provided by a bodyweight support system during slackline walking

Delft University of Technology

Informed Consent Form

This informed consent form is for individuals invited to and willing to participate in a balance assistance optimisation experiment at the TU Delft.

Researcher: Aneesh Ashok Kumar

Supervisor: Andrew Berry, Heike Vallery

Organization Name: Delft Technical University (TU Delft)

Faculty: Biomechanical Engineering Department, Mechanical, Materials and Maritime Engineering (3ME) Faculty, TU Delft

Below is a brief introduction to the study and your role in it. If you agree to participate after reading this information, please sign the certificate of consent at the end of this form. You will receive a full copy of your signed Informed Consent Form, upon request.

Information Sheet

Introduction:
The aim of the study is to study the benefits of optimizing control parameters in a balance assistance device to maximise task performance while keeping the assistance within a specific limit. Parameter tuning would be done i) using an optimisation algorithm and ii) by yourself, in separate trials. The task involves walking as far as possible on a slackline while being supported by the RYSEN (a bodyweight support system) using a safety harness. Certain restrictions would be imposed on the body motion to maintain sufficient task difficulty, based on your baseline performance evaluated when doing the task without the assistance of the RYSEN.

Qualification:
You are a healthy adult (18 years or older) who weighs less than 100 kg. To the best of your knowledge, you do not suffer from health issues which affect your movement or balance in daily life activities.

Your role and time commitment:
Before starting the experiment, you are weighed in order to optimize the experimental setup according to your weight. Following this, you are asked to try walking on the slackline a few times to evaluate your basic balance capability, and to get you familiarized with the task. Following this, you are asked to wear a full-body harness that is supported from the RYSEN and asked to repeat the activity for 8-10 trials while the RYSEN applies an upward force.

After this, you would be asked to repeat the task for 6 different modes during which lateral forces are applied by the RYSEN, and performance costs are evaluated for each trial based on the distance walked on the slackline before a step-off, and the assistance provided by the RYSEN. 2 of these modes would involve an algorithm-based adaptation of a force parameter; in 2 other modes you would be asked to adjust the parameter value in a way you think would reduce the cost shown to

you at the end of each trial; and the remaining 2 modes would involve uniform sampling of the parameter within its range. The experiment is expected to take at most 180 minutes.

Data acquisition:
You are advised to wear sports clothes in order to ensure the comfort of your walking pattern. The data is extracted from the RYSEN device: the time taken for completing each trial and the number of steps taken while walking will be recorded. We can also provide the appropriate clothing at the lab. Video may be recorded during the experiments to support post-processing of data. This would be done after notifying you. You may notify the experimenter if you do not wish to be recorded, in which case no recordings would be made.

Discomforts involved in participating:
Wearing a full body harness might make walking slightly restricted but will not pose a problem once you are accustomed to it.

Risks and safety measures:
Balancing on the slackline might be challenging for those new it, and there is a small risk of falling when attempting the task. The RYSEN, when used, prevents falling by supporting the user's body weight in case of loss of balance. Thus, you should be able to safely step off in case of a loss of balance on the slackline. Even in the initial trials without the RYSEN, 4 cm thick safety mats would be placed under the slackline, extending to 1 m on either side to cushion any falls. The slackline itself would be not more than 50 cm above the ground.
Rest intervals of 2-3 minutes would be provided after every 10-15 trials to ensure you do not get fatigued, and refreshments would be available during these intervals.

Confidentiality:
Any personal information, except for your weight, height, will not be collected and all the recorded data will be saved anonymous. Any identifiable data (such as name, email address, telephone number) are not linked to the recorded data and will not be kept longer than 6 months. All information will be archived so that no one except the researchers and supervisors as listed above will have access to the data. On request, you will have access to your own data and you will not be photographed or filmed without prior information. You may discuss with other participants after the study period, but please respect the confidentiality of others' participation in the study. All data is made anonymous for publication purposes. The anonymized data will be processed and uploaded to an online repository in the advent of a possible publication.

Participant's rights:
Participation in this research study is completely voluntary. Even after you agree to participate and begin the study, you are still free to withdraw at any time and for any reason. You have the right to ask that any data you have supplied to that point be withdrawn/destroyed, without penalty. You have the right to omit or refuse to answer or respond to any question that is asked, without penalty. You have the right to have your questions about the procedures answered (unless answering these questions would interfere with the study's outcome). If any questions arise as a result of reading this information sheet, you need to ask the investigators before the start of the experiment.

Cost, reimbursement and compensation:
No cost, reimbursement or compensation are applicable for this study.

Informed Consent Form

Please tick the appropriate boxes

	Study Participation and recorded data	**YES**	**NO**
1	I consent voluntarily to be a participant in this study. I understand that I can refuse to answer questions and that I can withdraw from the study at any time, without giving any reason.	☐	☐
2	I understand that taking part in the study involves video recordings being made that are identifiable. I agree that those video recordings are made during the experiments.	☐	☐
3	I understand that during the experiments sensor data is recorded by the RYSEN device itself.	☐	☐
4	I understand that I will be asked questions regarding my age and that my height and weight will be measured.	☐	☐
	Data Use		
5	I understand that information I provide will be used for the master thesis and a possible research article of Aneesh Ashok Kumar.		
6	I understand that personal information that can identify me (such as my name, email address, and telephone number) will not be shared beyond the research team.	☐	☐
7	I understand that personal information and recorded data will be stored separately.	☐	☐
8	I understand that any identifiable data (such as the video recordings) will be either removed or anonymized a maximum of 12 months after the experiments.	☐	☐
9	I agree that the recorded data in the experiments can be used (anonymized) in research outputs and can be published as open data.	☐	☐
10	I understand that I may request my data at any time, and that I can make corrections to any inaccurate data that I provided. I also understand that I have to 'right to be forgotten' and can request the deletion of my data.	☐	☐

For further information:
The investigator and supervisors listed above will gladly answer your questions about this study at any time. If you are interested in the final results of this study, you can contact the investigator or supervisors. For questions, please contact:

Aneesh Ashok Kumar – aneeshashokkumar@student.tudelft.nl – +31644559303

Consent Certificate:
I have read and understand the information above, and have had the opportunity to ask questions and my questions have been answered satisfactorily. By signing this form, I voluntarily consent to participate as a research participant in this study.

_____
Name of Participant (BLOCK CAPITALS)

_____ _____
Signature of Participant Date

_____
Name of Researcher (BLOCK CAPITALS)

_____ _____
Signature of Researcher Date

If you would like a copy of this consent form to keep, please ask the researcher.

H
Slackline Setup Design

Slackline Mounting Setup in BioMechaMotion Lab

Author: Aneesh Ashok Kumar

This document summarises the design considerations made for the installation of a slackline setup in the BioMechaMotion lab in 3mE, TU Delft.

Contents

I. Aim

The goal of this initiative is to install a slackline setup that:

- can be used by healthy adult participants weighing up to 100kg
- can be used in conjunction with the bodyweight support systems present in the gait lab
- has the maximum possible usable slackline length

In addition, it should be possible to dismount the setup with minimum effort after use (including ground anchors), to allow for the use of the gait lab for other tasks.

II. Overall Setup

Floor vs wall-mounted anchors: The anchors of a slackline should be able to withstand dynamic loads induced by webbing tension. A wall-mounted anchor would have an advantage of having the mounting bolts mainly under tensile loads, whereas floor-mounted anchors would fasteners subjected to shear forces and moments. A wall-mounted anchor also need not be removed after use. However, since the gait lab has only one solid wall at the ends of its length, at least one floor-mounted anchor is necessary. From discussions with the Campus Real Estate, TU Delft, it was decided that floor mounted anchors would be safer, considering the possible loads on the building. The anchors are Zinc coated steel plates bolted to the floor at each corner by M16 bolts. Each plate is placed over 2 Aluminium spacers, one on each side. The spacers are 1.5 cm thick and provide enough space to pass a load rated sling underneath the plates and connect to the slacklines.

Connecting elements: The slackline webbing is to be connected to the anchors at each end by 1 webbing sling (Endura HBE3010, purchased via Mennens NL) and 1 D-shackle (Green Pin G 4163, purchased via Mennens NL). Load ratings and further sources of information are given in Table 1.

Table 1: Load rating information and sources of further information on slackline webbing and connecting elements.

Element	Number (at each anchor point)	Specified load limits (kN)	Source of Information
Slackline webbing	1	40	E-mail communication with Gibbon (copy available in repository ((https://gitlab.tudelft.nl/GyroProject/slackline)))
Endura webbing	1	58.8 (29.4x2, based on loading configuration)	https://www.mennens.nl/en/products/textile-slings/webbing-sling-endura-p79944 (refer for part code HBE3010)
D-shackle	1	46.6	https://www.mennens.nl/en/products/shackles/dee-shackles-with-safety-bolt-g-4153-p108376 (refer for part code 11.30GPGDMB19)

Slack-frames: The slackline will be stretched over two slack-frames in between the anchors. Free standing slack-frames from Gibbon (ID Sports, Stuttgart, Germany) are considered in the design. These frames do not require floor-mounting and can be used indoors. The webbing is passed through one of three slots in each frame, which are at three different heights (30 cm, 50 cm and 70 cm). The frames themselves are free-standing units, their positions adjustable for achieving different line lengths. Thus, the frames are used to set the walkable length of the line and its height above the floor.

Slackline webbing and ratchet: The stiffness of the slackline depends on the webbing material used, and this determines the maximum sag of the slackline under loads, the generated tensions in the line and finally the difficulty level for the slackliner. High-stiffness low-stretch polyester webbings can be used for low-height setups, while being generally easier to maintain balance on than high-stretch nylon webbings. Due to the height constraint on the slackline, polyester webbings are considered in the setup.

The slackline webbing selected for the activity is the Gibbon Classic line, with a load rating of $40\ \mathrm{kN}$. The webbing itself is of low stretch polyester and is compatible with low height slackline setups.

The pre-tension in the webbing can be adjusted using a ratchet mechanism, which is provided by the slackline supplier.

The webbing, ratchet and a pair of slack-frames are available from Gibbon as an indoor hall kit (see https://www.gibbon-slacklines.com/en/products/slackline-frames/indoor-set-sports-halls/).

Safety mats: In order to ensure the safety of the participants during a complete loss of balance on a slackline, they could always be connected to a bodyweight support system, such that the fall is arrested in time. In addition, 4 cm thick judo mats could be laid below the slackline to cushion the landing.

A labelled diagram of the setup is shown in Figure 1.

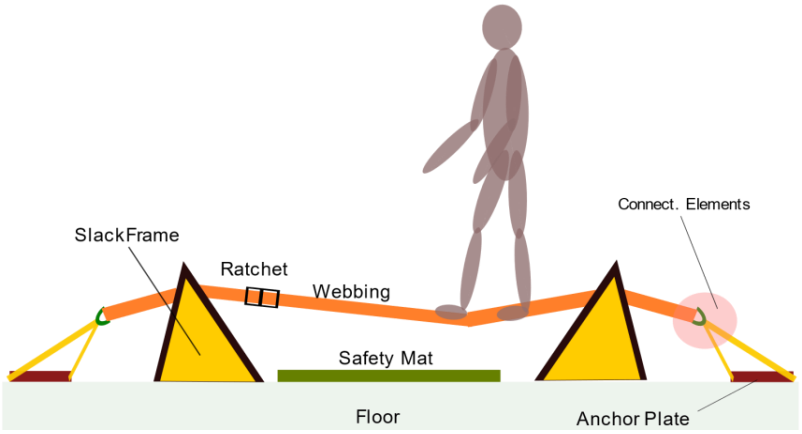

Figure 1. Proposed slackline layout, with line length l, and at a height h above the ground.

III. Estimating Maximum Possible Slackline Tension

A. Critical Load Calculations

1. Available information

The tensions induced in the Classic Line webbing— which would be used in the setup— during walking activities are estimated to be in the range of 5-12 kN based on experiments conducted by the manufacturer with a 90 kg participant (obtained via e-mail correspondence). The worst-case loading scenario would be when the participant loses balance and falls directly on the line. The lack of sufficient information on the properties of the Classic Line made it difficult to predict tensions in the worst-case scenario.

However, experimental data from the study by Athanasiadis [1] gives some insight into the properties of a slackline. The study focuses on the loading induced by leash falls, where a person falls from a slackline while connected to it by a leash rope of a specific length. The tightening of the leash during the fall causes a sudden impact load on the line. This could be compared to the loading induced when a person loses balance and falls onto the line.

Experimental data from the study [1] showed that slacklines exhibited different stiffness properties based on the loading, increasing in effective stiffness for a higher pre-tension and strain rate. The load characteristics exhibited in the experiments are shown in Figure 2 (taken from [1]), with the black plots being static load-deflection curves provided by the manufacturer and the red and green plots being the load-deflection curves during leash falls. The effective stiffness could be explained as the slope of the tension elongation curve, for the given pre-tension and strain rate. Since the Gibbon Classic Line is made from polyester, data from the polyester webbing is used to obtain an estimate of the stiffness for the

Classic Line under impact loading. The Classic Line is assumed to show a similar stiffness behaviour to the webbings from the study [1].

The Classic Line can be set to a maximum pretension of 5 kN, limited by the maximum load rating of the ratchet provided. Since Figure 2 shows an increase in effective stiffness with pre-tension, this maximum pre-tension is considered for estimating critical tension induced during a fall on the line.

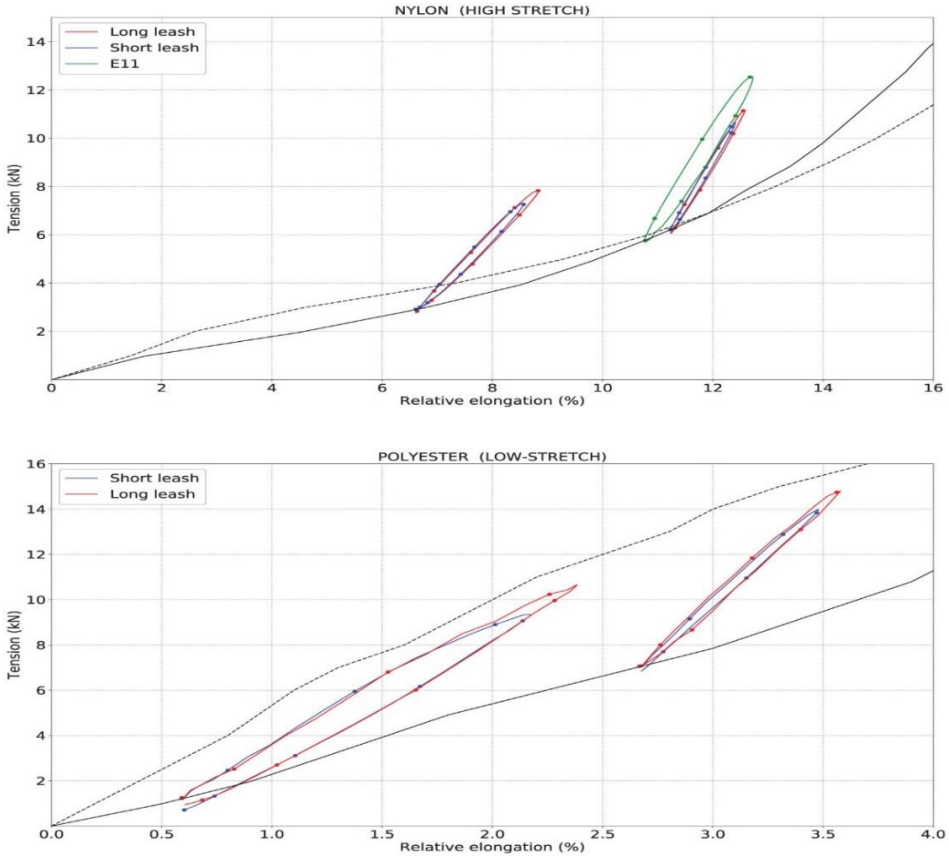

Figure 2: Tension elongation plots from the study by Athanasiadis[1]. Both nylon and polyester webbings show similar stiffness behaviour, with effective stiffness increasing with higher strain rate (impact loading) and higher pre-tensioning in the line.

During an impact load, the induced tension due to the relative elongation of the webbing is estimated in [1] as

$$T = T_0 + K_{\text{eff}}\epsilon \qquad 1$$

where T_0 is the pretension in the webbing, ϵ is the relative extension of the webbing with respect to the unstretched length of the line L, and K_{eff} is the effective stiffness of the webbing. Considering a leash fall

with a rope of length l, the following relation was derived between the pre-tension, the falling mass, and the length of the line [1]

$$\frac{K_{\text{eff}}}{mg}\epsilon^2 + \frac{2T_0}{mg}\epsilon - \sqrt{\epsilon(2+\epsilon)} = \frac{2l}{L} \qquad 2$$

Experimental data available for polyester webbing [1] was used to approximately estimate K_{eff} for the Classic Line for a maximum possible pre-tension. Estimating ϵ to be 0.9% (from Figure 2), the value of K_{eff} for an impact load applied for $T_0 = 7$ kN was calculated using Equation 2 to be approximately $9.8\text{x}10^2$ kN. Similarly, for $T_0 = 1.2$ kN, K_{eff} was estimated to be approximately 6x10^2 kN. Meanwhile, the maximum possible pre-tension for the Classic Line has been determined by the supplier to be around 5 kN. Experimental data is not available for this pre-tension value, and a relationship between the pretension and the effective stiffness has not been modelled. The higher value of $K_{\text{eff}} = 9.8 \text{ x } 10^2$ kN could be assumed for a pre-tension of 5 kN, being the more conservative estimate. However, this approach has two limitations:

- The properties of the webbings may differ significantly.

  The assumption of the polyester webbings having similar stiffness profiles is based purely on the material used. However, the quantity K_{eff} used in the study, while independent of line length, depends on the cross-sectional area of the webbing and structure of the webbing itself. The width of the webbings used in the experiments in [1] is not given. No response was obtained from the author (Athanasiadis) upon inquiry.

- The experiments in the study involved leash falls from lines under pre-tension without any pre-load from the weights used (The weights were supported by a different structure before being released for the fall). In contrast, when a person falls during a slackline walk, the line would be pre-loaded to a higher tension value due to the person's weight, which would imply a higher effective stiffness upon impact loading. However, the increase in relative elongation during a fall would be less pronounced, as there would already be sag in the line from the person's weight.

Hence, to account for the uncertainty from the above two points and have a conservative estimate of the tensions induced on impact, in addition to other differences caused by differences in material properties and webbing structure, the effective stiffness for the Classic Line is estimated using an uncertainty factor $UF = 2$:

$$K'_{\text{eff}} = UF\ K_{\text{eff}} = 2 \text{ x } 9.85 \text{ x } 10^2 = 19.7 \text{ x } 10^2\text{kN}$$

2. Comparing leash falls to a person falling on the line

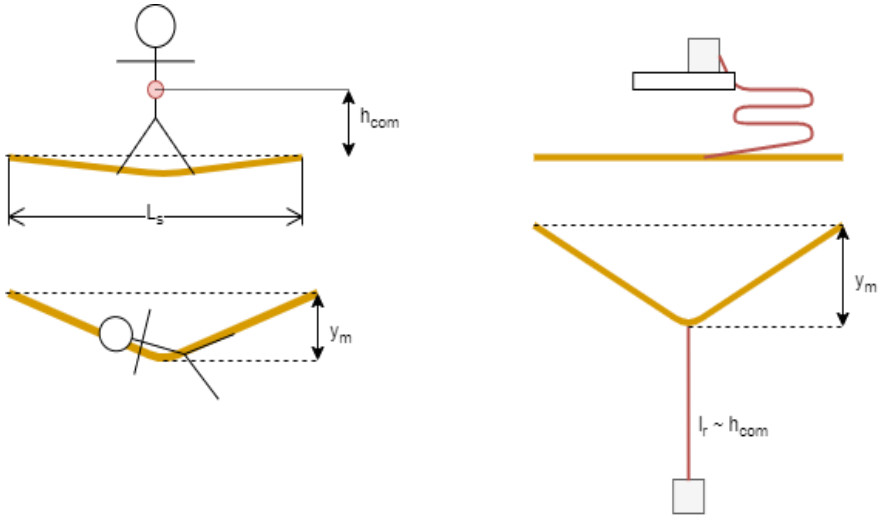

Figure 3: Visual comparison between the loading cases for a human falling completely on a slackline, and the leash-fall studies conducted in [1].

Both leash-falls and falling on the line cause impact loads. Considering a person of height 2 m, the height of their centre of mass above the slackline would be roughly 60 % of their full height [2], thus $h_{\mathrm{cm}} = 0.6 \text{ x } 2 = 1.2 \text{ m}$. Going with a point-mass approximation, the impact load from the fall is considered equivalent to that from an equal mass falling from a height h_{cm}above the slackline. This would also be a conservative approach, as in reality, the contact between the person and the line would slow down the fall, leading to a less steep impact loading on the line.

3. Obtaining the maximum elongation on impact based on energy considerations

When a point-mass *m* falls from a distance *h* above the slackline, the gravitational potential energy of the mass is converted into the elastic potential energy of the line. Considering a maximum vertical deflection *y* due to the impact load, the conversion in energy can be expressed as (from [1]):

$$mg(h+y) = T_0 x + \frac{1}{2}kx^2, \qquad 3,$$

where *x* is the absolute elongation in the line, in meters. Expressing in terms of relative elongation $\epsilon = \frac{x}{L_r}$, and $K'_{\mathrm{eff}} = kL_r$, where L_r is the length of the webbing under pre-tension, Equation 3 becomes

$$mg(h+y) = T_0 \epsilon L_r + \frac{1}{2}K'_{\mathrm{eff}}\epsilon^2 L_r \qquad 4.$$

The vertical deflection y can be expressed in terms of the relative elongation ϵ and the usable length of the webbing in between the slack-frames L_s.

$$y = \sqrt{\left(\frac{1}{2}(L_s + x)\right)^2 - \left(\frac{L_s}{2}\right)^2} = \frac{1}{2}\sqrt{x^2 + 2L_s x} = \frac{1}{2}\sqrt{\epsilon^2 L_r^2 + 2L_s \epsilon L_r} \qquad 5.$$

Substituting Equation 5 in 4, we get

$$\frac{1}{2}\frac{K'_{\text{eff}}}{mg}\epsilon^2 + \frac{T_0}{mg}\epsilon - \frac{1}{2}\frac{\sqrt{\epsilon^2 L_r^2 + 2\epsilon L_r L_s}}{L_r} = \frac{h}{L_r} \qquad 6.$$

Equation 6 can be numerically solved using MATLAB to compute the relative elongation from the impact of the falling mass, for a specific pre-tension and effective stiffness. The length of the webbing under pre-tension L_r can be computed from the geometry of the setup, for a given configuration of anchor positions and slackline lengths.

If the resulting maximum vertical deflection (from Equation 5) exceeds the slackline height above the ground, the slackline would touch the floor and the ground reaction force would relieve the webbing line of some of the impact load. In this case, the elongation corresponding to a deflection equal to the slackline height is computed to determine the maximum tension induced before the line touches the floor, using Equations 5 and 1 respectively.

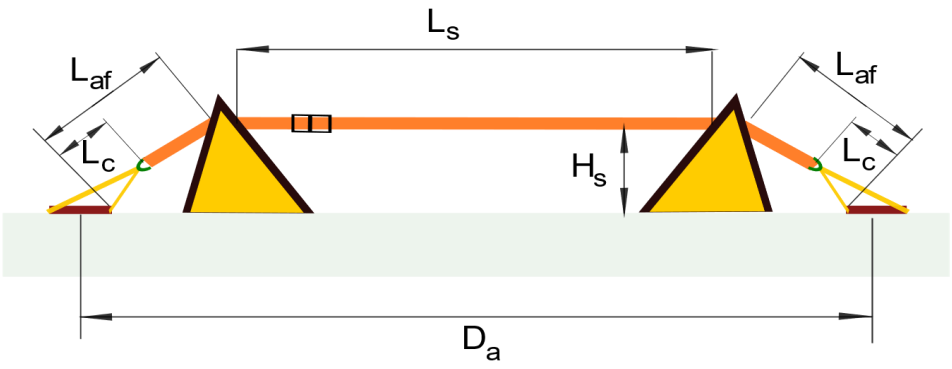

Figure 4: The distance between anchor points is D_a, the usable slackline length is L_s, the setup height is H_s, and the length of the connecting elements is L_c. Thus, $L_r = L_s + 2(L_{af} - L_c)$.

From the geometry of the setup shown in Figure 4, the webbing length under pre-tension L_r can be computed. The distance between the anchors D_a is set at 10.6 m (limited by the room length of 10.8 m). The length of the connecting elements L_c is considered to be 25 cm.

$$L_r = L_s + 2(\sqrt{H_s^2 + (0.5(D_a - L_s))^2} - L_c$$

Therefore, using MATLAB, the estimated maximum tension induced in the webbing from a fall is calculated for webbing lengths ranging from 1-10 m, for the following parameters:

$m = 100$ kg, $h_{\text{cm}} = 1.2$ m, $K'_{\text{eff}} = 1.97\text{x}10^2$kN and $T_0 = 5$ kN.

The induced tensions for slackline lengths from 1-10 m, in steps of 1 m, are given in Table 2, along with the vertical deflections. The line is at the maximum possible height of 0.7 m.

*Table 2: (i)Maximum induced tensions and vertical deflections in the slackline for various line lengths and a line height of 0.7 m, under critical loading. The tensions marked with * will not be reached as the slackline would touch the ground before the maximum elongation, reducing load on the line. (ii) Tensions required to maintain static deflections of 0.1 and 0.2 m, for various line lengths.*

L_s (m)		1	2	3	4	5	6	7	8	9	10
(i)Critical Loading	T_m (kN)	23.8	24.5	25.1	25.6	26.0	26.3	26.6	26.9*	26.9*	26.9*
	y_m (m)	0.22	0.32	0.39	0.47	0.53	0.58	0.63	0.68	0.70	0.70
(ii) T_{st} (kN) for:	y_{st} = 0.1 m	2.5	4.9	7.4	9.8	12.2	14.7	17.2	19.6	22.1	24.5
	y_{st} = 0.2 m	1.3	2.5	3.7	4.9	6.2	7.4	8.6	9.8	11.05	12.3

Thus, the maximum expected slackline tension is just under 27 kN, based on which the setup is designed.

B. Static Load Calculations

Next, the loads induced in the slackline during regular walking use are estimated for the maximum possible load of 100 kg.

A static sag y_{st} is considered for a load of mass m applied in the middle of a slackline of length l_s, which induces a static tension T_{st} in the line.

The study by Conley et al [3] determined the tension based on static equilibrium analysis.

$$T_{\mathrm{st}} = \frac{mg}{4}\sqrt{4 + \left(\frac{l_s}{y_{\mathrm{st}}}\right)^2} \tag{4}$$

The tensions required to maintain static deflections of 0.1 m and 0.2 m have been computed for setup lengths and are given in Table 2 (ii). It is important to note that these tensions are derived from the geometry of the setup, that would arise from the desired static deflection, and is not a result of the properties of the slackline itself. Given that the maximum pre-tension possible is around 5 kN, it would be unlikely to realise some of these tensions for the given deflections under static loading conditions, especially for the 0.1 m deflections with longer line lengths.

IV. Connecting Elements

The maximum tension under critical loading has been estimated to be nearly 27 kN. The slackline itself is rated for a load of 40 kN by Gibbon (with an unknown safety factor). The connecting elements are selected to maintain a safety factor above 4 for the setup.

Table 3: Safety factors of the connecting elements for the current application.

Connecting Element	**Number (at each end of line)**	**Working Load limits (kN)**	**Max Impact load (kN)**	**Specified Safety Factor**	**Safety Factor in application**
Endura sling	1	58.8 (29.4x2)	27	7	15.2
D-shackle	1	46.6	27	6	10.3

V. Anchor Design

The slackline webbing is stretched over the 2 slack-frames and connected to anchor plates at each end. Each floor-mounted anchor is to be mounted using 4 M16 (grade 12.9) bolts (see Figure 6). As seen in the End View, each plate has slot on its underside, through which the Endura textile webbings are looped around the plate. Both ends of the Endura webbing are connected to a D-shackle, which is also connected to the slackline webbing. The forces induced in the mounting bolts are evaluated based on a static equilibrium analysis. The line of action of the forces from the connecting elements are assumed to to pass through the centre of the plate. The forces transmitted by the connecting elements to the block are approximated as the force exerted by the webbing tension itself, acting at an angle α with the horizontal plane.

The tensile and shear forces induced in the bolts are evaluated based on a static equilibrium analysis in 2-D, considering the net forces in horizontal (along the length of the line) and vertical directions and the net moment in the plane to be zero.

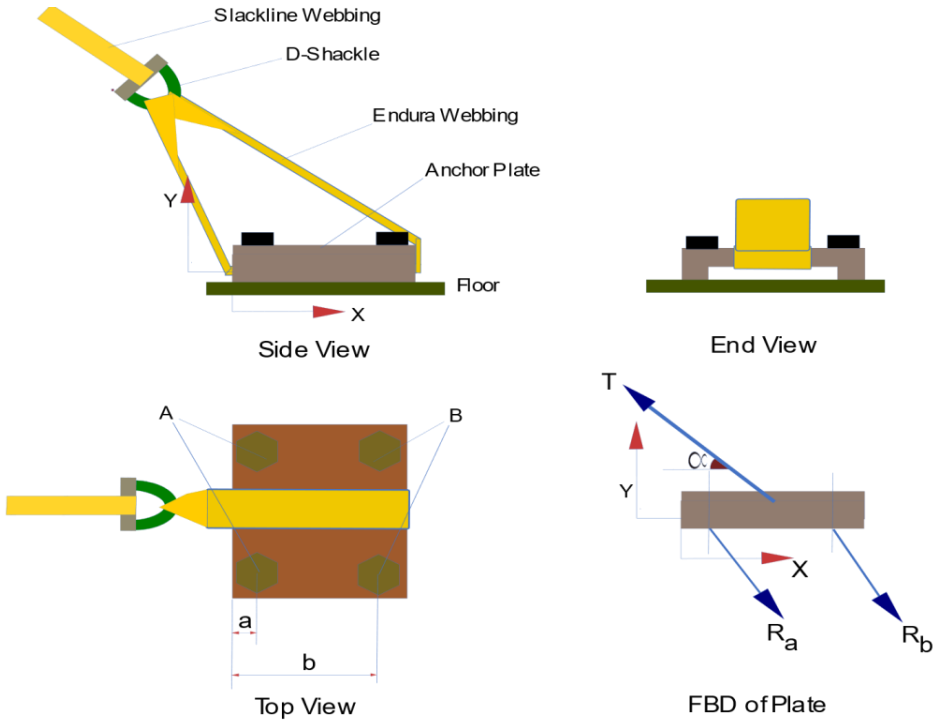

Figure 5: Orthogonal Views and Free Body Diagram of the anchor plates. The Tension in the Endura Webbing is assumed to act the Centroid of the Plate, and at an angle α with the horizontal.

Considering the symmetry of the block, this force is distributed equally over its left and right halves. In order to calculate the forces exerted on the floor-mounting bolts, the equations of static equilibrium of the block is considered. Thus, the x- and y- components of the forces on the block should cancel out, as should the moments in the z-axis about any point. Here the net moment about the origin (shown in Figure 6) is considered.

$$\Sigma F_x = 0 => R_{ax} + R_{bx} - T\cos\alpha = 0 \quad (5)$$

$$\Sigma F_y = 0 => T\sin\alpha - (R_{ay} + R_{by}) = 0 \quad (6)$$

$$\Sigma M_{0z} = 0 => 0.5T(t\cos\alpha + l\sin\alpha) - (R_{ay}a + R_{by}b) = 0 \quad (7)$$

Since there are 4 unknown bolt reaction force components (resolved in the x and y directions), and 3 equations of static equilibrium, a reasonable assumption is made that the x-components of the reaction forces are equal, and that the y-components are linearly related to the positions of the bolts along the x-axis.

$$R_{ax} = R_{bx} \quad (8)$$

It should be noted that the reaction forces of the bolts are assumed to be downwards and to the left, therefore, thus if the y-components of the reaction forces have negative values it implies upward reaction force acting on the block at that location, which would be provided by the floor.

Using equations 5-8, the reaction force components can be solved for different values of tension load, height and angle of tension load application, and floor-mounting bolt spacing. The anchor plates are

assumed to be at a distance of 10.4 m apart, with the distance between each slackframe-anchor pair considered to be equal. Then, for slackline lengths L_s from 0.2 to 10.2 m, and considering three possible slackline heights 0.3, 0.5 and 0.7 m, the loading at each bolt is calculated for a maximum webbing tension of 27 kN.

For the chosen M16 bolts (grade 12.9), the tensile endurance strength $S_e = 190\ \text{MPa}$, and the ultimate tensile strength $S_u = 1220\ \text{MPa}$ [4]. The endurance and ultimate strengths for shear loading are assumed to be half the corresponding axial strengths. The tensile stress cross-section area is given to be 157 mm^2. These values are used to compute the static safety factors on the bolts for each loading case. The minimum safety factor observed for tensile loads was 12.2 (corresponding to maximum L_s), while the minimum safety factor for shear loads was 6.4 (corresponding to minimum L_s).

The anchor plates should be removable when not in use. For this, the bolts are to be mounted on flush anchors in the ground. The flush anchors selected are M16x65 HKD from Hilti. The design tension and shear strengths are 17.6 kN and 27.0 kN. The loads computed on the expansion sleeves were always below these design ratings.

A further analysis for static and fatigue failure was done on SolidWorks 2019, to check for failure of the block itself. Considering a mild steel plate of dimensions 180x100x45 mm, and a yield stress of 220 MPa, a factor of safety above 4 could be achieved.

VI. Post-Installation Notes and Practical Considerations

With the current mounting design, a slackline can be set up along the length of the BioMechaMotion Lab and can be used along with the Bodyweight Support (BWS) Systems present in the lab. The setup is designed for a maximum user weight of 100 kg, but heavier loads could be considered with the use of appropriate bodyweight support while the user is on the slackline.

The slackline has been safely set to a length of 6 m and used for experiments along with BWS from the RYSEN. Longer setup lengths could be considered, but the space occupied by the slackframes, as well as the reachable workspaces of the support systems could become limitations. For safety, the setup of the slackline height should not be set to 0.7 m, including when used with BWS systems.

The fastening of the anchor plate bolts is to be done with the torque wrench provided by the contractor, to avoid over-tightening of the bolts into the expansion-sleeve anchors in the floor.

VII. References

[1] Athanasiadis, P. J. (2019). On the behavior of slackline webbings under dynamic loads and the simulation of leash falls. *Proceedings of the Institution of Mechanical Engineers, Part P: Journal of Sports Engineering and Technology*, *233*(1), 75-85.

[2] Clauser, C. E., McConville, J. T., & Young, J. W. (1969). *Weight, volume, and center of mass of segments of the human body*. Antioch Coll Yellow Springs OH.

[3] Conley, W. (2006). A Practical Analysis of Slackline Forces. *Zugriff am*, *20*, 2010..

[4] Mischke, C. R., & Shigley, J. E. (1996). *Standard handbook of machine design*. McGraw-Hill.

VIII. MATLAB Codes Used

The MATLAB codes used for the calculations of maximum webbing tensions are in the gitlab repository (https://gitlab.tudelft.nl/GyroProject/slackline) , in the directory 'MATLAB_codes\Webbing_tension_calcs'. The script 'Maximum_tension_estimator_main.m' can be run to obtain estimates of the maximum slackline webbing tensions for impact loading situations at different slackline lengths and heights.

The codes used to estimate the safety factors on the anchor mounting bolts and flush anchors are in the directory 'MATLAB_codes\FOS_calcs'. The script 'Max_load_static_FOS_main.m' can be run to compute the safety factors on the bolts and the flush anchors for different slackline lengths and heights.
Additional scripts for generating symbolic expressions as well as helper functions are also present in the respective directories, further information on these files can be found in the file 'MATLAB_codes\README.md'.